Long-Range Microbial Electron Transfer: Natural Mechanisms and Synthetic Models

by

Miyuki Thirumurthy

A Dissertation Presented in Partial Fulfillment
of the Requirements for the Degree
Doctor of Philosophy

Approved August 2019 by the
Graduate Supervisory Committee:

Anne Jones, Chair
Kevin Redding
Cesar Torres

ARIZONA STATE UNIVERSITY

December 2019

ABSTRACT

Exoelectrogenic microorganisms can grow by transferring electrons from their internal metabolism to extracellular substrates in a process known as extracellular electron transfer (EET). This dissertation explores the mechanisms of EET by both chemotrophic and phototrophic organisms and constructs a novel supramolecular structure that can be used as a model for microbial, long-range electron transfer. *Geobacter sulfurreducens* has been hypothesized to secrete and use riboflavin as a soluble, extracellular redox shuttle in conjunction with multi-heme, outer membrane, *c*-type cytochromes, but the required proteins and their properties have not been defined. To address the mechanism of extracellular electron transfer by *G. sulfurreducens*, the first part of this work explores the interaction between an outer membrane, octaheme, *c*-type cytochrome OmcZs from *G. sulfurreducens* and riboflavin. Interrogation via multiple physical techniques shows that OmcZs transfers electrons to riboflavin. By analogy to other characterized systems, riboflavin then likely interacts with extracellular acceptors directly. The second part of this work addresses the mechanisms of EET by the model cyanobacterium *Synechocystis* sp. PCC 6803. It has been hypothesized that *Synechocystis* employs conductive pili for production of extracellular current. However, the results herein show that a strain that does not have pili produces extracellular photocurrent in a direct electrochemical cell at a level similar to that by wild type cells. Furthermore, conductive atomic force microscopy (AFM) imaging is used to show that pili produced by the wild type organism are not conductive. Thus, an alternative EET

mechanism must be operable. In the third part of this work, a supramolecular structure comprised of peptide and cytochromes designed to serve as a model for long-range electron transfer through cytochrome rich environments is described. The *c*-type cytochromes in this synthetic nanowire retain their redox activity after assembly and have suitable characteristics for long-range electron transfer. Taken together, the results of this dissertation not only inform on natural microbial mechanisms for EET but also provide a starting point to develop novel, synthetic systems.

DEDICATION

To my rock, Dwarak Ravikumar, you mean the world to me.

To my loving parents, A.M. Thirumurthy and Shyamala Thirumurthy, you are the best.

ACKNOWLEDGMENTS

I am eternally thankful to Prof. Anne Jones for trusting me, guiding me and supporting through graduate school. She has been an inspiration to me in these 6 years and will always be. I have learnt a lot from Dr. Anne Jones who put her faith in me to learn a variety of techniques that I had no formal training in. I would like to thank her and Prof. Ian Gould for giving me this wonderful opportunity to study at Arizona State University.

I would like to thank my loving husband Dr. Dwarak Ravikumar for being my pillar of support in sickness and in health. Thank you for keeping me sane, focused and always being there for me. Graduate school would not have been possible without you guiding me every step of the way.

I want to thank my father, late Dr. A.M Thirumurthy and mother, Shyamala Thirumurthy for providing the most stable home one could ask for and for the unconditional love and unwavering support. I am thankful for my brother, Guhan Murthy who has been my friend, philosopher and guide right from day one. I would also like to thank my mother in law, Thara Ravikumar for her love through all these years.

I must thank Dr. Allison Rosenthal, Melody Griffith and Elysse Casson for their advice and support during the hardest period of my life. Thank you for being awesome.

I am thankful for my friends especially for being there for me through my highs and lows. I would like to thank Dr. Ashini Bolia and Rakesh Kukkamalla for all their

love and help through all these years in the United States of America. I sincerely thank Purnima Baskaran for all her support.

I want to acknowledge all the members of the Jones lab for their support. Thank you for putting up with me all these years. I would like to especially thank Samuel Williams and Dr. Christina Forbes for helping me with my experiments and data representation.

I would like to thank Dr. Mohammed El-Naggar and team for providing interesting ideas and helping me with complex electrochemical experiments. I would like to thank Dr. Kevin Redding for all the useful input and for allowing me to use his expensive lab equipment over the years. I want to acknowledge the National Science Foundation (Award Numbers 1359648 and 1105033) and Office of Naval Research Multidisciplinary University Research (Initiative Number N00014-18-1-2632) for funding my research over the last 6 years.

TABLE OF CONTENTS

Page

Page

Page

LIST OF TABLES

Table Page

LIST OF FIGURES

Figure Page

Chapter 1

Introduction, Scope and Summary of this Thesis

Miyuki A Thirumurthy[1]

[1]School of Molecular Sciences, Arizona State University, Tempe, USA

1.1 Electron transfer in biology

Electron transfer is essential for life, playing key roles in central biological processes such as metabolism and molecular biosynthesis. Biological energy transducing pathways depend on the transfer of electrons over distance scales from nanometers to centimeters. For example, in the electron transport chain of oxygenic respiration, electrons are transferred on distance scales from angstroms to microns through a series of proteins and soluble shuttles while concomitantly creating a proton gradient essential for production of adenosine triphosphate (ATP) by ATP synthase.[1] In a second example, some microorganisms can transfer electrons from internal metabolism to an external substrate in a process known as extracellular electron transfer (EET).[2,3] This involves electron transfer through length scales of microns and even longer and may be an essential process for communication and survival of microbial ecosystems.[4,5]

1.2 Exoelectrogens

Many microorganisms can vary their metabolism to utilize different electron donors and acceptors for growth in response to changes in chemical availability in their environment. Organisms from various genera also have the capacity to associate directly or indirectly with exogenous metals or metal oxides and use them either as terminal electron acceptors or as a primary electron donor for their metabolism.[6] Microorganisms with this ability are commonly referred to as exoelectrogens.[7] Microbes that interact with extracellular substrates have been identified in both the microbe oxidizing, i.e. reducing an extracellular substrate and the microbe reducing, i.e. oxidizing an extracellular

substrate, directions.[8,9] Furthermore, interactions are not limited to "naturally occurring" substrates; many isolated microbes as well as microbial communities have also been demonstrated to interact with solid-state electrodes.[10] These interactions with extracellular substrates have inspired a number of applications. For example, microbial fuel cells have been developed in which electrons transferred from internal metabolism can be used to generate electricity.[11] In the opposite direction, some microbes can be reduced by electricity from a solid-state electrode and use the electrons in metabolic processes. When the electrons drive synthesis of a chemical product, the process is referred to as microbial electrosynthesis.[12] Additionally, EET has been shown to play a role in bioremediation, waste water treatment, and renewable energy systems.[12,13] Despite its broad significance, key questions regarding the mechanisms, types, and components of EET remain, and the process has only been studied in a relatively small set of model organisms.

1.3 Mechanisms of short- range electron conduction in biological systems

To use exoelectrogenic microbes efficiently in industrial applications, the mechanisms of conduction and pathways of electron flow from metabolism to an abiotic surface must be characterized. There are several types of short-range (angstrom to nanometer) conduction mechanisms observed in in biological systems which can be described using an electron acceptor and donor. The four major mechanisms of short-range electron transfer are electron delocalization, tunneling, electron hopping, and flickering resonance.[14-19] In electron delocalization, electrons in valence atomic orbitals

overlap to form a continuous waveform, which results in electron transfer between the donor and acceptor molecules. This form of delocalized electron transfer can be observed in closely stacked aromatic groups, which result in π-π interactions, and leads to "metallic-like" transport.[14] Electron tunneling also relies on overlap of donor and acceptor wavefunctions and thus can only occur when the donor and acceptor are separated by less than approximately 2 nm. Super exchange is a single-step tunneling mechanism in which multiple bridge states provide an electronic pathway for electron transfer but remain formally unoccupied during electron transfer between a donor and an acceptor molecule. On the other hand, redox conduction and electron hopping are the most prevalent mechanism observed in metal-reducing bacteria. Electron hopping occurs when the charge moves between one or more stable sites, i.e. the electron "hops" between a donor and an acceptor. Redox conduction is multistep electron hopping through an arrangement of redox centers.[15] Electron hopping has been observed in many proteins including cytochromes, and other proteins of cellular respiration and photosynthesis.[14,15] Flickering resonance is a recently defined type of electron transport describing electron transfer between a donor and an acceptor molecule with bridging states having the same, temporary resonance.[20]

The above-mentioned short-range electronic conduction mechanisms typically occur within a single protein or peptide, and a series of sequential short-range electron conduction constitute long-range electron transfer (nanometers to centimeters range)

(Figure 1.1). However, long-range electron transfer in biological systems in general is much less understood.

1.4 EET mechanisms in exoelectrogens

Although many bacteria are capable of EET, the best studied model organisms are *Shewanella* and *Geobacter* species.[21,22] Based on studies of these organisms, three distinct mechanisms of electron transport and uptake have been hypothesized to play key roles in EET: direct contact, electron shuttles, and conductive appendages (Figure 1.2). Each will be described in more detail in the following paragraphs.

Electron transfer between a microbe and an electrode or other extracellular substrate can occur via direct, physical interaction between the two. This is important because the rate of electron transfer follows Marcus theory.[3] Thus for optimal electron transfer, the donor and acceptor must be spaced within 9 to 13 Å. Direct contact electron transfer has been hypothesized to be important for both *Shewanella* and *Geobacter* species. Under anaerobic growth conditions, these organisms can establish direct contact with numerous terminal acceptors like fumarate, nitrate, trimethylamine oxide (TMAO), dimethyl sulfoxide (DMSO), sulfite, thiosulfate and oxidized metals like Fe(III), Mn(III) and U(VI). Electrons are transferred from the microbes to the environment by direct contact between outer membrane redox components like cytochromes and extracellular electron acceptors. *Shewanella oneidensis* encodes 40 *c*-type cytochromes, but most EET is believed to be carried out by the metal respiratory (Mtr) proteins found in its outer membrane.[23-25] MtrABC (Figure 1.3, right side) is the best known outer membrane porin

complex and has paralogs like MtrDEF in the same organism. Mtr proteins can directly interact with the external surface or communicate with other outer membrane proteins like OmcA to reduce extracellular metals.[26] *Geobacter sulfurreducens*, a second well-studied exoelectrogen, encodes 100 genes for putative *c*-type cytochromes, a substantially higher number than other organisms reported to date.[27] EET by *G. sulfurreducens* is carried out by direct contact between a variety of characterized, outer membrane *c*-type cytochromes including OmcS, OmcZ, OmcB, and OmcC (Figure 1.3, left side) and the external environment.[28,29] The outer membrane OmcB/OmcC porin complex can directly interact with the external environment or transfer electrons to other outer membrane cytochromes like OmcZ or OmcS, which in turn transport the electron to the terminal electron acceptor.[30,31] However, the molecular interactions at the interface of the organism and the external environment are not completely understood.

In addition to direct interactions, it has been shown that some bacteria are capable of synthesizing and secreting small organic molecules, like flavins, which act as electron shuttles between the microbial cells and the environment.[32,33] Riboflavin has been identified as the dominant redox molecule present in the spent growth media of *Shewanella*, and the removal of riboflavin from the culture media results in reduced total current output in microbial electrochemical cells.[34,35] The riboflavin functions as a shuttle being reduced by cytochromes on the microbial surface and re-oxidized at the metal oxide surface. The process of electron shuttling repeats in cycles supporting microbial respiration. However, these cycles are only feasible with a high concentration of

accessible, endogenously secreted electron shuttles in the microbial environment with a relatively large diffusion coefficient in solution. Molecular dynamics and NMR studies have revealed that the outer membrane cytochromes like OmcA and MtrC from *Shewanella* have a weak affinity for electron shuttles like flavin and quinones, which allows for rapid turnover and an efficient shuttling mechanism.[36] Recent literature has shown that *G. sulfurreducens* also secretes flavin at concentrations comparable to that observed in *Shewanella* cultures.[31] Chapter 2 reports an interaction between riboflavin and an outer membrane cytochrome from *G. sulfurreducens*.

Metal-reducing bacteria have been hypothesized to employ micron-scale conductive appendages in electron transfer, adding a layer of complexity to the fundamental concepts of electron hopping occurring over short distances.[37,38] This type of long-range of EET is carried by structures often referred to as bacterial nanowires.[39] Although initially hypothesized to be pili, there is mounting evidence that alternative structures also play a key role in this type of long-range conduction.[38] For example, El-Naggar and coworkers have shown that *Shewanella* have conductive appendages which are distinct from the non-conductive, type IV pili.[40] Cryo-EM imaging suggests that the nanowires are extensions of the periplasm with encapsulated *c*-type, multi-heme cytochromes.[38,40,41] Cells which are remote from the external/electrode surface can transfer electrons to the cells that are close to the electrode by means of bacterial nanowires. Bacterial nanowires are involved not only in biofilm formation but also facilitate sustained cellular respiration and energy conservation.

1.5 Electrogenic phototrophs

Some of the earliest experiments interfacing microbes with electrodes used photosynthetic organisms which produced current upon photoillumination.[5,42] The efficiency of these devices is low but may be increased by understanding the mechanism of EET by phototrophs and optimizing the underlying biochemical process. *Synechocystis* sp. PCC 6803, a planktonic cyanobacterium, has been shown to produce photocurrent in a mediator-less bioelectrochemical system.[43] Several components have been hypothesized to be involved in this electron transfer including pili or bacterial nanowires, unknown redox-active components, or the extracellular polysaccharide. *Synechocystis* is not known to produce *c*-type cytochromes. Wild type *Synechocystis* sp. PCC 6803 do have two types of pili (thick and thin) observed during both photoautotrophic and photoheterotrophic growth.[44] Chapter 3 investigates the role of pili in Synechocystis EET by measuring the current produced by cells lacking pili *(ΔpilD*) and comparing it with the photocurrent produced by wild type cells.

1.6 Synthetic mimic of bacterial nanowire

Structural and mechanistic information regarding the source of conductivity in bacterial nanowires remains scarce. Deletion of the genes that encode for the outer membrane multiheme cytochromes like MtrC and OmcA in *Shewanella oneidensis* produces non-conductive appendages.[38] This has led to the hypothesis that electrons hop between adjacent hemes within and between cytochromes in conductive appendages during EET.[45] On the other hand, *Geobacter* pili have been hypothesized to have

conductivity similar to metals as a result of the overlap of π-orbitals of aromatic amino acids found in the pilA subunits.[46] However, a recent study by Malvankar and coworkers[47] has shown that *G. sulfurreducens* bacterial nanowires are not pili but instead are formed by micrometer-long polymerization of the hexa-heme cytochrome OmcS.[47,48] In the OmcS structure, the hemes are 3.5-6 Å apart which is sufficiently close for electron-hopping.

Inspired by bacterial nanowires, synthetic models have been created to understand the underlying mechanisms and limitations of natural and synthetic long-range EET. However, most self-assembling peptide and protein models developed so far have been devised to explore the delocalized transport conductance mechanism and have fallen in the range of semi-conducting to electrically insulating, with only a few exceptions.[15] On the other hand, Altamura and coworkers created nanofiber films from chimeric proteins composed of amyloid sequence and a redox-active, iron-sulfur protein, rubredoxin.[49] The nanowire film exhibited a conductivity of 3.1 μs/cm which is comparable to the conductivities of *G.sulfurreducens.*[49]

Cytochromes are believed to form the major conducting component in the bacterial nanowires of electrogenic bacteria, yet they have not been introduced into synthetic mimics to create a model system to evaluate hypotheses regarding electron transfer over long distances via redox hopping. Chapter 4 explores the electrical properties of nanowire assemblies by constructing a synthetic, supramolecular assembly of *c*-type cytochromes. This informs models of extracellular electron transfer and may

also provide a platform for engineering synthetic biological systems for enhanced long-range electron transfer.

1.7 Summary and scope of this dissertation

The research discussed in this dissertation seeks to define fundamental scientific mechanisms underpinning long-range biological electron transfer, to reproduce this functionality in synthetic systems, and to produce living components of electronic circuitry. The work focuses directly on mechanistic electrochemical and microscopic characterization of biological species and creation of protein-based synthetic systems.

This dissertation has two primary foci: natural extracellular electron transfer via protein, soluble electron shuttles, and conductive appendages; and synthetic models of long-range electron transfer in microbes. Chapter 2 describes the biophysical characterization of OmcZs, a *c*-type cytochrome from *Geobacter sulfurreducens* and its interactions with riboflavin. The results suggest that OmcZs functions directly in concert with riboflavin to transfer electrons from metabolism to the extracellular environment. Chapter 3 considers the role of *Synechocystis* pili in extracellular electron transfer by comparing photocurrent produced by wild type cells to that produced by variant cells that do not produce. No difference is detected, suggesting that pili do not play a functional role in extracellular electron transfer by *Synechocystis* and perhaps other phototrophs. Chapter 4 describes the construction of a synthetic nanowire comprised of *c*-type cytochromes. Incorporation of the protein into a supramolecular structure does not change the native redox properties. Together these results enhance our molecular

understanding of EET in a broad range of microorganisms. Finally, the implications of the studies described in this thesis will be discussed in Chapter 5. The knowledge gained from this work will encourage the introduction of exoelectrogenic proteins into heterologous hosts, which can prove to be useful in bioenergy and bioremediation applications. The flexibility of the synthetic nanowire model opens many potential applications based on protein and peptide nanoelectronics.

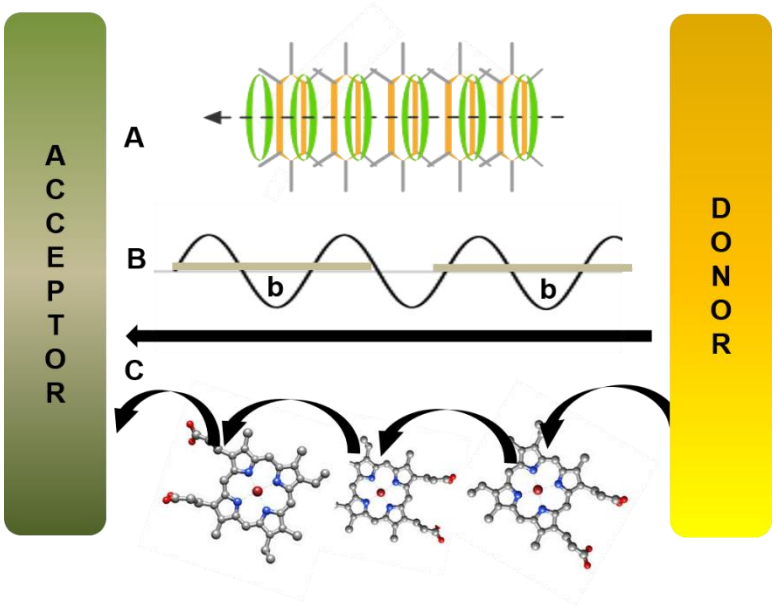

Figure 1.1. Schematic representation of three possible mechanisms of electron conduction in biological systems. The black arrows show the movement of electrons from the donor to the acceptor. (A) Delocalized electron transport through stacked aromatic molecules. (B) Tunneling through bridged states represented by "b". (C) Electron hopping through redox-active molecules.

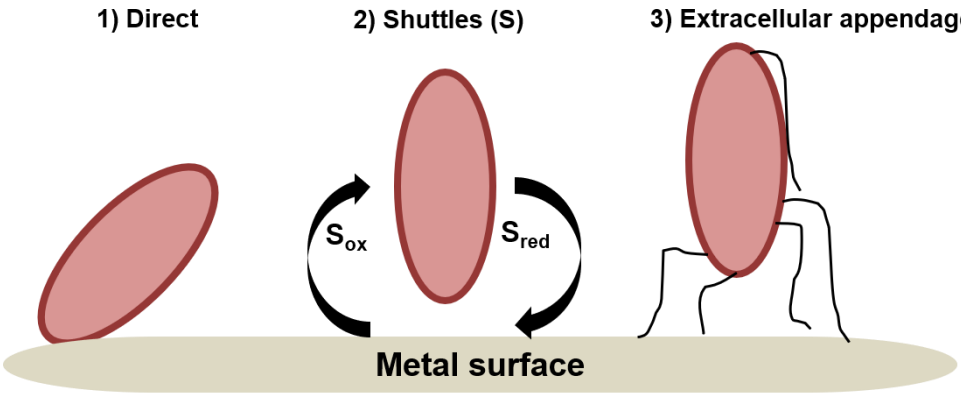

Figure 1.2. Schematic representation of three hypothesized mechanisms of EET by exoelectrogenic bacteria.

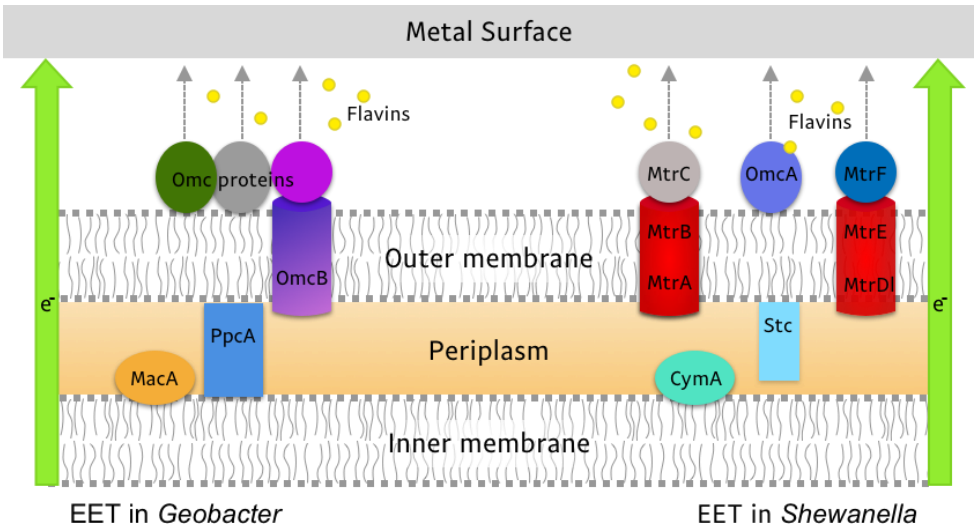

Figure 1.3. Schematic representation of EET models in *Geobacter* and *Shewanella*. Cytochrome-based, direct electron transfer and 13lavin-mediated electron transfer function in both types of bacteria.

1.8 References

1. Mitchell, P. Coupling of phosphorylation to electron and hydrogen transfer by a chemi-osmotic type of mechanism. *Nature* **4784**, 144–148 (1961).

2. Gray, H. B. and Winkler, J. R. Electron flow through metalloproteins. *Biochim. Biophys. Acta - Bioenerg.* **1797**, 1563–1572 (2010).

3. Marcus, R.A. and Sutin, N. Electron transfer in chemistry and biology. *Biochim. Biophys. Acta 811* **138**, 265–322 (1985).

4. Gralnick, J. A. and Newman, D. K. Extracellular respiration. *Mol. Microbiol.* **65**, 1–11 (2007).

5. Hernandez, M. E. and Newman, D. K. Extracellular electron transfer. *Cell. Mol. Life Sci.* **58**, 1562–1571 (2001).

6. Nealson, K.H. and Saffarini, D. Iron and Manganese in Anaerobic Respiration: Environmental Significance, Physiology, and Regulation. *Annu. Rev. Microbiol.* **48**, 311–343 (1994).

7. Kumar, R., Singh, L., Wahid, Z.A. and Din, M. F. M. Exoelectrogens in microbial fuel cells toward bioelectricity generation. *Int. J. energy Res.* **39**, 1048–1067 (2015).

8. Kumar, R., Singh, L. and Zularisam, A. W. Exoelectrogens: Recent advances in molecular drivers involved in extracellular electron transfer and strategies used to improve it for microbial fuel cell applications. *Renew. Sustain. Energy Rev.* **56**, 1322–1336 (2016).

9. Jiang, Y. and Zeng, R. J. Bidirectional extracellular electron transfers of electrode-biofilm: Mechanism and application. *Bioresour. Technol.* **271**, 439–448 (2019).

10. Bond, D. R., Bond, D. R., Holmes, D. E. and Tender, L. M. Electrode-Reducing Microorganisms That Harvest Energy from Marine Sediments. *Science (80).* **295**, 483–485 (2002).

11. Bretschger, O., Obraztsova, A., Sturm, C.A., Chang, I.S., Gorby, Y.A., Reed, S.B., Culley, D.E., Reardon, C.L., Barua, S., Romine, M.F. and Zhou, J. Current production and metal oxide reduction by *Shewanella oneidensis* MR-1 wild type and mutants. *Appl. Environ. Microbiol.* **73**, 7003–7012 (2007).

12. Rabaey, K. and Rozendal, R. A. Microbial electrosynthesis - Revisiting the electrical route for microbial production. *Nat. Rev. Microbiol.* **8**, 706–716 (2010).

13. Nealson, K. H., Belz, A. and McKee, B. Breathing metals as a way of life: Geobiology in action. *Antonie Van Leeuwenhoek* **81**, 215–222 (2002).

14. Ing, N. L., El-Naggar, M. Y. and Hochbaum, A. I. Going the Distance: Long-Range Conductivity in Protein and Peptide Bioelectronic Materials. *J. Phys. Chem. B* **122**, 10403–10423 (2018).

15. Creasey, R.C., Mostert, A.B., Nguyen, T.A., Virdis, B., Freguia, S. and Laycock, B. Microbial nanowires – Electron transport and the role of synthetic analogues. *Acta Biomater.* **69**, 1–30 (2018).

16. Bostick, C.D., Mukhopadhyay, S., Pecht, I., Sheves, M., Cahen, D. and Lederman, D. Protein bioelectronics: a review of what we do and do not know. *Reports Prog. Phys.* **81**, 026601 (2018).

17. Page, C.C., Moser, C.C., Chen, X. and Dutton, P. L. Natural engineering principles of electron tunneling in biological oxidation-reduction. *Nature* **402**, 47–52 (1999).

18. Gray, H. B. and Winkler, J. R. Electron tunneling through proteins. *Q. Rev. Biophys.* **36**, 341–372 (2003).

19. Hines, T., Diez-Perez, I., Hihath, J., Liu, H., Wang, Z.S., Zhao, J., Zhou, G., Müllen, K. and Tao, N. Transition from Tunneling to Hopping in Single Molecular. *J. Am. Chem. Soc.* **115**, 11658–11664 (2010).

20. Zhang, Y., Liu, C., Balaeff, A., Skourtis, S.S. and Beratan, D. N. Biological charge transfer via flickering resonance. *Proc. Natl. Acad. Sci.U.S.A* **111**, 10049–10054 (2014).

21. Myers, C.R; Nealson, K. H. Bacterial manganese reduction and growth with manganese oxide as the sole electron acceptor. *Science* **240**, 1319–21 (988).

22. Myers, C. R. and Nealson, K. H. Respiration-linked proton translocation couples to anaerobic reduction of manganese(IV) and iron(III) in *Shewanella putrefaciens* MR-1. *J. Bacteriol.* **172**, 6232–6238 (1990).

23. Rosso, K. M., Blumberger, J., Butt, J. N. and Breuer, M. Multi-haem cytochromes in *Shewanella oneidensis* MR-1: structures, functions and opportunities. *J. R. Soc. Interface* **102**, 20141117 (2015).

24. Pitts, K.E., Dobbin, P.S., Reyes-Ramirez, F., Thomson, A.J., Richardson, D.J. and Seward, H. E. Characterization of the *Shewanella oneidensis* MR-1 decaheme

cytochrome MtrA. *J. Biol. Chem.* **278**, 27758–27765 (2003).

25. Coursolle, D. and Gralnick, J. A. Modularity of the Mtr respiratory pathway of *Shewanella oneidensis* strain MR-1. *Mol. Microbiol.* **77**, 995–1008 (2010).

26. Myers, C. R. and Myers, J. M. Cell surface exposure of the outer membrane cytochromes of *Shewanella oneidensis* MR-1. *Lett. Appl. Microbiol.* **37**, 254–258 (2003).

27. Shi, L., Squier, T.C., Zachara, J.M. and Fredrickson, J. K. Respiration of metal (hydr)oxides by *Shewanella* and *Geobacter*: A key role for multihaem *c*-type cytochromes. *Mol. Microbiol.* **65**, 12–20 (2007).

28. Mehta, T., Coppi, M.V., Childers, S.E. and Lovley, D.R, Outer membrane *c*-type cytochromes required for Fe(III) and Mn(IV) oxide reduction in *Geobacter sulfurreducens*. *Appl. Environ. Microbiol.* **71**, 8634–8641 (2005).

29. Leang, C., Coppi, M.V. and Lovley, D. R. OmcB , a *c* -Type Polyheme Cytochrome , Involved in Fe (III) Reduction in *Geobacter sulfurreducens*. *J. Bacteriol.* **185**, 2096–2103 (2003).

30. Mehta, T., Coppi, M. V., Childers, S. E. and Lovley, D. R. Outer membrane *c*-type cytochromes required for Fe(III) and Mn(IV) oxide reduction in *Geobacter sulfurreducens*. *Appl. Environ. Microbiol.* **71**, 8634–8641 (2005).

31. Nevin, K.P., Kim, B.C., Glaven, R.H., Johnson, J.P., Woodard, T.L., Methé, B.A., DiDonato Jr, R.J., Covalla, S.F., Franks, A.E., Liu, A. and Lovley, D. R. Anode biofilm transcriptomics reveals outer surface components essential for high density current production in *Geobacter sulfurreducens* Fuel Cells. *PLoS One* **4(5)**, 5628 (2009).

32. Von Canstein, H., Ogawa, J., Shimizu, S. and Lloyd, J. R. Secretion of flavins by *Shewanella* species and their role in extracellular electron transfer. *Appl. Environ. Microbiol.* **74**, 615–623 (2008).

33. Brutinel, E. D. and Gralnick, J. A. Shuttling happens: Soluble flavin mediators of extracellular electron transfer in *Shewanella*. *Appl. Microbiol. Biotechnol.* **93**, 41–48 (2012).

34. Min, D., Cheng, L., Zhang, F., Huang, X.N., Li, D.B., Liu, D.F., Lau, T.C., Mu, Y. and Yu, H. Q. Enhancing Extracellular Electron Transfer of *Shewanella oneidensis* MR-1 through Coupling Improved Riboflavin Synthesis and Metal-Reducing Conduit for Pollutant Degradation. *Environ. Sci. Technol.* **51**, 5082–5089 (2017).

35. Yang, Y., Ding, Y., Hu, Y., Cao, B., Rice, S.A., Kjelleberg, S. and Song, H.

Enhancing bidirectional electron transfer of *Shewanella oneidensis* by a synthetic flavin pathway. *ACS Synth. Biol.* **4**, 815–823 (2015).

36. Paquete, C.M., Fonseca, B.M., Cruz, D.R., Pereira, T.M., Pacheco, I., Soares, C.M. and Louro, R. O. Exploring the molecular mechanisms of electron shuttling across the microbe/metal space. *Front. Microbiol.* **5**, 318 (2014).

37. Reguera, G., McCarthy, K.D., Mehta, T., Nicoll, J.S., Tuominen, M.T. and Lovley, D. R. Extracellular electron transfer via microbial nanowires. *Nature* **435**, 1098 (2005).

38. Gorby, Y.A., Yanina, S, McLean, J.S, Rosso, K.M, Moyles, D, Dohnalkova, A. Beveridge, T.J., Chang, I.S., Kim, B.H., Kim, K.S. and Culley, D. E. Electrically conductive bacterial nanowires produced by *Shewanella oneidensis* strain MR-1 and other microorganisms. *Proc. Natl. Acad. Sci.U.S.A* **103**, 11358–11363 (2006).

39. Strycharz-Glaven, S. M., Snider, R. M., Guiseppi-Elie, A. and Tender, L. M. On the electrical conductivity of microbial nanowires and biofilms. *Energy Environ. Sci.* **4**, 4366–4379 (2011).

40. El-Naggar, M.Y., Wanger, G., Leung, K.M., Yuzvinsky, T.D., Southam, G., Yang, J., Lau, W.M., Nealson, K.H. and Gorby, Y.A., Electrical transport along bacterial nanowires from *Shewanella oneidensis* MR-1. *Proc. Natl. Acad. Sci. U. S. A.* **107**, 18127–18131 (2010).

41. Subramanian, P., Pirbadian, S., El-Naggar, M. Y. and Jensen, G. J. Ultrastructure of *Shewanella oneidensis* MR-1 nanowires revealed by electron cryotomography. *Proc. Natl. Acad. Sci.U.S.A* **115**, E3246–E3255 (2018).

42. Berk, Richard S., and J. H. C. Bioelectrochemical Energy Conversion Technologies. *Appl. Microbiol.* **12**, 10–12 (1964).

43. Cereda, A., Hitchcock, A., Symes, M.D., Cronin, L., Bibby, T.S. and Jones, A. K. A bioelectrochemical approach to characterize extracellular electron transfer by *Synechocystis*. *PLoS One* **9**, e91484 (2014).

44. Bhaya, D., Bianco, N. R., Bryant, D. and Grossman, A. Type IV pilus biogenesis and motility in the cyanobacterium *Synechocystis* sp. PCC 6803. *Mol. Microbiol.* **37**, 941–951 (2000).

45. Pirbadian, S. and El-Naggar, M. Y. Multistep hopping and extracellular charge transfer in microbial redox chains. *Phys. Chem. Chem. Phys.* **14**, 13802–13808 (2012).

46. Malvankar, N.S., Vargas, M., Nevin, K.P., Franks, A.E., Leang, C., Kim, B.C., Inoue, K., Mester, T., Covalla, S.F., Johnson, J.P. and Rotello, V. M. Tunable metallic-like conductivity in microbial nanowire networks. *Nat. Nanotechnol.* **6**, 573–579 (2011).

47. Wang, F., Gu, Y., O'Brien, J.P., Sophia, M.Y., Yalcin, S.E., Srikanth, V., Shen, C., Vu, D., Ing, N.L., Hochbaum, A.I., Malvankar, N .S and Egelman, E. H. Structure of Microbial Nanowires Reveals Stacked Hemes that Transport Electrons over Micrometers. *Cell* **177**, 361–369 (2019).

48. Leang, C., Qian, X., Mester, T. and Lovley, D. R. Alignment of the *c*-type cytochrome OmcS along pili of *Geobacter sulfurreducens*. *Appl. Environ. Microbiol.* **76**, 4080–4084 (2010).

49. Altamura, L., Horvath, C., Rengaraj, S., Rongier, A., Elouarzaki, K., Gondran, C., Maçon, A.L., Vendrely, C., Bouchiat, V., Fontecave, M. and Mariolle, D. A synthetic redox biofilm made from metalloprotein-prion domain chimera nanowires. *Nat. Chem.* **9**, 157–163 (2017).

Chapter 2

Geobacter Cytochrome OmcZs binds Riboflavin: Implications for Extracellular Electron Transfer

Miyuki A Thirumurthy[1]*, and Anne K Jones*[1]

[1]School of Molecular Sciences, Arizona State University, Tempe, AZ, 85282, USA

1.1 Abstract

Geobacter sulfurreducens is an important model organism for understanding extracellular electron transfer (EET), i.e. transfer of electrons from the cell's interior (quinone pool) to an extracellular substrate. This exoelectrogenic functionality can be exploited in bioelectrochemical applications. Nonetheless, key questions remain regarding the mechanisms of this functionality. *G. sulfurreducens* has been hypothesized to employ both multi-heme cytochromes and soluble, small molecule redox shuttles, as the final, redox-active species in EET. However, interactions between 20lavin redox shuttles and outer membrane, redox proteins in *Geobacter* have not been demonstrated. Herein, the heterologous expression and purification from *E. coli* of a soluble form of the multi-heme cytochrome OmcZs from *G. sulfurreducens* is reported. UV-vis absorption assays show that riboflavin can be reduced by OmcZs with concomitant oxidation of the protein. Fluorescence assays show that oxidized OmcZs and riboflavin interact with a binding constant of 34 μM. Furthermore, expression of OmcZs in *E. coli* enables EET in the host, and the current produced by these *E. coli* in a bioelectrochemical cell increases when riboflavin is introduced. These results support the hypothesis that OmcZs functions in EET by transiently binding riboflavin, which shuttles electrons from the outer membrane to the extracellular substrate.

1.2 Introduction

Dissimilatory metal-reducing bacteria like *Geobacter* and *Shewanella* sp. can couple anaerobic growth to reduction of extracellular electron acceptors in a process

known as extracellular electron transfer (EET).[1,2] Electrons released during growth are transferred through the outer membrane to the extracellular terminal electron acceptor. This extraordinary functionality has applications in the development of biosensing technologies, microbial fuel cells, and bioremediation of redox-active pollutants.[3-6] For these and other bioenergy applications, molecular-level elucidation of the electron transfer process could lead to design of microorganisms with improved functionalities and new applications.

In response to environmental conditions, organisms capable of EET (exoelectrogens), can employ some combination of three different mechanisms to transfer electrons to abiotic surfaces. First, outer membrane bound *c*-type cytochromes[7-11] can be used to transfer electrons to adjacent cells or extracellular electron acceptors by direct contact. Second, conductive appendages, often referred to as bacterial nanowires or conductive pili may move electrons across large distances through biological assemblies of membrane and protein with unusual conductivity.[12,13] Third, small, soluble redox-active molecules such as flavins can shuttle electrons from the outer membrane to the external environment and return oxidized to the membrane to complete the cycle.[14-16]

Microorganisms including *Pseudomonas*, *Geothrix*, *Shewanella* and *Lactococcus* sp. can secrete soluble electron shuttles to transport electrons to electrode surfaces.[15-19] lthough both *Shewanella* and *Geobacter* sp. have served as model organisms to understand EET and despite the fact microbes genetically related to *G. sulfurreducens* often dominate the microbial communities found in bioelectrochemical systems, the

soluble, electron-shuttle-based EET mechanism of *Shewanella oneidensis* is better characterized.[20,21] *S. oneidensis* moves electrons from the menaquinone pool across the membrane through the Mtr pathway.[22] They are then transferred to the extracellular substrate by outer membrane cytochromes such as MtrC, OmcA, or MtrF via contact with the external surface either directly or in combination with electron shuttles such as flavins.[20] Until recently, *Geobacter* sp. were not known to produce electron shuttles. Genes responsible for the biosynthesis and secretion of flavins into culture media by *G. sulfurreducens* have been identified, and the amount of riboflavin detected in *G. sulfurreducens* culture supernatant can reach levels comparable to that present in *S. oneidensis* cultures.[14-16,23] This suggests flavins also play key roles in EET by *G. sulfurreducens*, but the molecular mechanisms of electron transfer involving riboflavin are yet to be identified.

Both *Geobacter* and *Shewanella* employ outer membrane, multi-heme cytochromes as central components in EET.[7,24] Interactions between the major *c*-type cytochromes of *Shewanella* such as OmcA, MtrC and MtrF with flavins including flavin mononucleotide and riboflavin have been defined,[21,25] and affinities have been shown to depend on the identities of both the flavin and the cytochrome. Like *S. oneidensis*, in *G. sulfurreducens* the majority of the multi-heme cytochromes localize in the outer membrane. However, there is minimal sequence similarity between cytochromes from these two species.[26] Thus, it is not trivial from *G. sulfurreducens* sequence information

and knowledge of *S. oneidensis* protein electron transfer networks to predict which *G. sulfurreducens* cytochromes might interact with flavins to form extracellular networks.

In this work, an interaction between the *G. sulfurreducens* multi-heme cytochrome OmcZs and riboflavin is identified. OmcZ has a long form ($OmcZ_L$) and a short form (OmcZs). The shorter form is the predominant, extracellular, cleaved product of $OmcZ_L$ and retains all the hemes. OmcZs was selected as a candidate for possible interactions with riboflavin for four reasons. First, *omcZ* is significantly upregulated in current-producing biofilms relative to cultures grown using fumarate as terminal acceptor, and its deletion severely inhibits current generation.[27] Furthermore, with respect to current production, *omcZ*-deficient cells cannot adapt to the loss even after relatively long growths, suggesting that other cytochromes cannot substitute the unique function of OmcZ.[27,28] Second, OmcZ localizes in the outer membrane. Third, OmcZ has an unusual heme binding motif ($CX_{14}CH$) like the flavin-binding, multi-heme cytochromes found in *Shewanella oneidensis*. Fourth, OmcZ can reduce small quinone molecules like anthraquinone-2,6-disulfonate (AQDS).[29] Suprisingly, the results herein show that OmcZs expression in *E. coli* confers on it the ability to perform EET in a bioelectrochemical cell in the presence of riboflavin. This result opens doors for developing *E. coli*, an important chassis for synthetic biology, for bioelectronic applications.

1.3 Methods

1.3.1 Plasmids, Strains, Media and Growth

E. coli strains were grown in Luria broth (LB) or on solid media containing 1% (w/v) agar. Antibiotics (kanamycin and chloramphenicol) were added to a final concentration of 50 μg mL^{-1} and 35 μg mL^{-1} respectively. Plasmids and strains used in this study are listed in Table 2.1.

1.3.2 Protein expression and purification

For expression of OmcZs, *E. coli* BL21 (DE3) was simultaneously transformed with pEC86 and pJ411 via heat shock, and transformants were identified by growth on agar plates containing kanamycin and chloramphenicol. A strain containing both pJ411 and pEC86 was grown aerobically with shaking (250 rpm, 15 h, 37° C) from a 0.1% inoculum from glycerol stocks in a 1.5 L culture in a 2.0 L flask. Cells were induced with 400 μM isopropyl β-D-1-thiogalactopyranoside (IPTG) in the log phase (OD_{600} ~ 0.5) and subsequently grown overnight. For anaerobic growth of *E. coli*, the volume of media was increased to 950 mL in a 1000 mL sealed glass bottle and incubated at 37° C without shaking to minimize aeration during growth. Soluble, folded OmcZs secreted into the culture medium was concentrated using Vivaflow filters 200,3000 MWCO (Sartorius, Germany) until the media turned its original color. The filtrate was then diluted with 50 ml, 50 mM Tris buffer pH 8 to obtain a clear reddish-brown solution. Protein purification was carried out using fast protein liquid chromatography (FPLC) on an AKTA prime plus using a diethylaminoethylene Sephadex A-25 (DEAE, 5.0 mL min^{-1},

5.0 mL fractions, 5.08 cm x 7.62 cm; buffer A (Tris buffer, 50.0 mM, pH 8.0). OmcZs was eluted from the column in 5 ml fractions using buffer B (50 mM Tris buffer, pH 8, 500 mM NaCl). The reddish-brown fractions were combined and concentrated using (Amicon Ultra 0.5 filters). Concentrated fractions containing OmcZs were further purified on Superdex 75 columns (GE Healthcare) equilibrated and eluted with 50 mM Tris buffer pH 8. Protein concentrations were determined using a Bradford assay kit with bovine serum albumin as the standard (Bio-Rad).

Protein purity was determined using SDS-PAGE with a 12% BisTris-SDS–polyacrylamide gel visualized by Coomasie staining. Gels were also stained with heme stain to check for the presence of *c*-type hemes using the method described by Francis et al.[30] For immunoblot analysis, proteins were separated on a 12% polyacrylamide gel, transferred to a nitrocellulose membrane (Immobilon-PVDF, 0.45 µm), and the membrane then blocked with 5% bovine serum albumin for 1 hr. His-tag monoclonal antibody [product6X His-tag monoclonal antibody (3D5), AP] from ThermoFisher Scientific was used to probe the membranes at a dilution of 1:100 and was incubated for 1 hr at 16 °C on a rocker and then washed in TBS-0.1%, Tween-20 solution. The membrane was washed three times in Tris-buffered saline and developed using the one step NBT/BCIP substrate kit Pierce from ThermoFisher Scientific.

1.3.3 UV-vis Spectroscopy

UV-vis absorbance spectra were measured using a Hewlett Packard 8453 UV-vis spectrophotometer with a gas-tight quartz cell of 1 cm path length at room temperature.

For spectroscopic experiments, the optical densities (OD_{600}) of the cultures were adjusted using LB medium at pH 7. A spectroscopic assay was used to monitor oxidation of the multiheme cytochrome by riboflavin. OmcZs (60 µg) was diluted in 0.9 mL of Tris-HCl (pH 8.0) and chemically reduced with 3 µl of mercaptoethanol under anaerobic conditions. The spectrum of the reduced OmcZs was recorded between 300 nm and 700 nm. Then, riboflavin (100 µl) was added from a stock solution (300 µM) to the reduced cytochrome solution, and the mixture incubated for 30 min before recording spectra.

1.3.4 Fluorescence quenching

Fluorescence spectra were measured at room temperature using a Perkin Elmer LS 55 fluorimeter with excitation and emission monochromator slits set at 3.0 nm and 1.5 nm, respectively. Before measuring, OmcZs and oxidized riboflavin were mixed anaerobically in a glovebox and incubated for 5 min. For each condition, three spectra were obtained to determine whether the fluorescence intensity changes with time. No changes were detected, and data presented are an average of all spectra obtained. Binding constants were determined from a Benesi- Hildebrand plot[31] of fluorescence intensity measured at 520 nm following excitation at 450 nm.

1.3.5 Electrochemistry

Electrochemical measurements were carried out in an anaerobic glovebox using a Squid Stat Prime potentiostat in a three-electrode electrochemical cell with a carbon cloth working electrode (625 mm^2, 1K plain weave ultralight carbon fiber fabric, 0.009-inch-thick, Fibre Glast Developments Corporation, Brookville, Ohio) poised at 0.2 V against a

saturated Ag/AgCl reference with a platinum wire counter electrode. Solutions were purged with nitrogen to remove oxygen before experiments. The OD_{600} of each suspension was adjusted to 0.7 using LB media (pH 7).

1.4 Results

1.4.1 Heterologous expression of OmcZs

A variant of the *Geobacter sulfurreducens c*-type cytochrome OmcZs was heterologously expressed in *E. coli* and purified to homogeneity. Figure 2.1 shows the sequence of the expressed protein. Three modifications to the original sequence were made. First, to facilitate secretion of the synthesized polypeptide into the *E. coli* periplasm for heme incorporation and post-translational processing, the transmembrane helical region of the native OmcZ sequence was replaced with the periplasmic signal peptide OmpA.[32] Second, analysis of the deduced amino acid sequence of OmcZs using the SignalP software (http://www.cbs.dtu.dk/services/SignalP) predicts a signal sequence cleavage site between residues Ala21 and Ala22; a His-tag was introduced after this cleavage site. Third, a Gly-Ser linker was introduced between the His-tag and the OmcZs sequence to facilitate proper folding of the heterologous protein.

For aerobic production of fully matured, *c*-type cytochromes in *E. coli*, a cytochrome maturation unit, referred to as ccm, is required.[33] Thus, to express OmcZs, *E coli* was co-transformed with a plasmid containing the *omcZs* gene (pJ411-*omcZs*) and a plasmid encoding the ccm operon (pEC86-*ccm*). The UV-vis absorption spectrum of the purified protein features local maxima at 408 nm (ε =910,230 M^{-1} cm^{-1}; γ Soret band)

and 537 nm (ε=103,127 M^{-1} cm^{-1}) (Figure 2). These features are characteristic of an oxidized, *c*-type cytochrome and also confirm incorporation of the hemes. The measured extinction coefficients are consistent with incorporation of all eight of the hemes predicted by the heme-binding sequence motifs. Yields of purified OmcZs are typically 3–5 mg of pure protein from a liter of *E. coli* culture.

As shown in Figure 2.3, lane 4, when induced by IPTG, these cells secrete full-length (31 kDa), soluble OmcZs into the growth medium. Following purification, the identity and correct maturation of this protein was confirmed both by heme staining (lane 2) and immunodetection of the his-tag (lane 5).

1.4.2 Reduction of riboflavin by OmcZs in *E. coli* supernatants

Flavins, in particular riboflavin, are believed to play a role in EET by *Shewanella*[34] and *Geobacter* sp[23], and analogies between these two organisms suggest that OmcZs can interact with riboflavin. As shown in Figure 2.4 and 2.5, oxidized riboflavin has a strong chromophore at 450 nm. A common characteristic of flavins is that this 450 nm absorbance decreases substantially in intensity upon reduction[35]. Thus, UV-vis spectroscopy was used to monitor the redox interaction between OmcZs and riboflavin. As shown in Figure 2.4, addition of supernatant from *E. coli* (pEC86 (*ccm* operon) + pJ411(*omcZs*)), a strain expressing both OmcZs and the ccm pathway, to a solution of oxidized 10 µM riboflavin and incubation for 12 hrs results in bleaching of the 450 nm chromophore of the oxidized riboflavin. In short, supernatant containing matured OmcZs can reduce the riboflavin. Furthermore, this reduction is reversible. The

riboflavin can be re-oxidized by exposure to air over the course of 2 hrs, with concomitant recovery of the 450 nm spectroscopic signature. Although spectroscopic features hemes are also dependent on redox state, features in the UV-vis spectra derived from the OmcZs cytochrome, especially the Soret band, are virtually unchanged throughout the entire experiment. This suggests that the majority of the OmcZs remains oxidized throughout.

To determine whether the riboflavin reduction requires fully matured OmcZs, control experiments were performed using *E. coli* BL21(pUC19), a strain with an empty expression plasmid, and BL21(pEC86), a strain expressing just the ccm operon without a *c*-type cytochrome. As shown in Figure 2.5, spectra show that in these experiments the riboflavin remains oxidized even after 12 hrs of incubation. This demonstrates that the *E. coli* supernatant without OmcZs is not sufficient for reduction of riboflavin. Instead, OmcZs is absolutely required for riboflavin reduction.

1.4.3 Oxidation of OmcZs by riboflavin

Data in the previous section shows that reduced *E. coli* supernatant containing mature OmcZs can be used to reduce riboflavin, and that the process depends strictly on the presence of OmcZs. However, those experiments could not detect a change in the oxidation state of the OmcZs. Analogous spectroscopic experiments using purified OmcZs successfully define the redox activity of the protein. As shown in Figure 2.6, chemically reduced, pure OmcZs produces a UV-vis spectrum including characteristic heme absorbances: a Soret absorance at 418 nm and sharp α-bands at 540 and 552 nm.

Anaerobic incubation of the pure OmcZs protein with 10 μM oxidized riboflavin for 30 min results in a change in the OmcZs UV-vis spectrum. As expected upon oxidation of hemes, the Soret peak shifts from 419 nm to 408 nm and the α-bands transform into a single broad peak at 537 nm. Control experiments show that the UV-vis spectrum of OmcZs without addition of riboflavin is unchanged over the same time period. Thus, riboflavin can oxidize OmcZs.

1.4.4 Fluorescence spectroscopy identifies binding between OmcZs and riboflavin

Riboflavin has strong fluorescence emission at 520 nm that can be quenched by nearby hemes.[36] Thus fluorescence spectroscopy was employed to probe binding of riboflavin to OmcZs by monitoring fluorescence intensity at 520 nm. A 10 μM solution of riboflavin was titrated with oxidized OmcZs (final concentrations 5 to 30 μM) while monitoring the fluorescence intensity at 520 nm. As shown in Figure 2.7, the riboflavin fluorescence decreases with increasing concentration of OmcZs. Using a Benesi-Hildebrand double reciprocal plot, the change in the fluorescence intensity at 520 nm was used to determine a disassociation constant (K_d) of 34 μM between oxidized OmcZs and riboflavin (Figure 2.8). Quenching of riboflavin fluorescence is not observed when riboflavin is incubated over the same time period alone or in the presence of a mono-heme cytochrome *c* from bovine heart.

1.4.5 OmcZs enables EET by *E. coli*

Electrons transferred out of a microbial cell to an electrode can be measured as current in a bioelectrochemical device. A bioelectrochemical cell with a carbon felt

working electrode was used to evaluate the impact of heterologously expressed OmcZs on extracelluar current production by *E. coli* under anaerobic conditions. *E. coli* is not noted for EET activity. Thus, as anticipated, *E. coli* strains not expressing the *G.sulfurreducens c*-type cytochrome OmcZs, i.e. containing the empty expression plasmid (pUC19) and only the *ccm* plasmid (pEC86), produce only very low currents on the order of 4.9 and 11.9 μA, respectively (Table 2.2 and Figure 2.9). On the other hand, the strain expressing both OmcZs and the ccm pathway (pEC86-ccm and pJ411-omcZs), i.e. a strain producing functional OmcZs, produces a significantly higher maximal current: 18.9 ± 0.84 μA. This suggests that expression of a functional OmcZs affords *E. coli* a new functionality, the ability to efficiently transfer electrons from metabolism to the carbon electrode.

Since the spectroscopic results suggest that riboflavin is a redox partner of OmcZs, the impact of riboflavin on extracellular current production by *E. coli* was also evaluated. As shown in Figure 2.6, addition of 5 μM riboflavin to electrochemical experiments does not impact the current produced by any of the control strains but increases the current produced by the strain expressing functional OmcZs by a factor of 1.5. Injection of 3 μM additional riboflavin to the electrochemical experiment after 45 min causes a further increase in current which clearly indicates that riboflavin plays a role in facilitating EET by interacting with OmcZs.

1.5 Discussion

While it has been hypothesized that outer membrane cytochromes *in Geobacter* sp[37] are capable of electron transport to extracellular acceptors through both direct contact[7] and via soluble electron shuttles,[23] the fundamental mechanistic details of these processes remain unexplored. Recently, it was shown that flavins play a crucial role in EET by anaerobic *Geobacter* cultures.[23] The presence of flavins like riboflavin or flavin mononucleotide in the media, either secreted or added, is required for optimal reduction of metal substrates. It has also been shown that the amount of riboflavin secreted in *Geobacter sulfurreducens* (~ 100 nM) culture media is comparable to *Shewanella oneidensis* under similar growth conditions.[14] Flavins in the media likely interact with redox proteins like cytochromes in the bacterial outer membranes to carry out EET.

Among the hundreds of putative *c*-type cytochromes encoded in the genome of *Geobacter sulfurreducens*, OmcZ has been described as the most essential for optimal extracellular current production in microbial fuel cells.[27] The *omcZ* transcript is abundant in current-producing cells, and the octaheme cytochrome OmcZ has an unusual heme binding motif ($CX_{14}CH$) like the flavin-binding cytochromes MtrC and OmcA found in *Shewanella oneidensis.*[39] Furthermore, recent studies have shown that OmcZ is essential for growth of *Geobacter sulfurreducens* strain ACL_{HF} using electrons from Fe(0). This suggests that OmcZ plays a key role in connecting internal metabolism to an external, flavin redox shuttle and may also be essential for direct electron transfer into the microbe.

In this work, complementary UV-vis absorption and fluorescence experiments have demonstrated a direct interaction between OmcZs and riboflavin, and that riboflavin oxidizes OmcZs. This strongly suggests that OmcZs and riboflavin are redox partners in the extracellular electron transport chain of *Geobacter sulfurreducens*. Furthermore, the dissociation constant of 34 μM determined between oxidized OmcZs and reduced riboflavin is relatively weak. It is also comparable to the 29 μM K_d reported for *S. oneidensis* OmcA interacting with flavin mononucleotide (FMN).[40] This provides additional evidence that *Geobacter* OmcZ and *Shewanella* OmcA play analogous functional roles in the two groups of organisms. Babanova and coworkers have used molecular docking simulations to predict the site of interaction between *Shewanella* OmcA and riboflavin as well as the energy of the interaction.[41] They have suggested that OmcA is actually a flavocytochrome with the flavin forming a relatively stable interaction with the protein by which it shuttles electrons to a nearby heme. Future biochemical and structural work on OmcZ may shed light on the question of how mobile riboflavin is in EET and whether OmcZ also interacts with other acceptors. This may be important since recent reports implicate OmcZ also as an intermediary in electron transfer into *Geobacter*.

The ability to electronically connect living cells with extracellular donors and acceptors is essential to develop technologies like microbial fuel cells or biophotovoltaics. Native organisms are often not ideal for these applications, and the tools of synthetic biology have proven useful in engineering relevant microorganisms.[42-

[46] This work shows that the current produced by *E. coli* cells expressing OmcZs is comparable to that of *E. coli* cells expressing the multi-protein MtrCAB complex from *Shewanella.*[47] This is important since expression of foreign proteins, especially those with complicated post-translational processing and transport like MtrCAB, often substantially stress the host.[42] Furthermore, functional expression of OmcZs in *E. coli* requires that it be correctly matured and transported in vivo, a non-trivial process. On the other hand, while the current produced by the *omcZs E. coli* strain is significant, it is lower than an *E. coli* strain with *cymAmtr* genes,[48] i.e. a strain producing both MtrCAB and CymA, a soluble, inner membrane component. This suggests that although OmcZs interacts with riboflavin and electronically connects the *E. coli* cells to extracellular acceptors, it is not coupling efficiently to the internal metabolism of *E. coli*. Co-expression of *G. sulfurreducens* OmcB,[49] a porin cytochrome complex that may interact with OmcZs, may improve current production by *E. coli* by creating a route for electron flow from internal metabolism to the outer membrane.

Table 1*: E. coli* Strains and Plasmids Used in This Study

Strain or Plasmid	Relevant characteristics or sequence	Source or reference
Plasmids		
pUC19	pMB1ori, lac promoter, lacZ marker, Amp^r	New EnglandBiolabs[50]
pEC86 (p*ccm*)	6.5 kb PCR fragment including *ccmABCDEFGH* with Cat^r	[51]
pJ411 (p*omcZ*)	*omcZs* with a N or C terminal OmpA signal peptide[32], kan^r	This study
E. coli strains		
BL21(DE3)	fhuA2 [lon] ompT gal (λDE3) [dcm] ΔhsdS λDE3 = λ sBamHIo ΔEcoRI-B int::(lacI::PlacUV5::T7 gene1) i21 Δnin5	New England Biolabs[52]

[a]The pEC86 plasmid was provided by D. Kramer's lab (Michigan State University); [b]The pJ411 plasmid was prepared by DNA 2.0.

Table 2.1: Currents Produced by *E. coli* Strains

Strain	Current (µA) without RFN	Current (µA) with RFN
no cells	2.4 ± 0.5	2.3 ± 0.3
pUC19 (no gene)	4.9 ± 0.4	5.1 ± 0.2
pEC86 (*ccm* operon)	11.9 ± 0.3	12.1 ± 0.4
pEC86 (*ccm* operon) + pJ411(*omcZs)*	18.9 ± 0.9	28.1 ± 0.5

Figure 2.1. OmcZs sequence expressed in this work. It contains only the soluble portion of the full-length protein with the transmembrane helical region replaced by a signal peptide sequence for secretion (pink) followed by a 10X histidine tag. Heme binding motifs are shown in blue. A Gly-Ser linker between the tag and the protein sequence is shown in green. The black arrow indicates the site for cleavage of the signal peptide between two alanine residues.

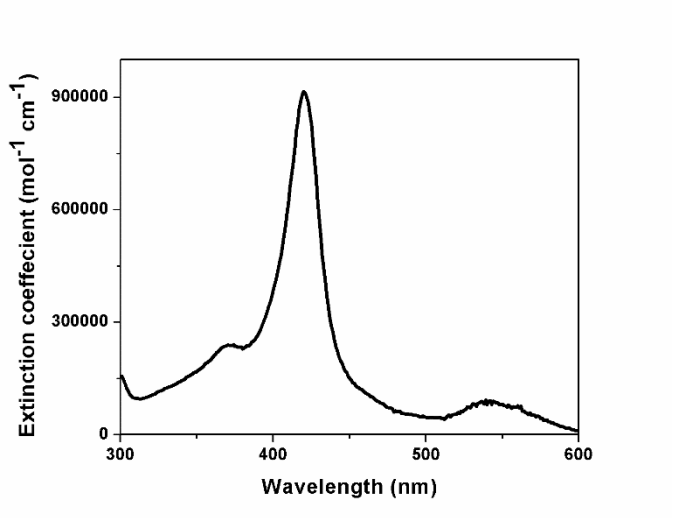

Figure 2.2. UV-visible absorbance spectrum of as-purified OmcZs. The absorbance maxima are at 408 nm and 537 nm.

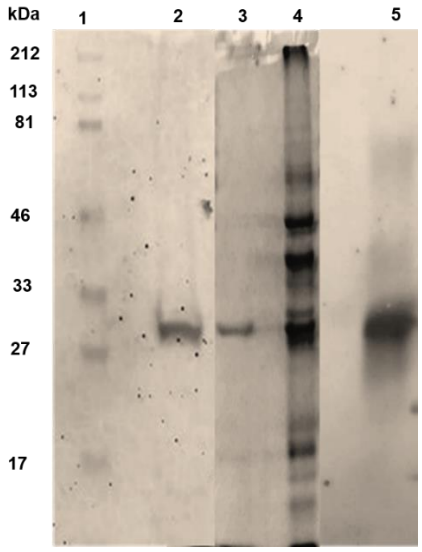

Figure 2.3. SDS-PAGE analysis of purified OmcZs and filtrate of the aerobic culture media. Lane 1: Protein standard (17 to 212 kDa); Lane 2: purified OmcZs visualized by heme staining; purified OmcZs (Lane 3) and the aerobic growth culture filtrate (Lane 4) visualized by Coomassie blue staining; Lane 5: Western blot analysis of purified OmcZs using anti-OmcZs antisera.

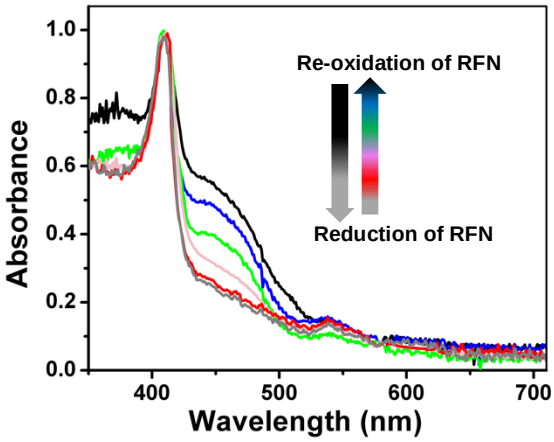

Figure 2.4. Reduction of riboflavin by OmcZs and re-oxidation of the flavin upon exposure to air. UV-vis absorption spectra from anaerobic *E. coli* (*pEC86 (ccm operon) + pJ411*(*omcZs*)) culture supernatant and 10 µM externally added, oxidized riboflavin (black line). The gray line shows the spectrum after 12 hrs of incubation. The experiment was then exposed to air to promote oxidation, and the spectra develop in the order red (30 min), pink (60 min), green (90 min), blue (120 min).

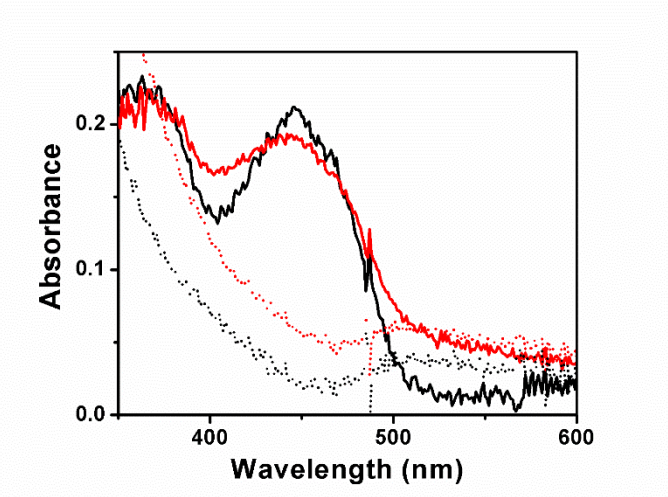

Figure 2.5. Riboflavin remains in the oxidized form in the absence of OmcZs. UV-vis absorption spectra from anaerobic *E. coli* cell culture supernatants from cells not expressing OmcZs in the absence (dotted lines) and presence (solid lines) of 10 µM externally added riboflavin after 12 hours of incubation. (Red lines) *E. coli* BL21 cells with pUC19 plasmid; (Black lines) BL21 cells expressing the *ccm* operon from the pEC86 plasmid.

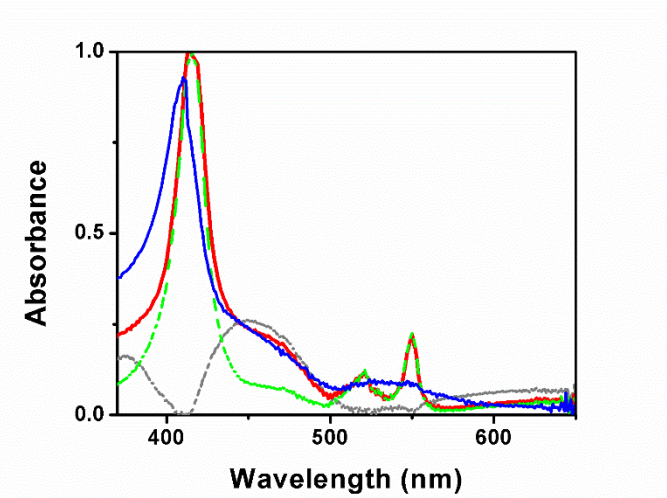

Figure 2.6. UV-vis spectra from oxidized riboflavin in the presence of reduced OmcZs. Oxidized flavin (gray, dotted line); Chemically reduced OmcZs before addition of 10 µM riboflavin (green, dotted line); chemically reduced OmcZs immediately after the addition of riboflavin (red, solid line). OmcZs in the presence of riboflavin after 30 min of incubation (blue, solid line).

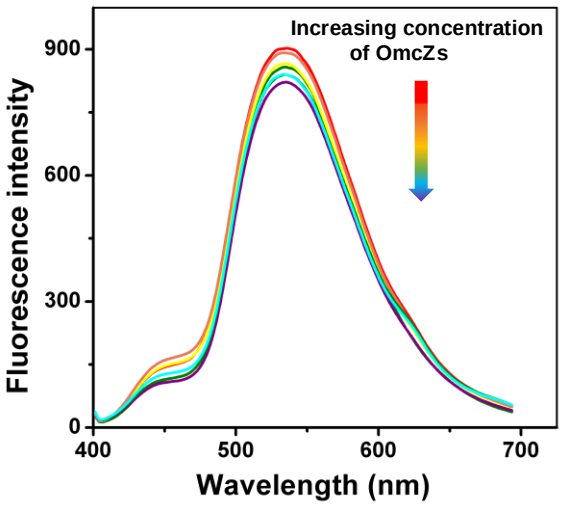

Figure 2.7. Quenching of the fluorescence from 10 µM riboflavin by OmcZs. Fluorescence emission spectra of a solution containing 10 µM riboflavin in the presence of OmcZs. The arrow shows the change in colors of the spectra corresponding to increasing concentrations of OmcZs. Spectra are shown for the following concentrations of OmcZs: 0, 5, 10, 15, 20, and 30 µM.

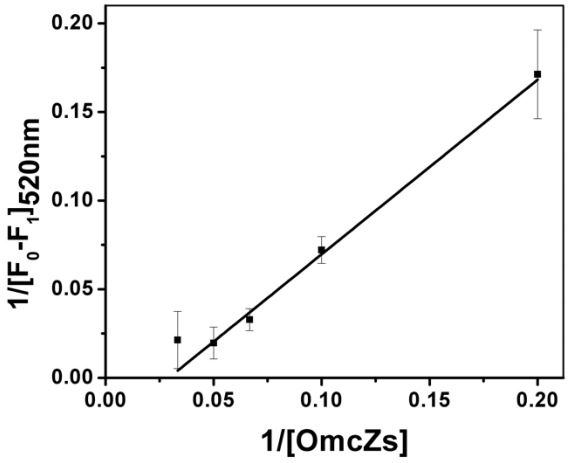

Figure 2.8. Benesi-Hildrebrand plot of fluorescence quenching of riboflavin by OmcZs. Fluorescence was measured at 520 nm following excitation at 450 nm over a variety of concentrations of OmcZs (oxidized). The line of best fit (solid black line) with a correlation coefficient (R^2) of 0.989 was used to calculate the average binding constant (K_d) of 34 µM. Error bars represent one standard deviation from the mean of three independent experiments.

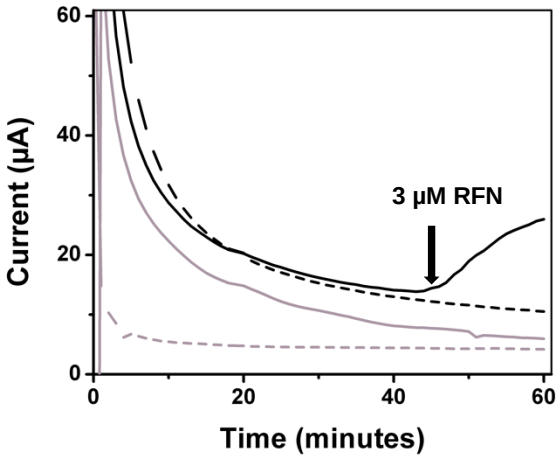

Figure 2.9. Presence of OmcZs and riboflavin significantly increases current production by *E. coli* cells. Current production in electrochemical reactors with a carbon cloth working electrode poised at 0.4 V vs SHE. Other conditions are defined in the methods. Dotted grey line is the current produced by an *E. coli* culture expressing the (pEC86-*ccm*), in the presence of 5 µM riboflavin. Solid gray line is the current production by an *E. coli* culture expressing both (pEC86-*ccm*) and (pJ411-*omcZs)*, in the absence of riboflavin. Dotted black line is the current production by *E. coli* culture expressing both the *ccm* operon (pEC86-*ccm*) and (pJ411-*omcZs)* in the presence of 5 µM riboflavin. Solid black line is the current production by by *E. coli* culture expressing both (pEC86-*ccm*) and (pJ411-*omcZs)* in the presence of 5 µM riboflavin. The spike in the current observed by the addition of 3 µM riboflavin after 45 min is represented by the solid black arrow.

1.6 References

1. Richter, K., Schicklberger, M. and Gescher, J. Dissimilatory Reduction of Extracellular Electron Acceptors in Anaerobic Respiration. *Appl. Environ. Microbiol.* **78**, 913–921 (2012).

2. Rev, A. and Lovley, D. R. Dissimilatory metal reduction. *Annu. Rev. Microbiol. 47.1 263-290.* **47(1**) 263–290 (1993).

3. Nealson, K. H., Belz, A. and McKee. B. Breathing metals as a way of life: Geobiology in action. *Antonie Van Leeuwenhoek* **81**, 215–222 (2002).

4. Liu, H., Ramnarayanan, R. and Logan, B.E., Production of Electricity during Wastewater Treatment Using a Single Chamber Microbial Fuel Cell, *Environ. Sci. Tech.* **38**, 2281–2285 (2004).

5. Lovley, D.R., Phillips, E.J., Gorby, Y.A. and Landa, E.R. Microbial reduction of uranium. *Nature* **350**, 413 (1991).

6. Rabaey, K. and Rozendal, R. A. Microbial electrosynthesis - Revisiting the electrical route for microbial production. *Nat. Rev. Microbiol.* **8**, 706–716 (2010).

7. Shi, L., Richardson, D.J., Wang, Z., Kerisit, S.N., Rosso, K.M., Zachara, J.M. and Fredrickson, J. K. The roles of outer membrane cytochromes of *Shewanella* and *Geobacter* in extracellular electron transfer. *Environ. Microbiol. Rep.* **1**, 220–227 (2009).

8. Hartshorne, R.S., Reardon, C.L., Ross, D., Nuester, J., Clarke, T.A., Gates, A.J., Mills, P.C., Fredrickson, J.K., Zachara, J.M., Shi, L. and Beliaev, A.S., Characterization of an electron conduit between bacteria and the extracellular environment. *Proc. Natl. Acad. Sci.U.S.A.* **106**, 22169–22174 (2009).

9. Myers, C.R. and Myers, J.M., Localization of Cytochromes to the Outer Membrane of Anaerobically Grown *Shewanella putrefaciens* MR-1. *J. Bacteriol.* **174**, 3429–3438 (1992).

10. Myers, J. M. and Myers, C. R. Role for outer membrane cytochromes OmcA and OmcB of *Shewanella putrefaciens* MR-1 in reduction of manganese dioxide. *Appl. Environ. Microbiol.* **67**, 260–269 (2001).

11. Myers, C. R. and Myers, J. M. Cell surface exposure of the outer membrane cytochromes of *Shewanella oneidensis* MR-1. *Lett. Appl. Microbiol.* **37**, 254–258 (2003).

12. Pirbadian, S., Barchinger, S.E., Leung, K.M., Byun, H.S., Jangir, Y., Bouhenni,

R.A., Reed, S.B., Romine, M.F., Saffarini, D.A., Shi, L. and Gorby, Y. A. *Shewanella oneidensis* MR-1 nanowires are outer membrane and periplasmic extensions of the extracellular electron transport components. *Proc. Natl. Acad. Sci. U.S.A.* **111**, 12883–12888 (2014).

13. Gorby, Y.A., Yanina, S., McLean, J.S., Rosso, K.M., Moyles, D., Dohnalkova, A., Beveridge, T.J., Chang, I.S., Kim, B.H., Kim, K.S. and Culley, D. E. Electrically conductive bacterial nanowires produced by *Shewanella oneidensis* strain MR-1 and other microorganisms. *Proc. Natl. Acad. Sci.U.S.A* **103**, 11358–11363 (2006).

14. Marsili, E., Baron, D.B., Shikhare, I.D., Coursolle, D., Gralnick, J.A. and Bond, D. R. *Shewanella* secretes flavins that mediate extracellular electron transfer. *Proc. Natl. Acad. Sci.U.S.A.* **105**, 3968–3973 (2008).

15. Von Canstein, H., Ogawa, J., Shimizu, S. and Lloyd, J.R., Secretion of flavins by *Shewanella* species and their role in extracellular electron transfer. *Appl. Environ. Microbiol.* **74**, 615–623 (2008).

16. Yang, Y., Ding, Y., Hu, Y., Cao, B., Rice, S.A., Kjelleberg, S. and Song, H., Enhancing Bidirectional Electron Transfer of *Shewanella oneidensis* by a Synthetic Flavin Pathway. *ACS Synth. Biol.* **4**, 815–823 (2015).

17. Watanabe, K., Manefield, M., Lee, M. and Kouzuma, A. Electron shuttles in biotechnology. *Curr. Opin. Biotechnol.* **20**, 633–641 (2009).

18. Hernandez, M. E. and Newman, D. K. Extracellular electron transfer. *Cell. Mol. Life Sci.* **58**, 1562–1571 (2001).

19. Glasser, N.R., Saunders, S.H. and Newman, D.K. The colorful world of extracellular electron shuttles. *Annu. Rev. Microbiol.* **71**, 731–751 (2017).

20. Kotloski, N. J. and Gralnick, J. A. Flavin Electron Shuttles Dominate Extracellular Electron Transfer by *Shewanella oneidensis*. *MBio* **4**, 10–13 (2013).

21. Brutinel, E. D. and Gralnick, J. A. Shuttling happens: Soluble flavin mediators of extracellular electron transfer in *Shewanella*. *Appl. Microbiol. Biotechnol.* **93**, 41–48 (2012).

22. Saffarini, D., Brockman, K., Beliav, A., Bouhenni, R. and Shirodkar, S. *Shewanella oneidensis* and extracellular electron transfer to metal oxides. in *Bacteria-Metal Interactions.* 21-40 (2015).

23. Okamoto, A., Saito, K., Inoue, K., Nealson, K.H., Hashimoto, K. and Nakamura,

R., Uptake of self-secreted flavins as bound cofactors for extracellular electron transfer in *Geobacter* species. *Energy Environ. Sci.* **7**, 1357–1361 (2014).

24. Xu, S., Jangir, Y. and El-Naggar, M. Y. Disentangling the roles of free and cytochrome-bound flavins in extracellular electron transport from *Shewanella oneidensis* MR-1. *Electrochim. Acta* **198**, 49–55 (2016).

25. Tokunou, Y., Hashimoto, K. and Okamoto, A. Acceleration of Extracellular Electron Transfer by Alternative Redox-Active Molecules to Riboflavin for Outer-Membrane Cytochrome *c* of *Shewanella oneidensis* MR-1. *J. Phys. Chem. C* **120**, 16168–16173 (2016).

26. Shi, L., Squier, T. C., Zachara, J. M. and Fredrickson, J. K. Respiration of metal (hydr)oxides by *Shewanella* and *Geobacter*: A key role for multihaem *c*-type cytochromes. *Mol. Microbiol.* **65**, 12–20 (2007).

27. Nevin, K.P., Kim, B.C., Glaven, R.H., Johnson, J.P., Woodard, T.L., Methé, B.A., DiDonato Jr, R.J., Covalla, S.F., Franks, A.E., Liu, A. and Lovley, D. Anode biofilm transcriptomics reveals outer surface components essential for high density current production in *Geobacter sulfurreducens* Fuel Cells. *PLoS One* **4(5)**, 5628 (2009).

28. Richter, H., Nevin, K.P., Jia, H., Lowy, D.A., Lovley, D.R. and Tender, L.M., Cyclic voltammetry of biofilms of wild type and mutant *Geobacter sulfurreducens* on fuel cell anodes indicates possible roles of OmcB, OmcZ, type IV pili, and protons in extracellular electron transfer. *Energy Environ. Sci.* **2**, 506–516 (2009).

29. Inoue, K., Qian, X., Morgado, L., Kim, B.C., Mester, T., Izallalen, M., Salgueiro, C.A. and Lovley, D.R..Purification and characterization of OmcZ, an outer-surface, octaheme *c*-type cytochrome essential for optimal current production by *Geobacter sulfurreducens*. *Appl. Environ. Microbiol.* **76**, 3999–4007 (2010).

30. Park, I. and Kim, B.C. Homologous overexpression of *omcZ*, a gene for an outer surface *c*-type cytochrome of *Geobacter sulfurreducens* by single-step gene replacement. *Biotechnol*, **33**(10), 2043 (2011).

31. Francis Jr, R.T. and Becker, R.R., Specific indication of hemoproteins in polyacrylamide gels using a double-staining process. *Anal. Biochem.* **136**, 509–514 (1984).

32. Hayashita, T., Taniguchi, S., Tanamura, Y., Uchida, T., Nishizawa, S., Teramae, N., Jin, Y.S., Lee, J.C. and Bartsch, R.A.,A dibenzo-16-crown-5 fluoroionophore for selective emission ratio sensing of Na^+ in basic aqueous dioxane solution. *J. Chem. Soc. Perkin Trans. 2* 1003–1006 (2002).

33. Pechsrichuang, P., Songsiriritthigul, C., Haltrich, D., Roytrakul, S., Namvijtr, P., Bonaparte, N. and Yamabhai, M. OmpA signal peptide leads to heterogenous secretion of *B. subtilis* chitosanase enzyme from *E. coli* expression system. *Springerplus* **5**, 1200 (2016).

34. Thony-Meyer, L., Fischer, F., Kunzler, P., Ritz, D. and Hennecke, H. *Escherichia coli* genes required for cytochrome *c* maturation. *J. Bacteriol.* **177**, 4321–4326 (1995).

35. Okamoto, A., Hashimoto, K., Nealson, K. H. and Nakamura, R. Rate enhancement of bacterial extracellular electron transport involves bound flavin semiquinones. *Proc. Natl. Acad. Sci. U. S. A.* **110**(19), 7856–61 (2013).

36. Macheroux, P. UV-visible Spectroscopy as a Tool to Study Flavoproteins. *Humana Press* **131**, 1–7 (1999).

37. Weber, G. Fluorescence of riboflavin and flavin-adenine dinucleotide. *Biochem. J.* **47**, 114 (1950).

38. Smith, J.A., Tremblay, P.L., Shrestha, P.M., Snoeyenbos-West, O.L., Franks, A.E., Nevin, K.P. and Lovley, D.R. Going Wireless: Fe(III) Oxide Reduction without Pili by *Geobacter sulfurreducens* Strain JS-1. *Appl. Environ. Microbiol.* **80**, 4331–4340 (2014).

39. Edwards, M.J., White, G.F., Norman, M., Tome-Fernandez, A., Ainsworth, E., Shi, L., Fredrickson, J.K., Zachara, J.M., Butt, J.N., Richardson, D.J. and Clarke, T.A. Redox Linked Flavin Sites in Extracellular Decaheme Proteins Involved in Microbe-Mineral Electron Transfer. *Sci. Rep.* **5**, 11677 (2015).

40. Paquete, C.M., Fonseca, B.M., Cruz, D.R., Pereira, T.M., Pacheco, I., Soares, C.M. and Louro, R.O., Exploring the molecular mechanisms of electron shuttling across the microbe/metal space. *Front.microbiol*, 5, 318 (2014).

41. Babanova, S., Matanovic, I., Cornejo, J., Bretschger, O., Nealson, K. and Atanassov, P., Outer membrane cytochromes/flavin interactions in *Shewanella* spp.—A molecular perspective. *Biointerphases*, **12**(2),021004 (2017).

42. Schuergers, N., Werlang, C., Ajo-Franklin, C.M. and Boghossian, A.A. A synthetic biology approach to engineering living photovoltaics. *Energ Environ Sci*, **10**(5),1102-1115 (2017).

43. TerAvest, M.A. and Ajo-Franklin, C.M., Transforming exoelectrogens for biotechnology using synthetic biology. *Biotechnol. Bioeng*, **113**(4), 687-697 (2016).

44. Tang, H.Y., Holmes, D.E., Ueki, T., Palacios, P.A. and Lovley, D.R., Iron Corrosion via Direct Metal-Microbe Electron Transfer. *Mbio*, **10**(3), e00303-19 (2019).

45. Li, F., Wang, L., Liu, C., Wu, D. and Song, H., Engineering exoelectrogens by synthetic biology strategies. *Curr. Opin. Echem*, **10**, 37-45 (2018).

46. Glaven, Sarah M. Bioelectrochemical systems and synthetic biology: more power, more products. *Microbiol. Biotechnol.* **12**, 819-823 (2019).

47. Jensen, H.M., Albers, A.E., Malley, K.R., Londer, Y.Y., Cohen, B.E., Helms, B.A., Weigele, P., Groves, J.T. and Ajo-Franklin, C.M. Engineering of a synthetic electron conduit in living cells. *Proc. Natl. Acad. Sci. U. S. A.* **107**, 19213–19218 (2010).

48. Jensen, H. M., TerAvest, M. A., Kokish, M. G. and Ajo-Franklin, C. M. CymA and Exogenous Flavins Improve Extracellular Electron Transfer and Couple It to Cell Growth in Mtr-Expressing *Escherichia coli*. *ACS Synth. Biol.* **5**, 679–688 (2016).

49. Mehta, T., Coppi, M. V., Childers, S. E. and Lovley, D. R. Outer membrane *c*-type cytochromes required for Fe(III) and Mn(IV) oxide reduction in *Geobacter sulfurreducens*. *Appl. Environ. Microbiol.* **71**, 8634–8641 (2005).

50. Yanisch-Perron, C., Vieira, J. and Messing, J., Improved M13 phage cloning vectors and host strains: nucleotide sequence of the M13mp18 and pUC19 vectors. *Gene* **33**, 103–119 (1985).

51. Yanisch-Perron, C.,Vieira, J. and Messing, J. Overproduction of the *Bradyrhizobium japonicum c*-Type Cytochrome Subunits of the cbb_3 Oxidase in *Escherichia coli*. *Biochem. Biophys. Res. Commun.* **251**, 744–747 (1998).

52. Studier, F. W. and Moffat, B. A. Selective expression of cloned genes directed by T7 RNA polymerase. *J. Mol. Biol.* **189**, 113–130 (1986).

Chapter 3

Pili do not play a significant role in the extracellular electron transfer by *Synechocystis PCC 6803*

Miyuki A Thirumurthy[1], Angelo Cereda[1], Andrew Hitchcock[2], John Heap[2], Jiawei Liu[3], Marko Chavez[4], Mohamed Y. El-Naggar[4], Robert Ros[3], Thomas S. Bibby[2], and Anne K. Jones[1]

[1]School of Molecular Sciences, Arizona State University, Tempe, AZ, 85287, USA

[2]Ocean and Earth Sciences, University of Southampton, Southampton, S014 3ZH, United Kingdom

[3]Department of Physics, Arizona State University, Tempe, AZ, 85287, USA

[4]Department of Physics and Astronomy, University of Southern California, Los Angeles, CA, 90484, USA

3.1 Abstract

Although photosynthetic organisms like *Synechocystis* sp. PCC 6803 can generate photocurrent with possible applications in bioenergy and bioelectronics, the mechanisms and components of electron transfer from phototrophs to an external environment have not been explored in detail. *Synechocystis*, like anaerobic exogenic bacteria, has thick and thin type IV pili which have been hypothesized to play a role in extracellular electron transport. Herein, a mediatorless electrochemical setup is used to compare the electrogenic output of wild type *Synechocystis* and a variant in which a protein essential for production of all types of pili has been genetically deleted *(ΔpilD*). No differences in photocurrent, i.e. current in response to light, are detectable. Conductivity measurements of individual pili of wild type cells using conductive atomic force microscopy also show these structures are not conductive. These results suggest that pili are not an active component in the cyanobacterial extracellular electron transport probed here.

3.2 Introduction

Electron transfer and redox reactions form the foundation for energy transduction in biological systems.[1] Some microbes have the capacity to transfer electrons beyond their cell wall to extracellular acceptors,[2] a function that may be important in microbial ecology and has been exploited in bioelectronic applications. Although electron transfer between redox-active sites separated by less than 1.6 nm is well understood to occur via electron tunneling described by Marcus theory, little is known about the mechanisms of electron transfer over larger distances, i.e. nanometers to micrometers, observed in biological ecosystems.[3] Long-range electron transfer in various microbes happen using soluble redox mediators or by conductive bacterial nanowires or pili.[4,5–9] Furthermore, an understanding of this activity forms the foundation for development of microbial fuel cells and photobiological electrochemical systems, devices that employ microbes to generate electricity.[10,11]

Two distinct mechanisms have been hypothesized to account for extracellular electron transfer in anaerobic bacteria: utilization of a soluble, diffusing redox shuttles like flavins to transfer electrons from the cellular interior to the extracellular surface,[12,13] and direct interaction between a redox-active component on the cell surface and the extracellular target.[14] The latter has been proposed to proceed via extracellular appendages that have come to be known as bacterial nanowires.[15,16] The composition of these nanowires is hypothesized to vary between different organisms and is not limited to pili. Recent work by El-Naggar and coworkers has shown that the nanowires of

Shewanella oneidensis MR-1 are comprised of outer membrane vesicles enclosing periplasmic proteins.[17] On the other hand, Lovely and coworkers reported that the nanowires of electrogenic *Geobacter* sp. are conductive pili.[18] Additionally, recent work by Malvankar and coworkers has shown that *Geobacter sulfurreducens* produces cytochrome-rich bacterial nanowires which are different from type IV pili. However, details about the types of charge carriers and mechanisms of interfacial electron transport within conductive appendages remain unclear.

It was recently reported that *Synechocystis* PCC 6803, a non-nitrogen fixing cyanobacterium, produces robust photocurrents in a mediatorless photoelectrochemical cell.[19] *Synechocystis* cells are known to produce morphologically distinct thick and thin pili peritrichously arranged on the cell surface, which are required for gliding motility and natural transformation competency.[20] There is one report that *Synechocystis* produces conductive pilus structures when CO_2 is limiting,[15] that remains to be corroborated. The PilD protein is a bifunctional membrane bound leader peptidase/methylase that processes PilA precursors and N-methylates the amino acid at position 1 in the mature protein.[21] As well as processing type IV prepilins, PilD is required for the biogenesis of type II secretion system (T2SS) psuedopilins in bacteria where a second prepilin peptidase is absent.[21] A Δ*pilD* mutant in a motile strain of *Synechocytsis* has been reported to be non-piliated, non-motile, and recalcitrant to transformation.[20] To ascertain whether pili are important for exoelectrogenesis, in this work, a *pilD* (*slr1120*) deletion mutant was generated in *Synechocystis*. Herein, the rates of extracellular electron transfer by this

mutant are compared to those of wild type by comparing the photocurrent production in a bioelectrochemical cell. The activity of the wild type and *ΔpilD* cells are indistinguishable, suggesting pili do not play a role in extracellular electron transfer by *Synechocystis* under the conditions investigated. Additionally, conductive AFM measurements suggest that thick and thin pili are not conductive appendages.

3.3 Materials and Methods

3.3.1 Biological materials and growth conditions

A glucose-tolerant (GT) strain of *Synechocystis* sp. PCC 6803 (provided by Prof. Peter Nixon, Imperial College London) was used as the wild type (WT),[22] and a *pilD* deletion mutant was generated in this strain background. *Synechocystis* was cultured in BG11 (blue-green) media under photoautotrophic or photomixotrophic conditions. For photoautotrophic growth, 200 ml cultures contained within 250 ml flasks were sparged with sterile air at 30°C under a constant illumination of approximately 50 μmol photons m^{-2} s^{-1}. For photomixotrophic growth, 5 mM glucose was added to the medium. Growth was monitored by measurement of the optical density of the culture at 750 nm (OD_{750}).

3.3.2 Deletion of *pilD*

Three fragments consisting of 685 bp including upstream flanking sequence and the first 28 codons of *pilD* followed by 2 TAA stop codons; the chloramphenicol acetyl transferase (*cat*) gene from pACYC184 (New England Biolabs (UK) Ltd, Hertfordshire, UK); and 500 bp beginning with the 12^{th}-from-last codon of *pilD* followed by flanking

downstream DNA were amplified separately by PCR using primer pairs p9-p10, p11-p12 and p13-p14, respectively (Figure 3.1). These fragments were joined by splicing overlap extension PCR and the resulting construct was cloned into the *EcoR1* and *HindIII* sites of pUC19 (New England biolabs Ltd, Hertfordshire, UK) and confirmed to be correctly assembled by automated DNA sequencing. This plasmid was used to transform wild type *Synechocystis*, and transformants selected with increasing chloramphenicol concentration (2.5-25 μg/ml) were screened by polymerase chain reaction (PCR) to confirm complete segregation to homozygous deletion mutants (Figure 3.1).

3.3.3 Electrochemical measurements

Electrochemical measurements were made in a three-electrode cell with carbon cloth as working electrode as described previously by Cereda et al.[19]

3.3.4 Motility assays

Synechocystis WT and *ΔpilD* were photoautotrophically grown in liquid BG11 medium to final OD_{750} 1.5. An aliquot of culture (15-20 μl) was spotted on BG11 agar plates and exposed to unidirectional light of approximately 50 μmol photons m^{-2} s^{-1} for five days at room temperature. For growth on plates, BG11 was supplemented with 10 mM TES (N-[tris(hydroxymethyl)methyl]-2-aminoethanesulfonic acid), 0.4% (w/v) agar, 0.3% (w/v) sodium thiosulphate, and 5 mM glucose.

3.3.5 Atomic Force Microscopy imaging of wildtype and mutant cells (*ΔpilD*)

Synechocystis WT and *ΔpilD* cells grown photoautotrophically in liquid BG11 or on BG11 agar plates were collected, washed 3 times and resuspended in 1 ml deionized

water. Aliquots of 5µl were spotted onto a mica support and air dried. After drying, samples were imaged with AFM (Asylum Research, MFP 3D, Santa Barbara, CA) in tapping mode using Tap300Al-G probes (with 40 N/m force constant, 300 kHz resonant frequency). The images were processed using Gwyddion software.

3.3.6 Scanning Electron Microscopy (SEM) imaging

Samples was fixed in 50 mM sodium phosphate buffer (pH 7.2) with 2% glutaraldehyde for 30 min at room temperature and then washed three times in the same buffer for a total of 30 min. After a second fixation step for 30 min at room temperature in the same buffer plus 0.5% osmium tetroxide, samples were washed three times with deionized water. Samples were critical point dried with carbon dioxide (Balzers CPD020 unit), mounted on Aluminum specimen stubs, and coated with approximately 15 nm of gold-palladium (Technics Hummer-II sputter-coater). Sample analysis was performed with a JEOL JSM-6300 SEM operated at 15 kV, and images were acquired with an IXRF Systems digital scanning unit.

3.3.7 Electrical characterization of pili using conductive AFM

Glass coverslips (43 X 50 NO. 1 Thermo Scientific Gold Seal Cover Glass), coated with 5 nm Titanium and then 100 nm Gold via electron beam evaporation, were used as conductive substrates. The Au-coated coverslips were rinsed with acetone, isopropanol, ethanol, and deionized (DI) water and then dried with nitrogen prior to use. Cyanobacteria, *Synechocystis* sp. PCC 6803 cells were drop casted onto the clean conductive substrates, rinsed with sterile water, and then left to dry overnight. An Oxford

Instruments Asylum Research Cypher ES Atomic Force Microscope (AFM) was used to make all pili electrical measurements. Dried samples were affixed and electrically connected to AFM discs with silver paint (TED PELLA, Inc.). The sample discs were then wired to the AFM upon loading. Si probes, with a Ti/Ir (5/20) coating, a resonant frequency of 75 kHz (58-97), a spring constant of 2.8 N/m (1.4-5.8), and a tip radius of 28 +/- 10 nm were used (Oxford Instruments AFM probe Model: ASYELEC.01-R2).

Pili electrical characterization was performed using Oxford Instruments Asylum research Fast Current Mapping (FCM). To generate FCM images, a bias is held between the probe and substrate while, for each pixel, current and force are measured with respect to the vertical distance of consecutive probe approaches and retractions over the sample. Each approach is terminated when a user-defined force is met (a force setpoint) and each retraction is terminated when a user-defined distance is met (a force distance). A bias of 5.00 V was used. A force setpoint of 51.14 nN and a force distance of 650 nm was used in the large pili (height 4-8 nm) measurements. A force set point of 27.86 nN and a force distance of 750 nm was used in the small pili (height 2-4 nm) measurements.

3.4 Results

3.4.1 Construction, growth, and phenotype of *ΔpilD* strain

As shown in Figure 3.1, amplification of relevant inserts was used to confirm successful construction of a *ΔpilD* strain as described in the methods section. Following transformation with the *pilD* mutagenesis construct (see experimental procedures), a larger PCR product corresponding to the chloramphenicol deletion construct (lane 2) was

amplified from transformant template DNA using primer pair p15-p16, compared to that using wild type DNA as template (lane 1). As the difference in size is only ~100 bp, the absence of wild type specific PCR products using primers internal to the deleted portion of the gene (p17 or p18) was also used to confirm complete segregation (wild type bands in lanes 3 and 5 absent in Δ*pilD* in lanes 4 and 6). A PCR using a reverse primer (p12) specific to the *cat* gene confirmed the deletion construct had integrated at the *pilD* locus (lane 7).

The *ΔpilD* mutant displays an obvious growth phenotype; cells aggregate into small clumps visible to the naked eye when grown on agar plates or in liquid medium (Figure 3.2). A similar phenotype has previously been reported in a non-motile mutant lacking thick pili.[23] The phenotype was much less apparent when cultures were well mixed by air bubbling during photoautotrophic or photomixotrophic growth, and *ΔpilD* grew comparably to the WT under these conditions (Figure 3.3).

As a measure of the impact of the *ΔpilD* mutation on photosynthesis, the chlorophyll a content of the mutant strain and the wild type strain were compared. Within the error of the measurement, chlorophyll a content is not impacted by the *ΔpilD* mutation (Figure 3.4), suggesting that the photosynthetic capacity of the strain should be relatively like that of the wild type.

Type IV pili are involved in phototaxis,[20] and thus the *pilD* gene deletion should abolish cell motility. A cell motility assay was performed as described in the methods.

Figure 3.2 shows that WT moves from the original spot in response to light exposure but the *ΔpilD* cells are unaffected by the light, i.e. not capable of phototaxis.

3.4.2 Electrochemical properties of *ΔpilD* strain

The light-dependent, electron transfer capacity of the wild type and *pilD* mutant *Synechocystis* was probed by measuring the photocurrent produced when a potential of +240 mV vs. SHE was applied. This potential was chosen as it has been previous shown to be sufficiently oxidizing for the cells to transfer electrons to an external substrate.[19] As shown in Figure 3.5 when *ΔpilD* cells are applied to the working electrode of a photo-bioelectrochemical cell followed by a few minutes incubation at the desired electrochemical potential, photocurrent production can be measured (red light with peak λ=660 nm, maximum intensity 20 W m^{-2} [110 µmol photons m^{-2} s^{-1}]). The photocurrent produced by the *pilD* mutant is comparable to the photocurrent produced by wild type (Figure 3.5). Electrochemical measurements were made for cells grown under two different conditions: photoautotrophic and photomixotrophic. In both cases, the observed photocurrent for the two strains was the same within the error of the experiments). For the Δ*pilD* strain, photocurrent increases linearly (R^2= 0.9854) with cell density to a magnitude (88±15%) comparable to the wild type (100±12%). This shows that for both strains the electrical output is directly related to the concentration of *Synechocystis* cells present in the electrochemical cell (Figure 3.6). Furthermore, it has been demonstrated previously that interruption of this electron transfer by inhibition or removal of essential components such as Photosystem I result in a significant decrease in observed

photocurrent.[19] This means that the direct microbial cell to anode electron transfer measured in this study is independent of type IV pili.

3.4.3 Atomic Force Microscopy(AFM) imaging of WT and *ΔpilD* cells

To rule out the possibility that growing cells planktonically under rapidly mixed conditions negatively impacts pili formation and stability via shearing action, AFM images for wild type *Synechocystis* grown under the condition mentioned above were acquired. Hair-like structures that may be pili are observed with similar densities on the cell surfaces of wild type cells (Figure 3.7). To ensure that the imaged cells are as morphologically like those used in the electrochemical measurements, samples were extensively washed in deionized water before AFM analysis to remove contaminants and to simulate the pretreatment conditions used for the electrochemical analysis. This rigorous washing treatment does not appear to have negatively impacted pili stability. On the other hand, AFM images of *ΔpilD* cells does not show the same hair-like structures (Figure 3.8). Since all known types of pili formation have been inactivated by deletion of *pilD*, the distinct and sparse structures observed in a few Δ*pilD* samples are likely extracellular polysaccharide or membrane extensions instead of pili.

3.4.4 Scanning Electron Microscopy (SEM) imaging of *Synechocystis* cells

SEM was used to define the physical interaction between *Synechocystis* cells and the carbon electrode. SEM micrographs of both wild type and mutant cells confirm uniform adhesion of cells to the carbon cloth electrode surface. Note, sample preparation for SEM imaging can affect the total number of cells attached to the electrode and can

underestimate the actual coverage. Nonetheless, in all images, cells are in direct contact with the carbon cloth electrode. High resolution images from wild type cells clearly show pili present between the cells and the carbon substrate (Figure 3.9). However, high resolution images from the *ΔpilD* strain show a complete absence of any type of pili (Figure 3.10), suggesting some other mechanism for the physical interaction with the electrode surface.

3.4.5 Current measurement using conductive AFM

Fast Current Mapping was used to generate topographical and current map images simultaneously of *Synechocystis* sp. PCC 6803 pili overtop a Au-coated glass coverslip. The large and small pili clearly visible in the topographical images (Figure 3.11a, d) show near zero current readings along their lengths in the current map images (Figure 3.11b, e). Representative point measurements of current as a function of time during probe approach and retraction (Figure 3.11c, f) show pili current readings comparable to background values when the probe contacts the pili with the same force used to observe current readings from the Au substrate. Our results indicate, within the sensitivity of our instrumentation, that the large and small type *Synechocystis* sp. PCC 6803 pili are not conductive.

3.5 Discussion

Conductive pili, or ‘microbial nanowires’, have been hypothesized to be important for long-range electron transport by various microorganisms including *Geobacter sulfurreducens* and *Shewanella oneidensis*. However, in many cases,

experiments show mechanisms that do not involve pili are also operational. Gorby and coworkers reported that under CO_2 limitation, scanning tunnelling microscopy images show that *Synechocystis* produces conductive filaments.[15] Unfortunately, these results have never been reproduced and controversy exists as to whether the structures observed could be true type IV pilus assemblies. Lovely and coworkers have suggested the diameter of the filaments is too large for type IV pili.[24] Furthermore, it has been hypothesized that *Shewenella oneidensis* structures observed by Gorby and coworkers in in the same study are filamentous extracellular polysaccharide (EPS) that arise as an artifact of dehydration during sample preparation or imaging.[25] Finally, although appendages produced by *S. oneidensis* have been shown to be conductive,[15,16] mutagenesis showed pili are not required for extracellular electron transfer,[26] and secreted flavins, a redox-active, soluble shuttle molecule have been detected in cultures of *Shewanella*. Thus, the question of whether *Synechocystis* employ pili in extracellular electron transfer is currently unanswered.

There is a broad collection of sub strains of *Synechocystis* sp. PCC 6803 that are used in laboratory studies, all of which are derivatives of the Berkeley strain 6803. Numerous substrain-specific mutations exist,[27] resulting in phenotypic alterations such as differences in sensitivity to glucose, motility and phototaxis.[23] A non-motile glucose-tolerant (GT) strain of *Synechocystis* sp. PCC 6803[28] was used as the wild type in this study, and the *ΔpilD* deletion mutant was generated in this background. There is some controversy generally in the literature as to whether GT strains produce pili. The lack of

motility in GT strains is due to a frameshift mutation in the *spkA* (*sll1574*) gene, which in motile strains encodes a functional Ser/Thr protein kinase.[29] It has also been also found that a 1 bp insertion that results in a frameshift mutation in the *pilC* (*slr0162/3)* gene in the non-motile GT Kazusa strain used for the genome sequence was absent in motile strains, and suggested the lack of motility in the Kazusa strain could be a consequence of this.[20,30] However, other GT strains, including the one used in the lab of Wim Vermaas, contain an intact *pilC* gene.[27] Furthermore, these stains are naturally transformable, whereas the Kazusa strain is non-competent for transformation with exogenous DNA,[23] indicating only the Kazusa strain lacks pili. Indeed, despite a report that an unspecified GT strain of *Synechocystis* lacks pili,[25] this strain was paradoxically naturally transformable, and others have found GT strains display both pilus morphotypes. Therefore, the transformation-competent, wild type strain used in this study should be capable of making pili.

The results herein show that the strain which lacks the *pilD* gene fails to produce pili and nonetheless can produce a similar amount of current as the wild type *Synechocystis* sp. PCC 6803. A bioelectrochemical system was used to measure the photocurrent produced by the mutant and the wild type grown under photomixotrophic and photoautotrophic growth conditions. This system does not depend on biofilm growth and is a rapid method to measure photocurrent production. The photocurrent is proportional to the optical density of the cells present in the electrochemical setup indicating that the entire process is photosynthetically driven (Figure 3.6). Both the

strains used in this study have similar photosynthetic capacity as the chlorophyll content of the mutant strain matches that of the wild type cells. The photocurrents produced by both strains grown planktonically were completely light-dependent confirming that the electrochemical readout corresponds to the cellular physiology, and this method is suitable to study the mechanism of extracellular electron transport used by wild type and mutants.

Direct contact between the *Synechocystis* cells and the carbon cloth electrode is confirmed by high-resolution SEM pictures which also show the complete absence of pili in the *pilD* mutant cells does not affect the adhesion of the mutant cells to the carbon cloth electrode. It is worth noting, however, that photocurrents produced by cyanobacterial in this system are much lower than those reported for anode-respiring bacteria. There are two distinct possible explanations. First, *Synechocystis* may only be able to use direct contact for electron transfer as opposed to pili or electron shuttles. Second, the metabolic pathways of cyanobacteria and especially electron sinks may be more tightly controlled such that electrons do not need to "escape" into the environment. Further investigation is necessary to distinguish between these possibilities.

The present findings show for the first time that deletion of *pilD* does not alter photocurrent production, indicating cell to electrode electron transfer must be mediated by an alternative mechanism in *Synechocystis*. Furthermore, conductive AFM measurements used in this study confirm the lack of conductivity of both the thick and thin pili of *Synechocystis*. Additionally, there is no evidence of flavin secretion by

Synechocystis, and current production by wild type and *pilD* mutant cells does not increase in the presence of an externally added mediator like ferricyanide (personal communication, Thomas Bibby). This suggests that for extracellular electron transfer *Synechocystis* must be in direct contact with the electron acceptor. Identifying the components responsible for this electron transfer is an important next step in exploiting cyanobacterial extracellular electron transfer.

Figures

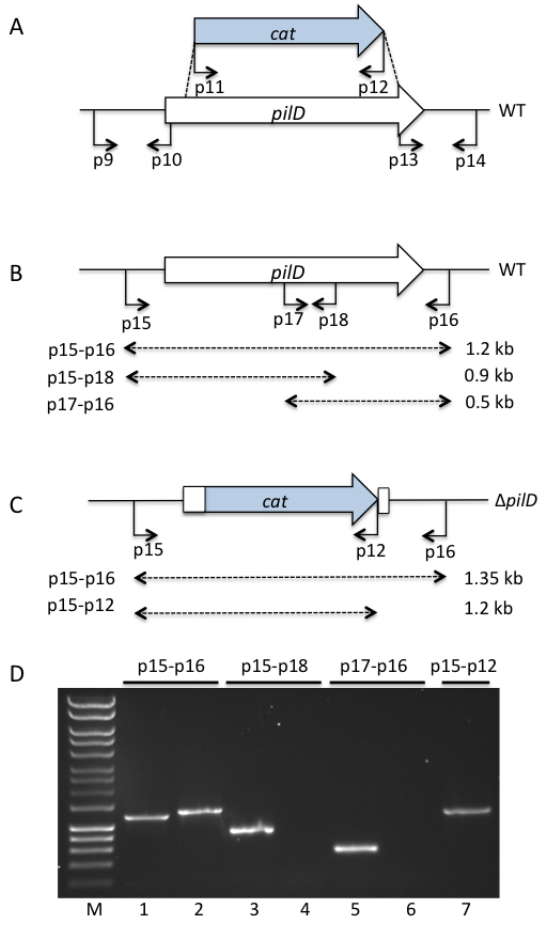

Figure 3.1. Scheme for deletion of *pilD*. (A) Strategy for replacement of *pilD* (*slr1120*) with the chloramphenicol acetyl transferase (*cat*) gene by splicing overlap extension PCR. Primer pairs p9-p10 or p13-p14 were used to amplify ~500-700 bp of the DNA upstream or downstream of the *pilD* locus; primers p10 and p13 contained sequence homology to the 5′ or 3′ end of the *cat* gene, respectively. The *cat* gene was amplified from pACYC184 using primers p11 and p12. When the three fragments were mixed in a subsequent PCR, single complementary strands annealed, and the full-length deletion construct was amplified using primers p9 and p14. This fragment was cloned into *Eco*R1/*Hind*III digested pUC19 and the plasmid was transformed into *Synechocytsis* sp. PCC 6803, with transformants segregated on chloramphenicol-containing plates. (B) The wild type *pilD* gene and flanking DNA. (C) The same region in Δ*pilD* transformants, in which the *cat* gene has replaced the majority of the *pilD* coding sequence. In (B) and (C) the positions of primer binding and the sizes of PCR products generated during

transformant screening are shown. (D) Agarose gel analysis of PCR amplicons confirming homozygous segregation of the deletion allele in Δ*pilD* (D). Lanes 1, 3 and 5 show PCR products amplified using template DNA from wild type, and lanes 2, 4, 6 and 7 from *ΔpilD*. The primer pair used in each reaction is indicated above the gel. Lane M = HyperLadder^{TM} I molecular weight marker (Bioline, UK). See text for further details.

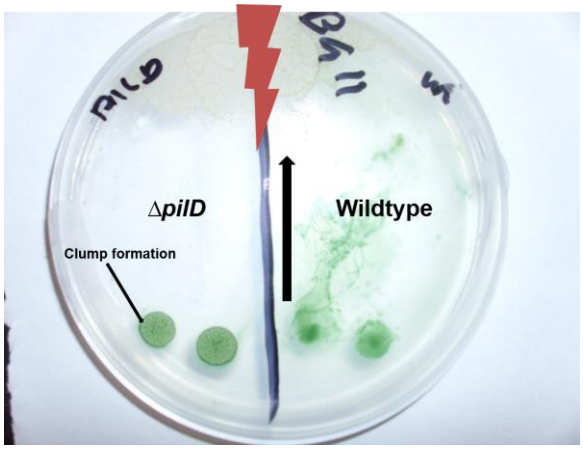

Figure 3.2. Photograph of *Synechocystis* directional motility assay. The black arrow shows the direction of cell movement towards light, wild type *Synechocystis* cells on the right and *ΔpilD* cells on the left.

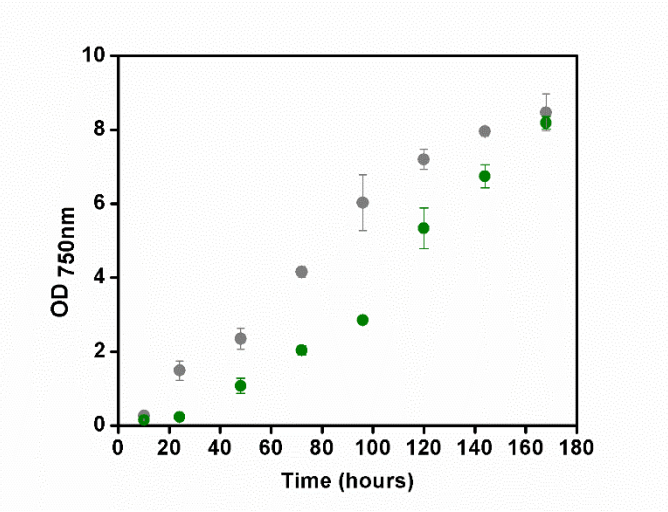

Figure 3.3. Growth curves for wild type and Δ*pilD Synechocystis.* The gray points show optical density at 750 nm of a wild type *Synechocystis* culture and the green points show optical density at 750 nm of a *ΔpilD* culture. Both the strains were grown under photoautotrophic conditions. Error bars represent one standard deviation from the mean of two independent experiments.

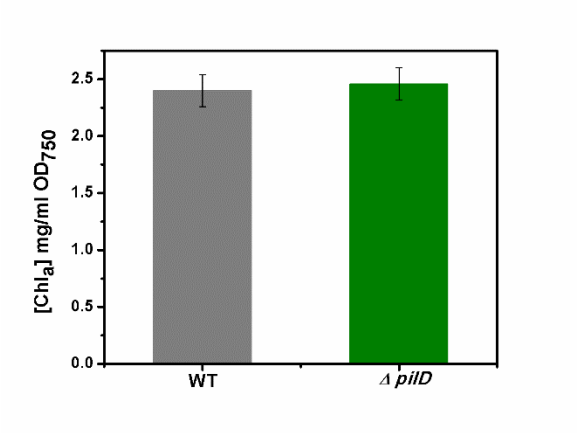

Figure 3.4. Chlorophyll content in wild type and *ΔpilD Synechocystis* cells. Error bars represent one standard deviation from the mean of three independent experiments.

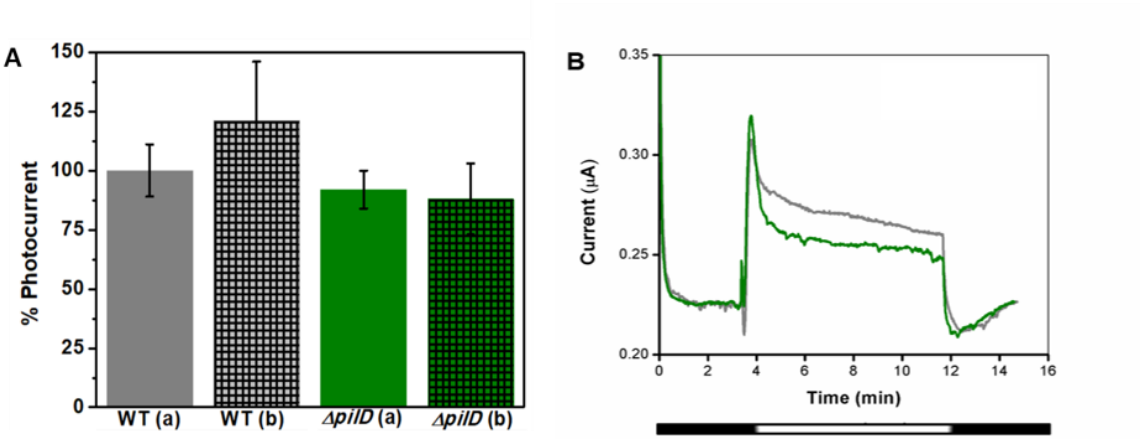

Figure 3.5. (A) Comparison of photocurrent produced by WT and *ΔpilD* mutant. The photocurrent is normalized to the cell density of the sample applied to the working electrode, and photocurrent produced by wild type (Photomixotrophic condition) is set at 100%. Strains were grown under photmixotrophic (a) or photoautotrophic (b) conditions (as described in experimental procedures) and harvested at a similar phase of growth (determined by OD_{750}). (B) Chronoamperograms showing photocurrent produced by *Synechocystis WT* cells and *ΔpilD* mutant cells immobilized on a carbon cloth electrode. The gray solid line shows a current-time trace for immobilized WT *Synechocystis* cells on a carbon cloth electrode. The current produced by *ΔpilD* mutant under light and dark conditions is shown as the green solid line. Current production in the dark was allowed to stabilize prior to illumination at which point a sudden increase in current is observed. After approximately 8 min, cells are returned to the dark and a sudden decrease in current is observed. The light and dark phases are shown schematically under the x-axis.

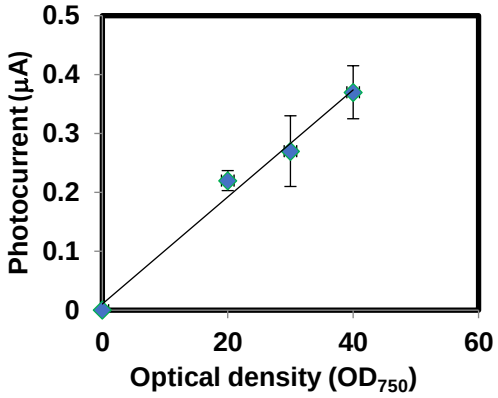

Figure 3.6. Observed photocurrent depends linearly on concentration of wild type *Synechocystis* cells present in the electrochemical experiments. The solid line is the line of best fit through the data with a correlation coefficient of $R^2 = 0.9854$. The error bars correspond to the uncertainty in both current and cell densities.

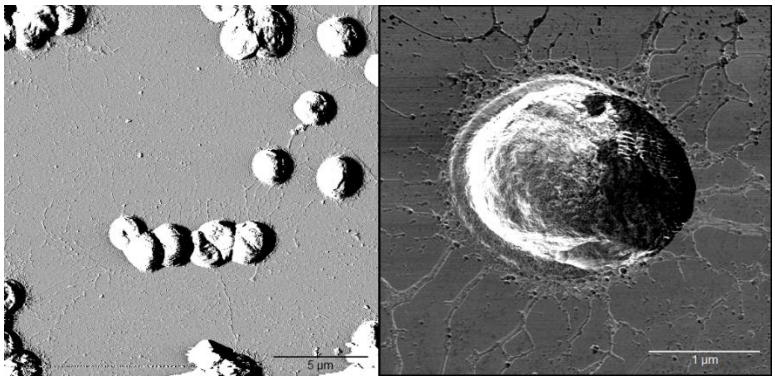

Figure 3.7. AFM images of wild type (planktonically grown) and magnified image of an individual cell with pili (right).

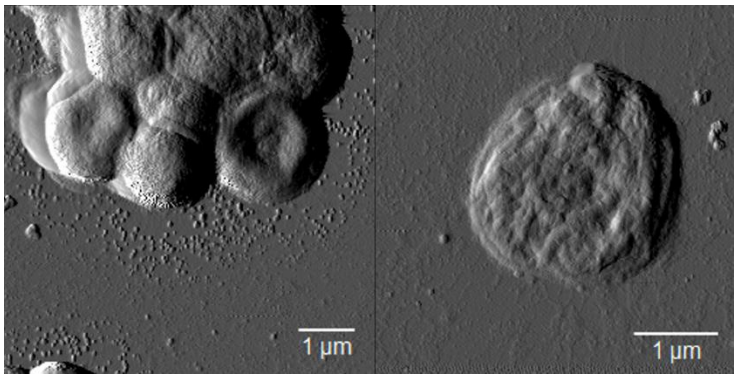

Figure 3.8. AFM image of planktonically grow cells of *ΔpilD* strain and a magnified image of a single *ΔpilD* cell (right).

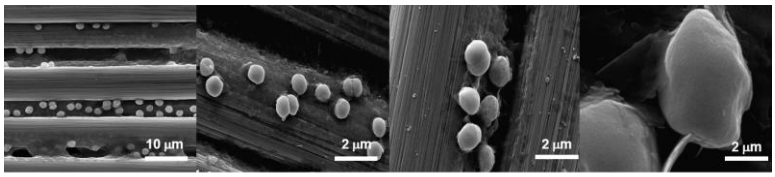

Figure 3.9. Scanning electron micrographs of wild type *Synechocystis* cells immobilized on a carbon cloth electrode at different magnifications (2500x, 6500x, 10000x, 50000x (left to right)).

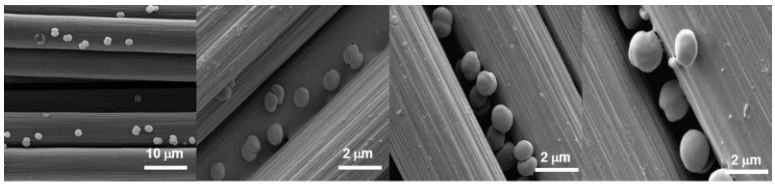

Figure 3.10. Scanning electron micrographs of *ΔpilD* mutant *Synechocystis* cells immobilized on a carbon cloth at different magnifications (2500x, 6500x, 10000x, 50000x (left to right)).

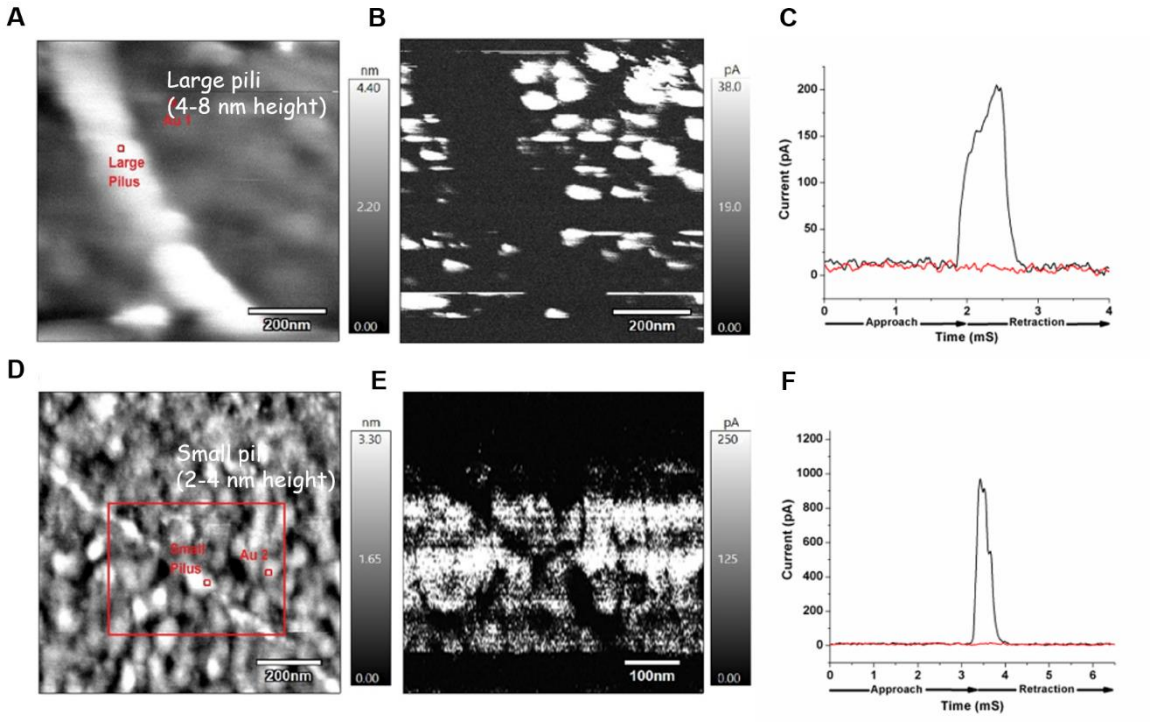

Figure 3.11. Topographical (a) and current map (b) images of a large *Synechocystis* sp. PCC 6803 pilus. (c) Current measured as a function of time during probe approach and retraction over the Au substrate (black) and over the large pilus (red). Topographical (d) and current map (e) images of a small PCC 6803 pilus. Note: (e) is a zoomed-in image of the area outlined by the red rectangle in (d). (f) Current measured as a function of time during probe approach and retraction over the Au substrate (black) and over the small pilus (red).

3.6 References

1. Marcus, R.A. and Sutin, N. Electron transfer in chemistry and biology. *Biochim. Biophys. Acta 811* **138**, 265–322 (1985).

2. Hernandez, M. E. and Newman, D. K. Extracellular electron transfer. *Cell. Mol. Life Sci.* **58**, 1562–1571 (2001).

3. Gray, Harry B., and J. R. W. Long-range electron transfer. *Proc. Natl. Acad. Sci.U.S.A* **102**, 3534–3539 (2005).

4. Reguera, G., McCarthy, K.D., Mehta, T., Nicoll, J.S., Tuominen, M.T. and Lovley, D. R. Extracellular electron transfer via microbial nanowires. *Nature* **435**, 1098–1101 (2005).

5. Brutinel, E. D. and Gralnick, J. A. Shuttling happens: Soluble flavin mediators of extracellular electron transfer in *Shewanella*. *Appl. Microbiol. Biotechnol.* **93**, 41–48 (2012).

6. Kotloski, N. J., Gralnick, J. A. and Newman, D. K. Flavin Electron Shuttles Dominate Extracellular Electron Transfer by *Shewanella oneidensis*. *MBio* **4**, 1–4 (2013).

7. Marsili, E., Baron, D.B., Shikhare, I.D., Coursolle, D., Gralnick, J.A. and Bond. D. R. *Shewanella* secretes flavins that mediate extracellular electron transfer. *Proc. Natl. Acad. Sci.U.S.A.* **105**, 3968–3973 (2008).

8. Yang, Yun, Yuanzhao Ding, Yidan Hu, Bin Cao, Scott A. Rice, Staffan Kjelleberg, and H. S. Enhancing Bidirectional Electron Transfer of *Shewanella oneidensis* by a Synthetic Flavin Pathway. *ACS Synth. Biol.* **4**, 815–823 (2015).

9. Kotloski, N. J.and Gralnick, J. A. Flavin Electron Shuttles Dominate Extracellular Electron Transfer by *Shewanella oneidensis*. *MBio* **4**, 10–13 (2013).

10. Kracke, F., Vassilev, I. and Krömer, J. O. Microbial electron transport and energy conservation - The foundation for optimizing bioelectrochemical systems. *Front. Microbiol.* **6**, 1–18 (2015).

11. Rabaey, K. and Verstraete, W. Microbial fuel cells: Novel biotechnology for energy generation. *Trends Biotechnol.* **23**, 291–298 (2005).

12. Watanabe, K., Manefield, M., Lee, M. and Kouzuma, A. Electron shuttles in biotechnology. *Curr. Opin. Biotechnol.* **20**, 633–641 (2009).

13. Glasser, N.R., Saunders, S.H. and Newman, D.K., The colorful world of extracellular electron shuttles. *Annu. Rev. Microbiol.* **71**, 731–751 (2017).

14. Shi, L., Richardson, D.J., Wang, Z., Kerisit, S.N., Rosso, K.M., Zachara, J.M. and Fredrickson, J. K. The roles of outer membrane cytochromes of *Shewanella* and *Geobacter* in extracellular electron transfer. *Environ. Microbiol. Rep.* **1**, 220–227 (2009).

15. Gorby, Y.A., Yanina, S., McLean, J.S., Rosso, K.M., Moyles, D., Dohnalkova, A., Beveridge, T.J., Chang, I.S., Kim, B.H., Kim, K.S. and Culley, D.E., Electrically conductive bacterial nanowires produced by *Shewanella oneidensis* strain MR-1 and other microorganisms. *Proc. Natl. Acad. Sci.U.S.A* **103**, 11358–11363 (2006).

16. El-Naggar, M.Y., Wanger, G., Leung, K.M., Yuzvinsky, T.D., Southam, G., Yang, J., Lau, W.M., Nealson, K.H. , Gorby, Y.A.Yang, J., Lau, W. M. and Nealson, K. H. Electrical transport along bacterial nanowires from *Shewanella oneidensis* MR-1. *Proc. Natl. Acad. Sci. U. S. A.* **107**, 18127–18131 (2010).

17. Pirbadian, S., Barchinger, S.E., Leung, K.M., Byun, H.S., Jangir, Y., Bouhenni, R.A., Reed, S.B., Romine, M.F., Saffarini, D.A., Shi, L. and Gorby, Y. A. *Shewanella oneidensis* MR-1 nanowires are outer membrane and periplasmic extensions of the extracellular electron transport components. *Proc. Natl. Acad. Sci.U.S.A***111**, 12883–12888 (2014).

18. Holmes, D. E., Dang, Y., Walker, D. J. F. and Lovley, D. R. The electrically conductive pili of *Geobacter* species are a recently evolved feature for extracellular electron transfer. *Microb. Genomics* **2**, 1–20 (2016).

19. Cereda, A., Hitchcock, A., Symes, M.D., Cronin, L., Bibby, T.S. and Jones, A. K. A bioelectrochemical approach to characterize extracellular electron transfer by *Synechocystis*. *PLoS One* **9**, e91484 (2014).

20. Bhaya, D., Bianco, N. R., Bryant, D. and Grossman, A. Type IV pilus biogenesis and motility in the cyanobacterium *Synechocystis* sp. PCC 6803. *Mol. Microbiol.* **37**, 941–951 (2000).

21. Stroml, M. S. and Lory, S. Structure-function and biogenesis of the type IV. *Fish. Sci.* **47**, 565–96 (1993).

22. Tichý, M., Bečková, M., Kopečná, J., Noda, J., Sobotka, R. and Komenda, J. Strain of *Synechocystis* PCC 6803 with Aberrant Assembly of Photosystem II Contains Tandem Duplication of a Large Chromosomal Region. *Front. Plant Sci.* **7**, 1–10 (2016).

23. Ikeuchi, M. and Tabata, S. *Synechocystis* sp. PCC 6803 – a useful tool in the

study of the genetics of cyanobacteria. *Photosynth. Res.* **70**(1) 73–83 (2001).

24. Lovley, D. R. Electromicrobiology. *Annu. Rev. Microbiol.* **66**, 391–409 (2012).

25. Tajima, N., Sato, S., Maruyama, Kaneko, Sasaki, N.V., Kurokawa, Ohta, H., Kanesaki, Y.U., Yoshikawa, H., Tabata, S. and Ikeuchi, M. Genomic Structure of the Cyanobacterium *Synechocystis* sp. PCC 6803 Strain GT-S. *DNA Res.* **18**, 393–399 (2011).

26. Bouhenni, R.A., Vora, G.J., Biffinger, J.C., Shirodkar, S., Brockman, K., Ray, R., Wu, P., Johnson, B.J., Biddle, E.M., Marshall, M.J. and Fitzgerald, L. A. The role of *Shewanella oneidensis* MR-1 outer surface structures in extracellular electron transfer. *Electroanalysis* **22**, 856–864 (2010).

27. Danika, T., Bjorn, V., Annegret, W., Salim, A. and Wolfgang, R. H. Microevolution in Cyanobacteria: Re-sequencing a Motile Substrain of *Synechocystis* sp PCC 6803. *DNA Res.* **19**, 435–448 (2012).

28. Williams, J. G. K. Construction of Specific Mutations in Photosystem II Photosynthetic Reaction Center by Genetic Engineering Methods in *Synechocystis* 6803. *Methods Enzymol.* **167**, 766–778 (1988).

29. Kamei, A., Yuasa, T., Geng, X. and Ikeuchi, M. Biochemical examination of the potential eukaryotic-type protein kinase genes in the complete genome of the unicellular cyanobacterium *Synechocystis* sp. PCC 6803. *DNA Res.* **9**, 71–78 (2002).

30. Kaneko, T., Sato, S., Kotani, H., Tanaka, A., Asamizu, E., Nakamura, Y., Miyajima, N., Hirosawa, M., Sugiura, M., Sasamoto, S. and Kimura, T. Sequence Analysis of the Genome of the Unicellular Cyanobacterium *Synechocystis* sp. Strain PCC6803. II. Sequence Determination of the Entire Genome and Assignment of Potential Protein-coding Regions. *DNA Res.* **3**, 185–209 (1996).

Chapter 4

Assembly of Redox Proteins into Supramolecular Nanowires

Miyuki A. Thirumurthy[1], Jiawei Liu[2], Shuai Xu[3], Robert Ros[2], Mohamed Y. El-Naggar[3]

and Anne K. Jones[1]

[1]School of Molecular Sciences, Arizona State University, Tempe, AZ, 85287, USA

[2]Department of Physics, Arizona State University, Tempe, AZ, 85287, USA

[3]Department of Physics and Astronomy, University of Southern California, Los Angeles, CA, 90484, USA

4.1 Abstract

Many dissimilatory metal-reducing bacteria such as *Geobacter* and *Shewanell*a can grow by transferring electrons from cellular metabolism to external substrates like metal oxides. Some of these microorganisms employ structures referred to a "bacterial nanowires", micron-scale, conductive, pilus-like appendages, in this process. Conductivity along these nanowires is believed to be sufficiently high for them to serve as the conduit for electron flux from metabolism, but little is known about the mechanisms of long-distance conductivity. Variously, electron transfer via stacked organic residues of a proteinaceous structure, hopping through structures of *c*-type cytochromes, and soluble redox mediators have all been hypothesized to play a role. This work reports a nanoscale supramolecular structure comprised of a self-assembling peptide and a modified *Shewanella c*-type cytochrome that can be used as a model to explore electron transfer. The nanofiber structure is formed via self-assembly of a peptide and a small tetraheme cytochrome (STC) tagged with a complementary peptide assembly domain. TEM and fluorescence microscopy show that the linear nanofibers contain protein. Furthermore, electrochemical studies show that the STC retains its native redox properties within the nanofiber. The resulting structure is a first-generation model to probe how assemblies of redox proteins within bacterial filaments may participate in long-range electron transfer.

4.2 Introduction

Long-range electron transfer is to essential to myriad bioenergetic and biosynthetic processes.[1] Electron transfer within complexes involved in oxidative phosphorylation and photosynthesis usually takes place between protein-bound metal ions separated by distances of approximately 9-13 Å.[2] There are also bioenergetic processes involving longer distance electron exchange between microorganisms and their environment.[3-4] For example, dissimilatory, metal-reducing bacteria can transfer electrons to metals or metalloids that serve as terminal electron acceptors.[5] The relative insolubility of these metal acceptors necessitates extracellular electron transfer (EET), *i.e.* transfer of electrons to the extracellular medium. [4,7] Despite the importance of this process in microbial metabolism, the mechanisms of EET and the components involved remain largely unknown.

Three distinct mechanisms have been hypothesized to be operative in EET to electrodes or interspecies electron transfer. First, EET can be facilitated by chemical mediators such as organic electron shuttles like flavins produced and secreted by cells or by natural compounds found in the extracellular environment. Second, extracellular electron shuttles and acceptors may be directly reduced by redox-active molecules like *c*-type cytochromes on the outer surface of cells.[6] Third, electrons can be transported through long, electrically conductive filaments called "microbial nanowires" that have been identified in metal reducers like *Geobacter* and *Shewanella* sp.[7,8] Studies have

suggested that the physiological roles and mechanisms of EET may be distinct in these two organisms or even in a single species exposed to various growth conditions.[9,10]

The mechanisms of electron transfer via bacterial nanowires have been studied predominantly in *Shewanella oneidensis* and *Geobacter sulfurreducens*.[6,11] Two competing mechanisms for conductivity along bacterial nanowires have been outlined in the literature: conductivity arising from electron hopping between highly concentrated cytochromes and metallic-like conductivity arising from π-π stacking along the bacterial structure. There is relative agreement that the conductivity of *Shewanella* nanowires arises from cytochromes. El-Naggar and coworkers have shown that the conductive filaments of *S. oneidensis* are cytochrome-rich extensions of the outer membrane and periplasm and are distinct from pili.[12-13] They have hypothesized that electron transfer along *S. oneidensis* nanowires occurs via electron hopping between cytochromes present at high concentration along the length of the filament. A Monte Carlo kinetic model has been constructed that suggests such a multi-step hopping model could account for the observed conductivity along *S. oneidensis* nanowires.[14] However, cytochrome-to-cytochrome electron hopping or tunneling has yet to be demonstrated in vivo. In contrast, there is less agreement regarding the mechanisms of conductivity along *Geobacter* nanowires. Lovley and coworkers have interpreted scanning tunneling microscopy results to indicate that the conductivity of nanowires in *Geobacter* is not a result of cytochromes. They argue that the spacing of cytochromes in *Geobacter* is not ideal for electron tunneling or hopping.[15] Instead, based on four types of experiments, they hypothesize that

the nanowires of *Geobacter* are "pili", and the entire structure exhibits metal-like conductivity arising from the overlapping of π orbitals of key aromatic amino acids. [16,17] First, electrostatic force microscopy has shown metallic-type conductivity of pili and the absence of electron hopping in *G. sulfurreducens.*[15] Second, the conductivity of pili does not decrease at lower temperatures as would be expected for an electron hopping mechanism.[9, 18] Third, genetically altered pili and flagella do not exhibit charge propagation like the wild type pili, suggesting that the components in the pilus may contribute to their conductivity.[19] Fourth, X-ray diffraction studies of pili have provided structural evidence for π-π stacking of aromatic amino acids in *Geobacter* pili and bolstered claims of metal-like conductivity.[20] On the other hand, recently Malvakar and coworkers published the cyro-electron microscopy structure of bacterial nanowires in *Geobacter* showing that the conductive appendages are not pili and have OmcS cytochrome monomers along their length.[21,22] These nanowires are slightly thicker than the pili and their conductivity is hypothesized to result from the presence of cytochromes.

Structurally defined and tunable models of conductive filaments could prove key in discriminating between the two competing hypotheses explaining conductivity. The goal of this project is to construct an artificial, one-dimensional array of *c*-type cytochromes and to characterize the electrical properties of this supramolecular assembly. The β-tail/Q11 system is used as a platform to assemble the multi-component nanofibers.[23] This tailorable system has the following features that make it ideal for construction of arrays of biologically active proteins. First, the protein of interest is

expressed in a soluble state. Second, proteins with diverse biophysical properties have been integrated into supra-molecular structures using this system. Third, the tag has slow fibrillation kinetics, which minimizes misfolding or aggregation because of the tag during microbial expression. The small tetraheme *c*-type cytochrome (STC) from *Shewanella oneidensis* has been chosen for incorporation into superstructures. This protein was selected because it has the lowest amino acid to heme ratio known for a cytochrome.[24] Additionally, STC has been extensively characterized structurally, spectroscopically, and electrochemically, making it an excellent candidate for a monomeric protein building block for nanostructure formation.

As shown in Figure 4.1, in this study, the "β-tail" peptide tag (MALKVELEKLKSELVVLHSELHKLKSEL) is expressed as a fusion to the *S. oneidensis* STC to facilitate assembly of the desired nanostructure. The results herein show that the fused peptide tag does not interfere in the production and purification of a soluble, properly folded, fusion *c*-type cytochrome protein. The β–tail peptide undergoes a structural change from α-helix to β-sheet upon binding with a short, de novo, fibrillizing peptide: Q11 (QQKFQFQFEQQ). The Q11 peptide self–assembles in aqueous salt solutions to form β-sheet nanofibers.[25] Also, the fibrillization of the β-tail peptide is not affected by large protein cargo. The array of *c*-type cytochromes is imaged using atomic force microscopy and transmission electron microscopy and determine the electrochemical properties using thin film electrochemistry. The benefits of this study include not only a better understanding of the mechanism of long-range electron transfer

in nature but also the development of new nanostructures for the emerging fields of electro-microbiology and bioelectronics.[16]

4.3 Methods

4.3.1 Construction of the plasmid with the *β–tail stc* gene (pJ411)

All strains and plasmids used in this project are defined in Table 4.1. The expression plasmid (pJ411) containing the gene coding for β–tail STC with the OmpA leader sequence upstream was produced by DNA 2.0. The leader sequence targets the associated protein to the periplasm for post-translational heme incorporation. The Nde1 and Xba1 restriction sites were incorporated into the flanking DNA and the entire construct is under the control of a T7 promoter. The pJ411 plasmid contains the gene coding for β–tail STC, the product of which confers kanamycin resistance on *E. coli*.

4.3.2 Media and growth conditions

E. coli strains were grown in Luria broth (LB) or on solid media containing 1% (w/v) agar. Antibiotics (kanamycin and chloramphenicol) were added to a final concentration of 50 μg mL^{-1} and 35 μg mL^{-1}.

4.3.3 Co-expression of pJ411 and pEC86

E. coli expression strain BL21 (DE3) was transformed via heat shock simultaneously with plasmids pEC86 and pJ411. The transformed cells were grown on agar plates containing both kanamycin and chloramphenicol to obtain single colonies containing both plasmids.

4.3.4 Protein expression and preparation of cell extract

To express β–tail STC, cultures were grown aerobically with shaking (250 rpm, 15 hrs, 37° C) from a 0.1% inoculum from glycerol stocks in a 1.5 L culture in a 2.0 L flask. Cells were induced in the log phase (OD_{600} ~ 0.5) using 0.4 μm isopropyl β-D-1-thiogalactopyranoside (IPTG) and subsequently grown overnight. Periplasmic extracts were obtained by adding lysozyme to a final concentration of 50 μg mL^{-1} in phosphate buffer (100 mM, 20% sucrose, pH 7.4). The resulting soluble extract was cleared by centrifugation (18,000 g, 30 min, at 4° C) to obtain a clear pink supernatant. The supernatant was dialyzed using Fisher brand dialysis tubing (6,000–8,000 NMWCO) against 100 mM potassium phosphate buffer (pH 7.4) overnight.

4.3.5 Protein purification

Protein purification was carried out using fast protein liquid chromatography (FPLC) on an AKTA prime plus using a diethylaminoethylene Sephadex A-25 (DEAE, 5.0 mL min^{-1}, 5.0 mL fractions, 5.08 cm x 7.62 cm; buffer A (100 mM potassium phosphate buffer, pH 7.4). β–tail STC was eluted from the column in 5 ml fractions using buffer B (100 mM potassium phosphate buffer, pH 7.4, 500 mM NaCl). Reddish-brown fractions were combined and concentrated using Amicon Ultra 0.5 filters. Concentrated fractions containing β–tail STC were further purified on Superdex 75 columns (GE Healthcare) equilibrated and eluted with 100 mM potassium phosphate buffer at pH 7.4. Protein concentrations were determined using a Bradford assay kit with bovine serum albumin as the standard (Bio-Rad).

4.3.6 Electrophoresis and gel staining for his-tagged protein and heme

Protein purity was determined using SDS-PAGE with a 12% BisTris-SDS–polyacrylamide gel visualized by Coomasie staining and Invision his-tag in gel staining. Gels were also stained for the presence of *c*-type hemes using the method described by Francis et al.[26]

4.3.7 Q11 Peptide synthesis and purification

A Protein Technologies PS3 automated peptide synthesizer was used to synthesize the peptide N-QQKFQFQFEQQ-C (Q11) on a 0.4 mmol scale using standard fluorenylmethoxycarbonyl (Fmoc) solid-phase synthesis using rink amide resin (0.156 mmol/g, 100-150 mesh). Activation was performed with 0.45 M HOBt/HBTU in DMF. Q11 was acetylated and cleaved from the resin as described previously.[25] Cleavage products were collected by centrifugation, dissolved in acetonitrile, lyophilized, and stored at -20 °C. Crude, lyophilized Q11 could be dissolved in acetonitrile only following addition of 0.1% Trifluoroacetic acid (TFA). The crude peptide was purified using a Waters 2996 HPLC system equipped with a photodiode array detector and a column, in a 0%-40% acetonitrile gradient. The identity of the peptide was confirmed by MALDI-TOF (linear mode at 25,000 V; laser repetition rate of 20 Hz) using saturated sinapinic acid as matrix.

4.3.8 Protein-peptide nanofiber preparation

Purified Q11 was dissolved in ultrapure water to a final concentration of 10 mM by continuously vortexing and sonicating for 10 min. Freshly prepared aqueous Q11

solutions were diluted tenfold with 1 X Phosphate buffer saline (PBS) containing β–tail STC at total protein concentration between 0.25 and 1.5 μM. The mixture was incubated overnight to assemble to nanofibers. Nanofibers were sedimented by centrifugation at 18,000 rpm for 5 min. Supernatant containing free protein and peptide was discarded. The pellet was resuspended in fresh PBS.

4.3.9 UV–Vis spectroscopy

UV–visible absorbance spectra were obtained with a Hewlett-Packard 8453 spectrophotometer using quartz cuvettes with a 1 cm path length.

4.3.10 Enzyme linked immunosorbent assay (ELISA)

A 100 μL aliquot of purified protein was added to the wells of a 96 well maxi-sorp ELISA plate and incubated for 2 hrs at room temperature. The excess liquid was decanted, and the wells were washed with ultrapure water repeatedly. Three different peptide antibodies which target different antigenic determinants of the β–tail STC (SELHKLKSELGSGGGGSGGGGSGGGGSA, ESGGCESCHKDGTP, or GKLSEMDAVHKPHD) were raised for imaging purposes. Aliquots of 100 μL of the three different primary detection peptide (anti-STC) antibodies were added to individual wells and they were incubated for an hour at room temperature. After repeated rinsing, 100 μL horse radish peroxide conjugate was added to each of the wells and incubated for 30 min. Chromogenic substrate was added to the wells after repeated washing and the plates were incubated in the dark for 30 min. Stop solution (100 μl of 0.16 M, sulfuric acid) was added to the wells, and a color change from blue to yellow was noted in most

wells. Absorbance of each well was read 550 nm using a Perkin Elmer 2104 multilabel reader.

4.3.11 Transmission Electron Microscopy (TEM)

TEM was used to visualize the (β–tail STC-Q11**)** integrated nanofibers. Nanofiber samples were absorbed onto a 200-mesh carbon grid which was later blocked with 2% acetylated bovine serum albumin (BSA) /0.1% cold water fish skin gelatin. After which, the carbon grids were placed onto a series of droplets containing monoclonal mouse anti-STC antibody (1:4) in 1 X phosphate buffer saline, goat anti-mouse Ig-G with 10 nm gold particles and 1% uranyl acetate in water. The carbon grids were washed three times after each step. Grids were analyzed with a Philips CM 12 TEM.

4.3.12 Fluorescence microscopy

A sample of integrated nanofibers was spotted on poly-lysine coated slides. Primary monoclonal mouse anti-STC antibody was added to the surface and incubated for 1 hr. Incubation was followed by repeated washing using PBS with 0.1% Tween 20 (PBST). Anti-mouse antibody conjugated with Alexa Fluoro 647 was added, and the slide was incubated for 20 min followed by washing with PBST and rinsing with PBS. The sample was the covered and sealed with a coverslip and imaged using the Leica TCS Leica TCS SP5 AOBS Spectral Confocal System.

4.3.13 Atomic force microscopy

Nanofiber solution (10 μl) was left to absorb over 60 min on a mica (1.5 cm x 1.5 cm, Ted Pella, Inc.) surface cleaved and the cleaned with ultrapure water. After

evaporating the liquid, samples were immediately AFM imaged (Asylum Reseach, MFP 3D, Santa Barbara, CA) in tapping mode using Tap300Al-G probes (with 40 N/m force constant, 300 kHz resonant frequency, Budget Sensors). Images were processed using Gwyddion software.

4.3.14 Circular dichroism

Circular dichroism was performed using a JASCO J-815 spectropolarimeter, using a quartz cuvette with a path length of 0.1 cm. CD spectra were recorded from 260 to 190 nm in 1 nm increments.

4.3.15 Electrochemistry

Electrochemical measurements were carried out in an anaerobic glovebox using an Autolab potentiostat in a three-electrode electrochemical cell with a 1.6 mm diameter gold electrode (99.95% purity) from BASi, as the working electrode. The reference and counter electrodes were Ag/AgCl and platinum, respectively. The reference electrode was encased within a glass sheath equipped with CoralPor frit (BASi, West Lafayette, IN) and filled with 3.5 M potassium chloride. Experiments were performed in 100 mM potassium phosphate buffer at pH 7.4. Solutions were purged with nitrogen to remove oxygen before experiments. Background capacitance was removed from voltammograms using Qsoas to obtain "baseline-corrected" versions.[27]

4.3.16 Electrochemical gating

Nanowire samples were drop cast onto gold interdigitated array electrodes (IDA) and dried in air for 4–12 hrs to complete dryness before measuring. The electrochemical

cell consists of the IDA as working electrode (both source and drain) (ALS Co., Ltd, Japan), an external Ag/AgCl reference electrode, and a platinum counter electrode. The IDA consists of 65 pairs of parallel gold "electrode arms" (each arm is 2 mm long x 2 μm wide). Electrochemical gating measurements were performed in PBS at pH 7.4. Gating was performed with 20 mV offset between source and drain, 1 mV s^{-1} scan rate, -600–300 mV potential range vs. Ag/AgCl. Copper wires were affixed to the terminal contact pads or each working electrode using silver paint (SPI Supplies, West Chester, PA) and the connections were sealed with epoxy (Gorilla Glue, Cincinnati, OH).

4.4 Results

4.4.1 Nanofiber design

As depicted schematically in Figure 4.1, the nanofibers constructed in this work are comprised of two components: a self-assembling peptide known as "Q11" that forms fibrils via self-assembly and a co-peptide, known as the "β-tail", that can be incorporated into the Q11 fiber structure and is appended as a tag to a redox protein. This system was selected largely because the β-tail transitions slowly from random coil to β-sheet with concomitant supramolecular structure formation. When using the β-tail as a tag in a protein construct, the slow fibrillization kinetics minimize protein aggregation or misfolding in *E.coli.* Furthermore, Q11 can be readily synthesized using solid-phase peptide synthesis.

The redox protein selected for this study is the small tetraheme cytochrome (STC) from *Shewanella oneidensis*.[24,28] It was selected for three main reasons. First, it has the

highest heme to amino acid ratio reported; this means that the distance electrons must travel "through protein" as opposed to through redox cofactors is minimal. Second, it is an easily expressed, soluble protein that has been well characterized spectroscopically and structurally. Third, its redox properties are well-characterized and include inter- and intra-molecular electron transfer.[24,28,29]

4.4.2 Protein design and purification

A gene encoding a modified STC for this project was generated commercially within an IPTG-inducible construct. The STC construct includes four distinct parts: a sequence encoding the OmpA signal peptide[30] to target the expressed protein to the periplasm of *E coli*; a sequence encoding the β-tail to promote supramolecular assemble; the structural gene for STC; and finally a sequence encoding a C-terminal his-tag linked to the structure sequence via a gly-ser linker (Figure 4.2). The resulting chimeric, β-tail STC has a total of 155 residues and a molecular weight of 16.45 kDa. Analysis of the deduced amino acid sequence using SignalP (http://www.cbs.dtu.dk/services/SignalP) predicts a cleavage following the OmpA sequence at a cleavage site between residues Ala26 and Met27. To facilitate expression of holo-protein in *E. coli*, cells were co-transformed with the plasmid encoding the STC construct as well as a plasmid encoding *ccmABCDEFGH*, the operon responsible for *c*-type cytochrome maturation in *E. coli*. Co-expression of these two plasmids leads to growth of pink colonies, but the cells are not colored if the maturation plasmid is omitted. This indicates the maturation genes are essential for holo-STC production.

Holo-β-tail STC was purified from *E. coli* periplasmic extracts as defined in the methods. Figure 4.3A shows that purified β-tail STC can be visualized at the appropriate molecular weight using Coomassie staining, staining for the presence of hemes, or staining in response to the his-tag. Furthermore, Figure 4.3B shows that β-tail STC has a UV-vis absorption spectrum with local maxima at 408 and 551 nm characteristic of an oxidized hemoprotein with an extinction coefficient of 103 mM^{-1} cm^{-1} $heme^{-1}$ at 408 nm and 24 mM^{-1} cm^{-1} $heme^{-1}$ at 551 nm. The purity assessed by the ratio of absorbance at 280 nm to the absorbance at 408 nm (Soret peak) ranged from 0.06 to 0.08 for this fusion protein with four hemes. Single heme proteins have 280 nm/Soret peak absorbance of 0.15 to 0.2. Typical yields of pure β-tail STC are 5.3 mg L^{-1}.

4.4.3 Synthesis, purification and self-assembly of Q11

Q11 was synthesized via solid-phase peptide synthesis and purified to greater than 90% by HPLC. The identity of the purified peptide was confirmed via MALDI-MS (Figure 4.4). Circular dichroism spectra show that Q11 transitions from a random coil to a β-sheet when incubated in phosphate buffered saline (Figure 4.5). This structural transformation can also be observed using TEM imaging which shows that the sheet structure is a fibril (Figure 4.6).

4.4.4 Nanofiber Assembly

To determine the optimal conditions for the integration of β–tail STC with Q11 to form nanofibers, protein and peptide were mixed using varying concentrations of protein in the range 0.5 μM to 1.5 μM and peptide in the range 1 mM to 5 mM. The quantity of

β–tail STC integrated into the fiber was estimated by measuring the concentration of protein in solution before and after nanofiber assembly. As shown in Figure 4.7, under static conditions, incubation results in formation of nanofibers that can be sedimented via centrifugation within a few hours of initial assembly. A Q11:β–tail STC ratio of 1000:1 results in formation of distinct nanofibers after 12 hrs of incubation (Figure 4.7). Other peptide to protein ratios were investigated but yield fibers less than 5 nm in length or clumps of short strands (data not shown).

4.4.5 Structural analysis

Structural analysis reveals that the dimensions of the Q11/β-tail STC nanofibers are comparable to naturally occurring nanowires in *Shewanella*. Naturally occurring nanowires in *Shewanella oneidensis* are ~20 nm in thickness and are 150 nm to 1 μm in length depending on the growth environment.[31] TEM shows that Q11/β-tail STC fibers have a length between 1 and 150 μm and a width in the range of 2-20 nm (Figure 4.8). Atomic force microscopy shows that the nanofibers are approximately 4 nm high. Nanofibers consisting of only Q11 as well as Q11 mixed with β-tail STC were imaged. The presence of STC does not have a significant effect on the observed nanofiber height.

Both immunogold and fluorescence labelling of β-tail STC were used to confirm its incorporation into the nanofibers and evaluate its distribution throughout the fiber. Nanofibers assembled in the presence of β–tail STC were labelled with primary peptide antibodies specific to two different sequences on the β-tail STC protein. The affinity of

these peptide antibodies for β-tail STC was confirmed using ELISA (Figure 4.9a). Secondary antibodies with gold nanoparticles were used to visualize the protein locations in individual nanofibers in TEM images. Images show localization of β–tail STC within Q11 nanofibers. Within a single fiber, the distance between the gold nanoparticles ranges from 1 to 50 nm (Figure 4.9b), showing the redox protein is trapped within the structure of the nanofiber and relatively evenly distributed throughout. However, an inherent limitation of immunogold labelling is that the gold particles are not exactly at the place where the primary antibody is bound, and the exact distance between the components in the micrograph cannot be determined. To overcome this limitation and provide complementary information regarding the distribution of protein, fluorescent antibody labelling was also used to determine the locations of proteins in nanofibers. Fluorescence images like that in Figure 4.10 show that β-tail STC is distributed throughout the entire fiber, providing independent confirmation of the results of TEM imaging.

4.4.6 Redox properties of the nanowires

To confirm that β-tail STC retains redox activity similar to STC when incorporated into nanofibers, assembled nanofibers were deposited on a gold electrode and interrogated electrochemically. A 10-15 μL aliquot of nanofiber suspension was dried on the surface of an electrode, and excess or weakly bound fibers were removed by rinsing with ultrapure water. Then the sample was imaged using AFM to confirm the presence of dense fibrils before electrochemical experiments (Figure 4.11).

For electrochemical measurements, nanofiber samples (10 to 15 μl) were drop cast on gold electrodes and allowed to dry in the glove box until a thin film of sample was seen on the surface. A thin film of the sample was successfully formed only on gold electrodes, and the sample did not adhere to indium tin oxide or glassy carbon electrodes. As shown in Figure 4.12, cyclic voltammograms feature reversible oxidation and reduction peaks centered at $E_{1/2}$ = -98 mV vs. SHE. The same reduction potential is reported for native STC.[24] The electrochemical signals obtained from β-tail STC(chimeric protein) and β-tail STC integrated into nanofibers are similar. The most significant difference is the peak widths. Isolated protein gives rise to signals with 90 mV width at half height. However, the half-height peak width of signals from protein embedded in nanofibers is larger at approximately 130 mV. There may be two reasons to explain the relatively broader peak width for signals from STC in nanofibers relative to isolated protein. First, within the nanofiber the STC monomers may be close enough to one another to introduce dispersion of the heme potentials as a result of electronic interactions. Second, the interactions of each STC with the electrode may be slightly different resulting in a dispersion of potentials that arises from difference in kinetics of electron transfer between the protein and the electrode. Although these explanations are distinct and one is thermodynamic whereas the other is kinetic, both mechanisms may play a role in practice in the observed peak broadening. No redox signal was observed in cyclic voltammograms obtained from Q11 fibers without β-tail STC dried on gold electrode (Figure 4.12).

Electrochemical gating experiments were performed to evaluate the conductivity along the length of individual nanofibers. Distinct electrochemical features were not observed in either the raw data or the processed gating results. Visual investigation of fibers dried on the IDA surface shows they peel away from the electrode surface and form sediments in the electrolytic solution. Variations in drying conditions did not enhance adhesion of the nanofibers to the IDA surface.

4.5 Discussion

The supramolecular structure described here is one of several recent examples of peptide or protein-based bioelectronic materials that have been inspired by EET and especially the "nanowires" of *Shewanella* and *Geobacter*.[32] Each of these structures has the potential to offer unique insights into mechanistic questions and to provide opportunities to design synthetic bioelectronic components more suited to applications than naturally occurring systems. This discussion considers the significance of the STC nanowire system created in this work in the context of these other materials.

Self-assembling peptides have been reported to form a range of diverse structures, and a number of groups have attempted use these as a platform to create bioelectronic materials either by incorporating aromatic amino acids into repeating structures or by introducing redox-active moieties. However, none of these structures have conductivity comparable to naturally occurring nanowires.[33,34] For example, ferrocene-tagged peptide nanowires have been described, but their conductivity ranges from the semi-conducting to the insulating range.[35,36] Similarly, Fry and coworkers have employed simple peptides

to scaffold heme binding and material formation. The heme environment in these materials has the advantage of being highly homogeneous with close contact between hemes, but measurements of bioelectronic properties have not been done.[37] Thus, it is unclear to what extent that system models electron transfer through microbial nanostructures. Finally, Ing and coworkers have reported construction of conductive nanofibers based on an α-helical peptide sequence from *Geobacter*.[38] They argue that the conductivity of this structure does not arise from redox-active cofactors or stacking of π amino acids but is instead related to the structural regularity and helical content. The physical details of such a hypothesis remain unclear.

There are relatively fewer examples of self-assembly of redox proteins into conductive materials, but three systems are relevant for comparison to our STC work. Altamura and coworkers have employed a prion domain to assemble a synthetic nanofiber of rubredoxin, an [FeS] protein.[39] The iron centers in this synthetic scaffold are 1 nm apart, and biofilms have conductivities comparable to *G. sulfurreducens*.[40] However, the conductivity of the individual nanofibers of rubredoxin was not reported, and the reported results are insufficient to demonstrate electron hopping within the nanowires. Kijihara and coworkers have constructed supramolecular assemblies based on self-assembly of a modified cytochrome b_{562}. They can assemble the cytochrome chains using a mixture of Zn and Fe porphyrins to demonstrate photoinduced charge separation and subsequence recombination on the seconds timescale.[41] Kinetic analysis suggests the observed charge separation is a single-step electron transfer reaction though and that

longer distance conductivity is not observed. Thus, this system is likely not yet a good model for long-range microbial electron transfer. Amdursky and coworkers have described hemin incorporation into bovine serum albumin mats resulting in a material with the highest measured conductance for a protein-based material and electron transport over cm length scales.[42] Measurements of AC impedance and DC current-voltage are consistent with charge transport through the material via electron hopping between adjacent hemins. However, it is also worth noting that the hemin environment is anticipated to be highly heterogeneous, and the cofactor, although relatively stable, is non-covalently associated with a non-native protein. Thus, while this material is particularly exciting for bioelectronic applications, it has limited relevance as a model for natural systems.

This work uses a strategy to produce β–sheet nanofibers which display redox-active cytochromes throughout their length and retain their biological activity. Since two components are involved in assemble, these fibers are less regularly ordered than the systems described above. That may make them more analogous to "bacterial nanowires" that are likely not rigid supramolecular assemblies. The Q11 peptide associates with β-tail STC to form stable nanofibers with a local concentration of cytochrome high enough to achieve good electrochemical signals using cyclic voltammetry. The native redox characteristics of the STC remain unaltered by the supramolecular assembly. Furthermore, transmission electron microscopy and fluorescence microscopy suggest a dense organization of cytochromes close enough for electron transfer through the length

of the nanofibers which could allow electron transfer through electron hopping mechanism. Further experiments will be necessary to test that hypothesis. Detection of STC in the nanofibers using three antibodies with distinct epitopes suggests that the STC may be very exposed in the nanofibers, highly mobile in the nanofibers, or heterogeneously organized in the nanofibers. Any one of these offers both advantages and disadvantages. For example, heterogeneous organization may decrease conductivity by introducing orientations in which the heme-to-heme distance is too large for efficient electron transfer. On the other hand, structural flexibility may be required for efficient electron transfer since it may allow small movements to bring hemes into appropriate contact.

To date, electrochemical gating experiments to evaluate conductivity along individual nanowires have not been successful with the synthetic nanowires created in this work because they do not adhere well to interdigitated array electrodes. Future work will test immobilization or encapsulation methods to avoid sample loss from electrode surfaces and pursue these measurements. Additionally, high surface area electrodes may be evaluated.

Finally, this system provides an excellent starting point for engineering functional nanofibers with tunable composition and can be used to test fundamental mechanisms of electron transport in biological systems as well as to develop bioelectronics components. Since both components can be expressed in soluble forms in vivo, it may be used as a

first step in development of synthetic “living electronics” that can be assembled in response to environmental stimuli.

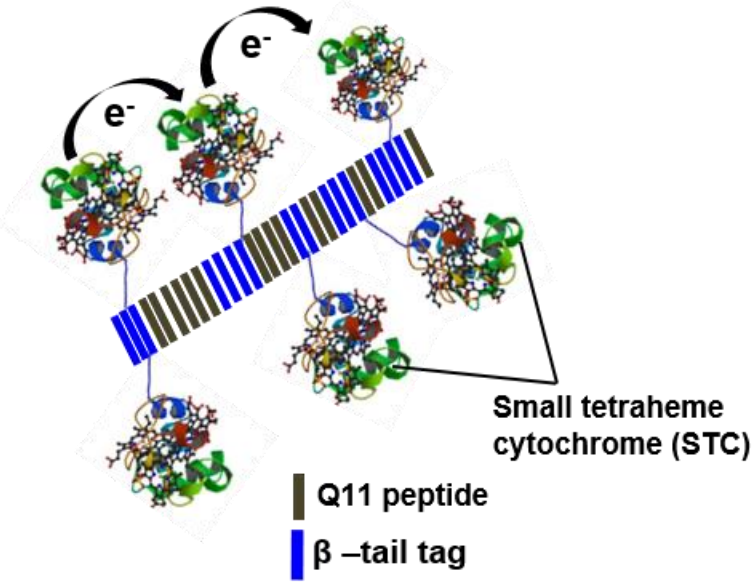

Figure 4.1. Schematic representation of the Q11/β-tail STC supramolecular assembly.

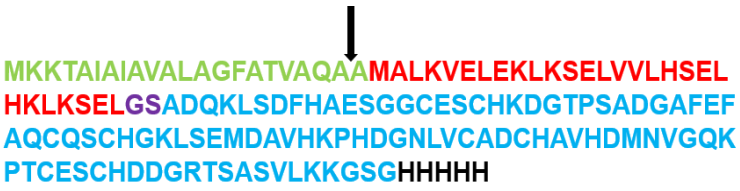

Figure 4.2. β-tail STC sequence expressed in this work. The OmpA leader sequence is shown in green followed by the β-tail tag in red. A Gly-Ser linker between the tag and the protein sequence is shown in purple. The black arrow indicates the site for cleavage of the signal peptide. The STC sequence is shown in blue with a his-tag in its C-terminus in black.

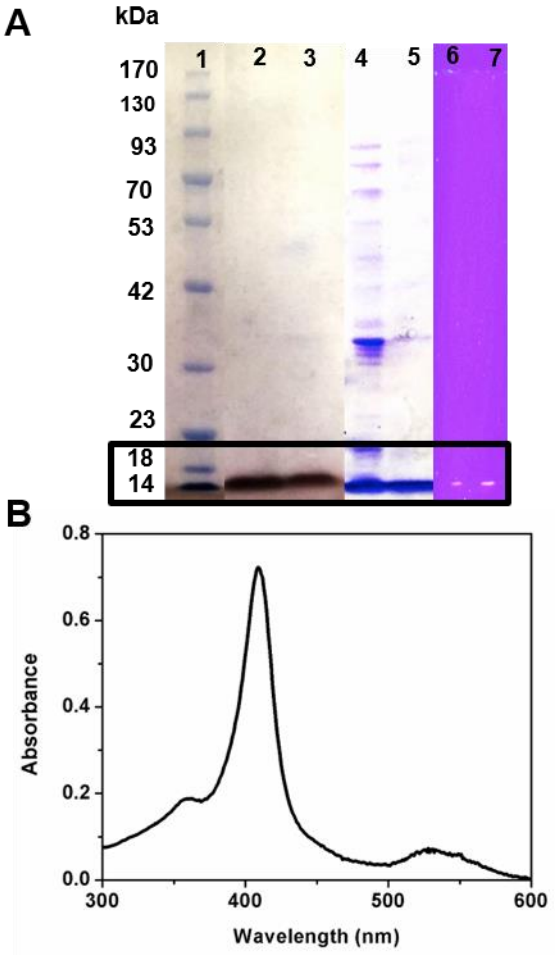

Figure 4.3. (A) SDS-PAGE (12%) analysis to confirm the presence of β-tail STC. Cell lysate (lanes 2,4, and 6) and purified β-tail STC (lanes 3, 5, and 7). Lanes 2 and 3 are stained for the presence of heme. Lanes 4 and 5 are stained with Coomassie blue. Lanes 6 and 7 are stained with stain specific for His-tagged proteins. Lane 1 shows the protein molecular weight standard. Purified β-tail STC is present as a prominent 16 kDa band in all three gels. (B) UV-visible absorbance spectrum of pure β-tail STC in the oxidized form.

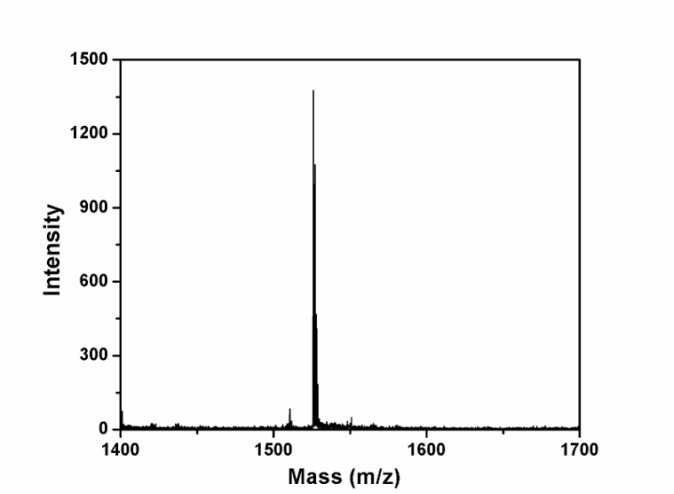

Figure 4.4. MALDI-TOF Mass spectrometry of Q11 peptide. Calculated m/z for Q11:1526.70, observed 1526.70. Scans were averaged over 150 laser shots.

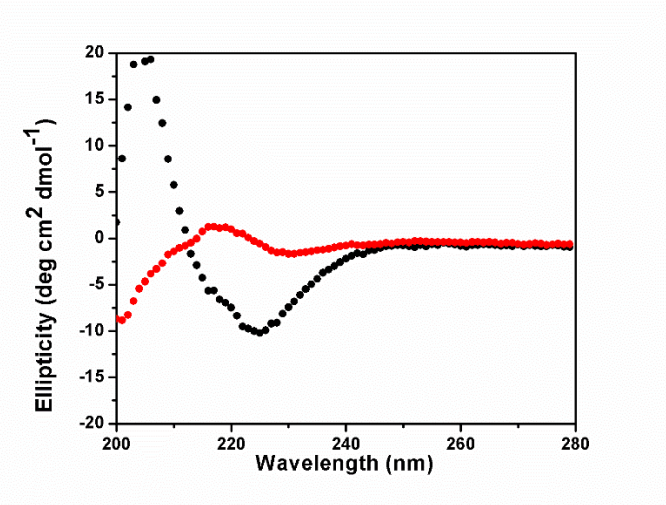

Figure 4.5. CD spectra of Q11 peptide in water (red) and PBS (black) after 12 hrs of incubation.

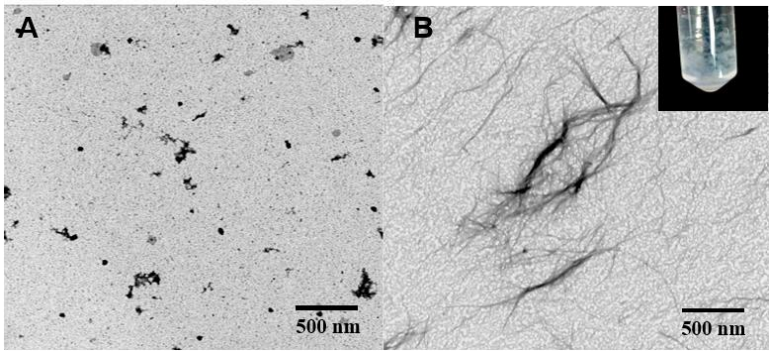

Figure 4.6. (A) Transmission electron micrographs of Q11 in water and (B) in PBS after incubation for 12 hrs. The inset in image (B) shows a picture of Q11 nanofibers which can be sedimented by centrifugation after incubation on the time scale of hours.

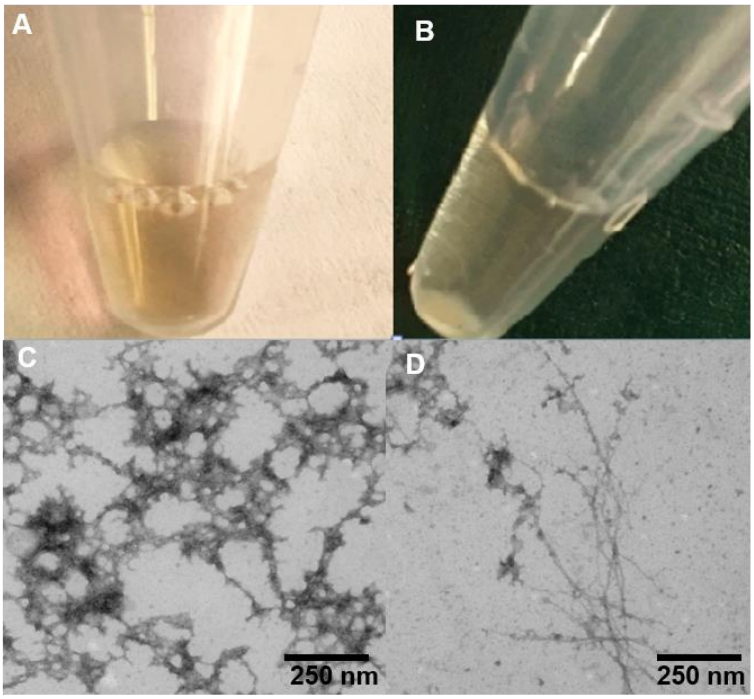

Figure 4.7. (A) Digital photograph of a 1000:1 mixture of Q11 and β-tail STC before overnight incubation, and (B) nanofibers collected via centrifugation after overnight incubation of the peptide and protein. Transmission electron micrographs of nanofibers formed from the peptide-protein mixture (C) before incubation and (D) after incubation.

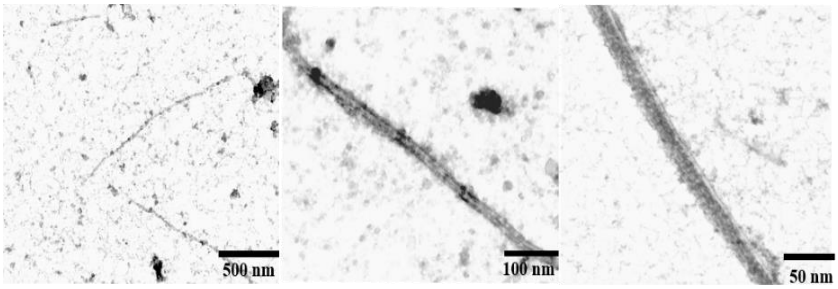

Figure 4.8. TEM images of a collection and individual Q11-β-tail STC nanofibers (left to right). The nanofibers were stained using 1% uranyl acetate.

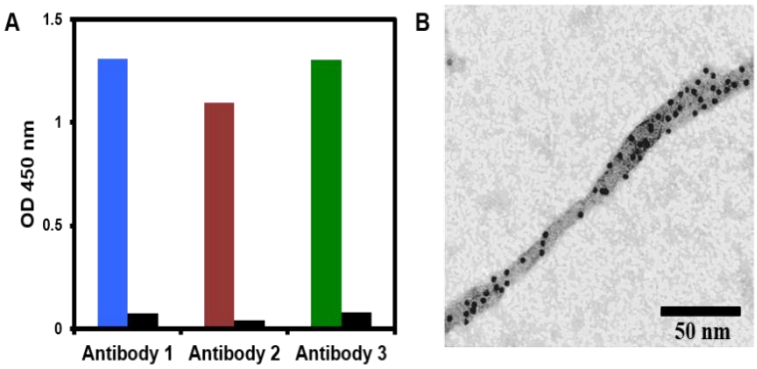

Figure 4.9. (A) ELISA of three different peptide antibodies against β-tail STC. Black bars show each peptide antibody tested against bovine serum albumin. (B) Transmission electron micrograph of a Q11-β-tail STC nanofiber displaying gold nanoparticle-labelled β-STC along the fiber.

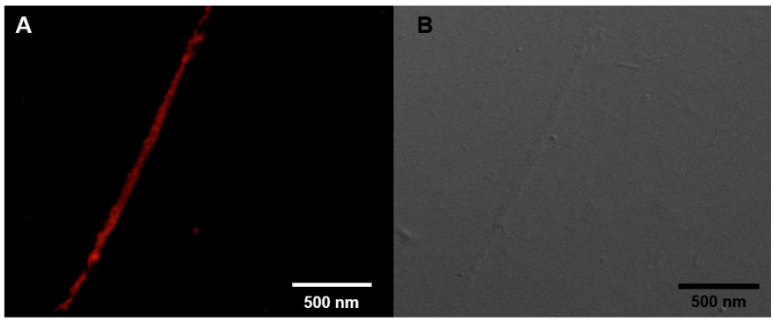

Figure 4.10. Fluorescence micrographs of a single Q11-β-tail STC nanofiber displaying the presence of fluorescent antibodies bound to β-tail STC through the entire length of the fiber (A) with its corresponding amplitude micrograph (B).

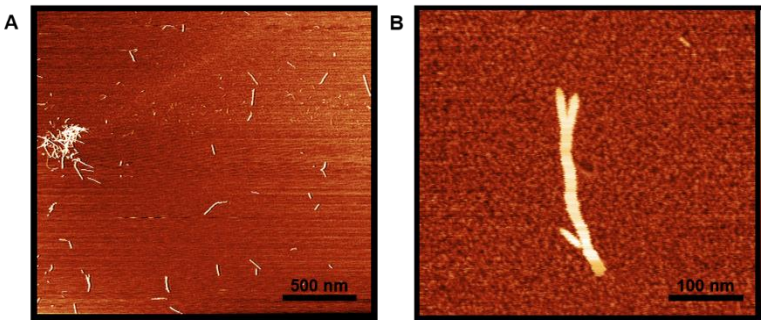

Figure 4.11. Atomic force micrographs of Q11-β-tail STC nanofibrils on mica at different scales.

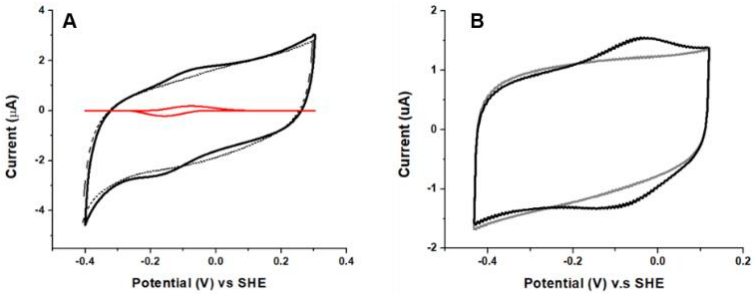

Figure 4.12. (A) Cyclic voltammogram of Q11-β-tail STC nanofiber (10 μl dried onto the electrode surface) in an anaerobic solution of 100 mM potassium phosphate buffer at pH 7.4 (black). Cyclic voltammogram recorded at 100 mV s^{-1} with a sweep window of (-0.5 V to 0.5 V) starting from the reducing side). The red trace is the baseline-corrected (to remove capacitance) version of the same voltammogram. (Dotted black) Cyclic voltammogram of Q11 nanofibers without β-tail STC under the same experimental conditions. (B) Cyclic voltammogram of β-tail STC (200 μM) (10 μl dried onto the electrode surface) in an anaerobic solution of 100 mM potassium phosphate buffer at pH 7.4 (black). Cyclic voltammogram recorded at 100 mV s^{-1} with a sweep window of (-0.5 V to 0.3 V) starting from the reducing side. Gray line is a control cyclic voltammogram in the absence of protein or nanofiber under the same experimental conditions as above.

Table 4.1: *E. coli* strains and plasmids used in this study

Strain or Plasmid	Characteristics or Sequence	Source
E. coli		
DH5α	fhuA2 Δ(argF-lacZ)U169 phoA recA1 relA1 endA1 thi-1 hsdR17	New England Biolabs
BL21 (DE3)	fhuA2 [lon] ompT gal (λDE3) [dcm] ΔhsdS λDE3 = λ sBamHIo ΔEcoRI-B int::(lacI::PlacUV5::T7 gene1) i21 Δnin5	New England Biolabs[43]
Plasmids		
pEC86	ccm operon genes, Cat^r	[12]
pJ411	Beta tail fused with STC gene, kan^r	This study

4.6 References

1. Gray, Harry B., and Jay R. Winkler. Long-range electron transfer. *Proc. Natl. Acad. Sci.* **102**, 3534–3539 (2005).

2. Gray, H. B. and Winkler, J. R. Electron flow through metalloproteins. *Biochim. Biophys. Acta - Bioenerg.* **1797**, 1563–1572 (2010).

3. Williams, R. J. P. Overview of Biological Electron Transfer. *Adv. Chem. Transf. Biol. Solid State* 3–23 (2009).

4. Gralnick, J. A. and Newman, D. K. Extracellular respiration. *Mol. Microbiol.* **65**, 1–11 (2007).

5. Lovley, D. R. Dissimilatory metal reduction. *Annu. Rev. Microbiol.* **47**, 263–290 (1993).

6. Shi, L., Dong, H., Reguera, G., Beyenal, H., Lu, A., Liu, J., Yu, H.Q. and Fredrickson, J. K. Extracellular electron transfer mechanisms between microorganisms and minerals. *Nat. Rev. Microbiol.* **4**, 651–662 (2016).

7. Gorby, Y.A., Yanina, S., McLean, J.S., Rosso, K.M., Moyles, D., Dohnalkova, A., Beveridge, T.J., Chang, I.S., Kim, B.H., Kim, K.S. and Culley, D. E. Electrically conductive bacterial nanowires produced by *Shewanella oneidensis* strain MR-1 and other microorganisms. *Proc. Natl. Acad. Sci.U.S.A* **103**, 11358–11363 (2006).

8. Reguera, G., McCarthy, K.D., Mehta, T., Nicoll, J.S., Tuominen, M.T. and Lovley, D. R. Extracellular electron transfer via microbial nanowires. *Nature* **435**, 1098 (2005).

9. Malvankar, N. S. and Lovley, D. R. Microbial nanowires: A new paradigm for biological electron transfer and bioelectronics. *ChemSusChem* **5**, 1039–1046 (2012).

10. Malvankar, N. S. and Lovley, D. R. Microbial nanowires for bioenergy applications. *Curr. Opin. Biotechnol.* **27**, 88–95 (2014).

11. El-Naggar, M.Y., Wanger, G., Leung, K.M., Yuzvinsky, T.D., Southam, G., Yang, J., Lau, W.M., Nealson, K.H. , Gorby, Y.A.Yang, J., Lau, W. M. & Nealson, and K. H. Electrical transport along bacterial nanowires from *Shewanella oneidensis* MR-1. *Proc. Natl. Acad. Sci. U. S. A.* **107**, 18127–18131 (2010).

12. Pirbadian, S., Barchinger, S.E., Leung, K.M., Byun, H.S., Jangir, Y., Bouhenni,

R.A., Reed, S.B., Romine, M.F., Saffarini, D.A., Shi, L. and Gorby, Y. A. *Shewanella oneidensis* MR-1 nanowires are outer membrane and periplasmic extensions of the extracellular electron transport components. *Proc. Natl. Acad. Sci.U.S.A* **111**, 12883–12888 (2014).

13. El-Naggar, M.Y., Gorby, Y.A., Xia, W. and Nealson, K. H. The molecular density of states in bacterial nanowires. *Biophys. J.* **95**, 10–12 (2008).

14. Pirbadian, S. and El-Naggar, M. Y. Multistep hopping and extracellular charge transfer in microbial redox chains. *Phys. Chem. Chem. Phys.* **14**, 13802–13808 (2012).

15. Malvankar, N.S., Tuominen, M.T. and Lovley, D. R. Lack of cytochrome involvement in long-range electron transport through conductive biofilms and nanowires of *Geobacter sulfurreducens*. *Energy Environ. Sci.* **5**, 8651–8659 (2012).

16. Angenent, L.T., Karim, K., Al-Dahhan, M.H., Wrenn, B.A. and Domíguez-Espinosa, R., Production of bioenergy and biochemicals from industrial and agricultural wastewater. *Trends Biotechnol.* **22**, 477–485 (2004).

17. Vargas, M., Malvankar, N.S., Tremblay, P.L., Leang, C., Smith, J.A., Patel, P., Synoeyenbos-West, O., Nevin, K.P. and Lovley, D. R. Aromatic Amino Acids Required for Pili Conductivity and Long-Range Extracellular Electron Transport in *Geobacter sulfurreducens*. *MBio* **4**, 1–6 (2013).

18. Malvankar, N. S., Yalcin, S. E., Tuominen, M. T. and Lovley, D. R. Visualization of charge propagation along individual pili proteins using ambient electrostatic force microscopy. *Nat. Nanotechnol.* **9**, 1012–1017 (2014).

19. Feliciano, G.T., da Silva, A.J., Reguera, G. and Artacho, E., Molecular and electronic structure of the peptide subunit of *Geobacter sulfurreducens* conductive pili from first principles. *J. Phys. Chem. A* **116**, 8023–8030 (2012).

20. Malvankar, N.S., Vargas, M., Nevin, K., Tremblay, P.L., Evans-Lutterodt, K., Nykypanchuk, D., Martz, E., Tuominen, M.T. and Lovley, D. R. Structural basis for metallic-like conductivity in microbial nanowires. *MBio* **6**, e00084 (2015).

21. Filman, D.J., Marino, S.F., Ward, J.E., Yang, L., Mester, Z., Bullitt, E., Lovley, D.R. and Strauss, M. Structure of a cytochrome-based bacterial nanowire. *bioRxiv* 492645 (2018).

22. Wang, F., Gu, Y., O'Brien, J.P., Sophia, M.Y., Yalcin, S.E., Srikanth, V., Shen,

C., Vu, D., Ing, N.L., Hochbaum, A.I., Malvankar, N .S and Egelman, E. H. Structure of Microbial Nanowires Reveals Stacked Hemes that Transport Electrons over Micrometers. *Cell* **177**, 361–369 (2019).

23. Hudalla, G.A., Sun, T., Gasiorowski, J.Z., Han, H., Tian, Y.F., Chong, A.S. and Collier, J. H. Gradated assembly of multiple proteins into supramolecular nanomaterials. *Nat. Mater.* **13**, 829–36 (2014).

24. Qian, Y., Paquete, C.M., Louro, R.O., Ross, D.E., LaBelle, E., Bond, D.R. and Tien, M. Mapping the Iron Binding Site(s) on the Small Tetraheme Cytochrome of *Shewanella oneidensis* MR-1. *Biochemistry* **50**, 6217–6224 (2011).

25. Collier, J. H. and Messersmith, P. B. Enzymatic modification of self-assembled peptide structures with tissue transglutaminase. *Bioconjug. Chem.* **14**, 748–55 (2003).

26. Francis Jr, R.T. and Becker, R.R., Specific indication of hemoproteins in polyacrylamide gels using a double-staining process. *Anal. Biochem.* **136**, 509–514 (1984).

27. Fourmond, V. QSoas: A Versatile Software for Data Analysis. *Anal. Chem.* **88**, 5050–5052 (2016).

28. Leys, D., Meyer, T.E., Tsapin, A.S., Nealson, K.H., Cusanovich, M.A. and Van Beeumen, J. J. Crystal structures at atomic resolution reveal the novel concept of 'electron-harvesting' as a role for the small tetraheme cytochrome *c*. *J. Biol. Chem.* **277**, 35703–11 (2002).

29. Paquete, C. M. and Louro, R. O. Unveiling the details of electron transfer in multicenter redox proteins. *Acc. Chem. Res.* **47**, 56–65 (2014).

30. Pechsrichuang, P., Songsiriritthigul, C., Haltrich, D., Roytrakul, S., Namvijtr, P., Bonaparte, N. and Yamabhai, M. OmpA signal peptide leads to heterogenous secretion of *B. subtilis* chitosanase enzyme from *E. coli* expression system. *Springerplus* **5**, 1200 (2016).

31. Subramanian, P., Pirbadian, S., El-Naggar, M. Y. and Jensen, G. J. Ultrastructure of *Shewanella oneidensis* MR-1 nanowires revealed by electron cryotomography. *Proc. Natl. Acad. Sci.U.S.A* **115**, E3246–E3255 (2018).

32. Chong, G.W., Karbelkar, A.A. and El-Naggar, M. Y. Nature's conductors: what can microbial multi-heme cytochromes teach us about electron transport and biological energy conversion? *Curr. Opin. Chem. Biol.* **47**, 7–17 (2018).

33. Tan, Y., Adhikari, R.Y., Malvankar, N.S., Pi, S., Ward, J.E., Woodard, T.L., Nevin, K.P., Xia, Q., Tuominen, M.T. and Lovley, D. R. Synthetic Biological Protein Nanowires with High Conductivity. *Small* **12**, 4481–4485 (2016).

34. Creasey, R.C., Mostert, A.B., Solemanifar, A., Nguyen, T.A., Virdis, B., Freguia, S. and Laycock, B. Biomimetic Peptide Nanowires Designed for Conductivity. *ACS Omega* **4**, 1748–1756 (2019).

35. Wang, J., Li, D., Yang, M. and Zhang, Y. A novel ferrocene-tagged peptide nanowire for enhanced electrochemical glucose biosensing. *Anal. Methods* **6**, 7161–7165 (2014).

36. Yemini, M., Reches, M., Rishpon, J. and Gazit, E. Novel electrochemical biosensing platform using self-assembled peptide nanotubes. *Nano Lett.* **5**, 183–186 (2005).

37. Christopher Fry, H., Wood, A. R. and Solomon, L. A. Supramolecular control of heme binding and electronic states in multi-heme peptide assemblies. *Org. Biomol. Chem.* **15**, 6725–6730 (2017).

38. Ing, N.L., Spencer, R.K., Luong, S.H., Nguyen, H.D. and Hochbaum, A. I. Electronic Conductivity in Biomimetic α-Helical Peptide Nanofibers and Gels. *ACS Nano* **12**, 2652–2661 (2018).

39. Altamura, L., Horvath, C., Rengaraj, S., Rongier, A., Elouarzaki, K., Gondran, C., Maçon, A.L., Vendrely, C., Bouchiat, V., Fontecave, M. and Mariolle, D. A synthetic redox biofilm made from metalloprotein-prion domain chimera nanowires. *Nat. Chem.* **9**, 157–163 (2017).

40. Malvankar, N.S., Vargas, M., Nevin, K.P., Franks, A.E., Leang, C., Kim, B.C., Inoue, K., Mester, T., Covalla, S.F., Johnson, J.P. and Rotello, V. M. Tunable metallic-like conductivity in microbial nanowire networks. *Nat. Nanotechnol.* **6**, 573–579 (2011).

41. Kajihara, R., Oohora, K. and Hayashi, T. Photoinduced electron transfer within supramolecular hemoprotein co-assemblies and heterodimers containing Fe and Zn porphyrins. *J. Inorg. Biochem.* **193**, 42–51 (2019).

42. Amdursky, N., Wang, X., Meredith, P., Riley, D.J., Payne, D.J., Bradley, D.D. and Stevens, M. M. Electron Hopping Across Hemin-Doped Serum Albumin Mats on Centimeter-Length Scales. *Adv. Mater.* **29**, 1700810 (2017).

43. Studier, F. W. and Moffat, B. A. Selective expression of cloned genes directed by T7 RNA polymerase. *J. Mol. Biol.* **189**, 113–130 (1986).

Chapter 5

Conclusion

Miyuki A Thirumurthy[1]

[1]School of Molecular Sciences, Arizona State University, Tempe, AZ, 85287, USA

This dissertation has focused on investigation of the natural mechanisms of extracellular electron transfer in microbes and built a synthetic model to probe a possible mechanism for long-range electron transport in biological systems.

Chapter 2 describes the role of a *c*-type cytochrome, OmcZs in transporting electrons from the metabolism of *Geobacter sulfurreducens* to an external electrode. Spectroscopy and electrochemistry are used to characterize an interaction between OmcZs and riboflavin, showing for the first time that this protein clearly plays a role in EET that relies on a flavin as a soluble redox shuttle. Furthermore, expression of OmcZs in *E. coli* confers on it the ability to produce extracellular current which can be enhanced by addition of riboflavin. This is a non-native functionality that opens doors for engineering of *E. coli* for new bioelectronic applications. In parallel, future work will aim to study the flavin binding sites present in the multi-heme cytochrome and to identify other components involved in mediated electron transfer in current producing organisms like *Geobacter sulfurreducens*.

Chapter 3 addresses the question of whether *Synechocystis* pili are involved in extracellular electron transfer (EET). This is an important question since little is known about EET by phototrophs. Photocurrents produced by wild type cells and cells which cannot produce pili are similar in a mediator less biochemical cell suggesting pili do not play a role in EET under these conditions. Furthermore, in contrast to previous reports in the literature, conductive AFM suggests the pili are not conductive. In the future, it will be important to establish whether this is a general result for cyanobacteria or other

phototrophs. Future studies will also seek to identify approaches to improve the extracellular current production by this organism by identifying components essential for EET.

Chapter 4 describes the first synthetic, nanoscale model for electron transfer built using *c*-type cytochromes. Fibers on the scale of μm incorporate protein throughout with an intermolecular distance of 1 to 50 nm and the redox properties of the protein are not modified by incorporation into a fiber. Unfortunately, the nanofibers do not adhere well to the electrode surface for electrochemical gating experiments. Future studies will involve conductivity measurements of individual nanofibers using modified electrode surfaces and will also focus on building systems with a fixed distance between the redox-active components to ensure effective electron transfer. This system is the first step in designing new nanostructures which prove useful in the field of bio-nanoelectronics.

In conclusion, this dissertation has provided insights into biological EET using both natural and synthetic systems. It serves as a foundation to build novel, synthetic systems.

References

1. Gray, H. B. and Winkler, J. R. Electron flow through metalloproteins. *Biochim. Biophys. Acta - Bioenerg.* **1797**, 1563–1572 (2010).

2. Marcus, R.A. and Sutin, N. Electron transfer in chemistry and biology. *Biochim. Biophys. Acta 811* **138**, 265–322 (1985).

3. Mitchell, P. Coupling of phosphorylation to electron and hydrogen transfer by a chemi-osmotic type of mechanism. *Nature* **4784**, 144–148 (1961).

4. Hunt, K. A., Flynn, J. M., Naranjo, B., Shikhare, I. D. and Gralnick, J. A. Substrate-level phosphorylation is the primary source of energy conservation during anaerobic respiration of *Shewanella oneidensis* strain MR-1. *J. Bacteriol.* **192**, 3345–3351 (2010).

5. Nealson, K.H. and Saffarini, D. Iron and Manganese in Anaerobic Respiration: Environmental Significance, Physiology, and Regulation. *Annu. Rev. Microbiol.* **48**, 311–343 (1994).

6. Bond, D. R, Holmes, D. E. and Tender, L. M. Electrode-Reducing Microorganisms That Harvest Energy from Marine Sediments. *Science (80).* **295**, 483–485 (2002).

7. Bretschger, O., Obraztsova, A., Sturm, C.A., Chang, I.S., Gorby, Y.A., Reed, S.B., Culley, D.E., Reardon, C.L., Barua, S., Romine, M.F. and Zhou, J. Current production and metal oxide reduction by *Shewanella oneidensis* MR-1 wild type and mutants. *Appl. Environ. Microbiol.* **73**, 7003–7012 (2007).

8. Rabaey, K. and Rozendal, R. A. Microbial electrosynthesis - Revisiting the electrical route for microbial production. *Nat. Rev. Microbiol.* **8**, 706–716 (2010).

9. Nealson, K. H., Belz, A. and McKee, B. Breathing metals as a way of life: Geobiology in action. *Antonie Van Leeuwenhoek* **81**, 215–222 (2002).

10. Ing, N. L., El-Naggar, M. Y. and Hochbaum, A. I. Going the Distance: Long-Range Conductivity in Protein and Peptide Bioelectronic Materials. *J. Phys. Chem. B* **122**, 10403–10423 (2018).

11. Creasey, R.C., Mostert, A.B., Nguyen, T.A., Virdis, B., Freguia, S. and Laycock, B. Microbial nanowires – Electron transport and the role of synthetic analogues. *Acta Biomater.* **69**, 1–30 (2018).

12. Lovley, D. R. Dissimilatory metal reduction. *Annu. Rev. Microbiol.* **47**, 263–290 (1993).

13. Shi, L., Squier, T.C., Zachara, J.M. and Fredrickson, J. K. Respiration of metal (hydr)oxides by *Shewanella* and *Geobacter*: A key role for multihaem *c*-type cytochromes. *Mol. Microbiol.* **65**, 12–20 (2007).

14. Kranz, R. G., Richard-Fogal, C., Taylor, J.-S. and Frawley, E. R. Cytochrome *c* Biogenesis: Mechanisms for Covalent Modifications and Trafficking of Heme and for Heme-Iron Redox Control. *Microbiol. Mol. Biol. Rev.* **73**, 510–528 (2009).

15. Myers, C. R. and Myers, J. M. Cell surface exposure of the outer membrane cytochromes of *Shewanella oneidensis* MR-1. *Lett. Appl. Microbiol.* **37**, 254–258 (2003).

16. Myers, J. M. and Myers, C. R. Role for outer membrane cytochromes OmcA and OmcB of *Shewanella putrefaciens* MR-1 in reduction of manganese dioxide. *Appl. Environ. Microbiol.* **67**, 260–269 (2001).

17. Myers, C. R. and Myers, J. M. Localization of cytochromes to the outer membrane of anaerobically grown *Shewanella putrefaciens* MR-1. *J. Bacteriol.* **174**, 3429–3438 (1992).

18. Gray, Harry B., and J. R. W. Long-range electron transfer. *Proc. Natl. Acad. Sci. U.S.A* **102**, 3534–3539 (2005).

19. White, G.F., Shi, Z., Shi, L., Wang, Z., Dohnalkova, A.C., Marshall, M.J., Fredrickson, J.K., Zachara, J.M., Butt, J.N., Richardson, D.J. and Clarke, T. A. Rapid electron exchange between surface-exposed bacterial cytochromes and Fe(III) minerals. *Proc. Natl. Acad. Sci. U. S. A.* **110**, 6346–51 (2013).

20. Rosso, K. M., Blumberger, J., Butt, J. N. and Breuer, M. Multi-haem cytochromes in *Shewanella oneidensis* MR-1: structures, functions and opportunities. *J. R. Soc. Interface* **102**, 20141117 (2015).

21. Myers, C.R and Nealson, K. H. Bacterial manganese reduction and growth with manganese oxide as the sole electron acceptor. *Science* **240**, 1319–21 (988).

22. Myers, C. R. and Nealson, K. H. Respiration-linked proton translocation couples to anaerobic reduction of manganese(IV) and iron(III) in *Shewanella putrefaciens* MR-1. *J. Bacteriol.* **172**, 6232–6238 (1990).

23. Pitts, K.E., Dobbin, P.S., Reyes-Ramirez, F., Thomson, A.J., Richardson, D.J. and Seward, H. E. Characterization of the *Shewanella oneidensis* MR-1 decahemecytochrome

MtrA. *J. Biol. Chem.* **278**, 27758–27765 (2003).

24. Coursolle, D. and Gralnick, J. A. Modularity of the Mtr respiratory pathway of *Shewanella oneidensis* strain MR-1. *Mol. Microbiol.* **77**, 995–1008 (2010).

25. Mehta, T., Coppi, M. V., Childers, S. E.and Lovley, D. R. Outer membrane *c*-type cytochromes required for Fe(III) and Mn(IV) oxide reduction in *Geobacter sulfurreducens*. *Appl. Environ. Microbiol.* **71**, 8634–8641 (2005).

26. Nevin, K.P., Kim, B.C., Glaven, R.H., Johnson, J.P., Woodard, T.L., Methé, B.A., DiDonato Jr, R.J., Covalla, S.F., Franks, A.E., Liu, A. and Lovley, D. R. Anode biofilm transcriptomics reveals outer surface components essential for high density current production in *Geobacter sulfurreducens* Fuel Cells. *PLoS One* **4(5)**, 5628 (2009).

27. Von Canstein, H., Ogawa, J., Shimizu, S. and Lloyd, J. R. Secretion of flavins by *Shewanella* species and their role in extracellular electron transfer. *Appl. Environ. Microbiol.* **74**, 615–623 (2008).

28. Brutinel, E. D. and Gralnick, J. A. Shuttling happens: Soluble flavin mediators of extracellular electron transfer in *Shewanella*. *Appl. Microbiol. Biotechnol.* **93**, 41–48 (2012).

29. Min, D., Cheng, L., Zhang, F., Huang, X.N., Li, D.B., Liu, D.F., Lau, T.C., Mu, Y. and Yu, H. Q. Enhancing Extracellular Electron Transfer of *Shewanella oneidensis* MR-1 through Coupling Improved Riboflavin Synthesis and Metal-Reducing Conduit for Pollutant Degradation. *Environ. Sci. Technol.* **51**, 5082–5089 (2017).

30. Yang, Y., Ding, Y., Hu, Y., Cao, B., Rice, S.A., Kjelleberg, S. and Song, H. Enhancing bidirectional electron transfer of *Shewanella oneidensis* by a synthetic flavin pathway. *ACS Synth. Biol.* **4**, 815–823 (2015).

31. Paquete, C.M., Fonseca, B.M., Cruz, D.R., Pereira, T.M., Pacheco, I., Soares, C.M. and Louro, R. O. Exploring the molecular mechanisms of electron shuttling across the microbe/metal space. *Front. Microbiol.* **5**, 318 (2014).

32. Reguera, G., McCarthy, K.D., Mehta, T., Nicoll, J.S., Tuominen, M.T. and Lovley, D. R. Extracellular electron transfer via microbial nanowires. *Nature* **435**, 1098 (2005).

33. Gorby, Y.A., Yanina, S., McLean, J.S., Rosso, K.M., Moyles, D., Dohnalkova, A., Beveridge, T.J., Chang, I.S., Kim, B.H., Kim, K.S. and Culley, D. E. Electrically conductive bacterial nanowires produced by *Shewanella oneidensis* strain MR-1 and other microorganisms. *Proc. Natl. Acad. Sci. U.S.A* **103**, 11358–11363 (2006).

34. Strycharz-Glaven, S. M., Snider, R. M., Guiseppi-Elie, A. and Tender, L. M. On the electrical conductivity of microbial nanowires and biofilms. *Energy Environ. Sci.* **4**, 4366–4379 (2011).

35. El-Naggar, M.Y., Wanger, G., Leung, K.M., Yuzvinsky, T.D., Southam, G., Yang, J., Lau, W.M., Nealson, K.H. , Gorby, Y.A.Yang, J., Lau, W. M. & Nealson, and K. H. Electrical transport along bacterial nanowires from *Shewanella oneidensis* MR-1. *Proc. Natl. Acad. Sci. U. S. A.* **107**, 18127–18131 (2010).

36. Reardon, P. N. and Mueller, K. T. Structure of the type IVa major pilin from the electrically conductive bacterial nanowires of *Geobacter sulfurreducens*. *J. Biol. Chem.* **288**, 29260–29266 (2013).

37. Aklujkar, M., Coppi, M.V., Leang, C., Kim, B.C., Chavan, M.A., Perpetua, L.A., Giloteaux, L., Liu, A. and Holmes, D.E., Proteins involved in electron transfer to Fe(III) and Mn(IV) oxides by *Geobacter sulfurreducens* and *Geobacter uraniireducens*. *Microbiology* **159**, 515–535 (2013).

38. Subramanian, P., Pirbadian, S., El-Naggar, M. Y. and Jensen, G. J. Ultrastructure of *Shewanella oneidensis* MR-1 nanowires revealed by electron cryotomography. *Proc. Natl. Acad. Sci. U.S.A* **115**, E3246–E3255 (2018).

39. Berk, R.S. and Canfield, J.H., Bioelectrochemical Energy Conversion Technologies. *Appl. Microbiol.* **12**, 10–12 (1964).

40. Hernandez, M. E. and Newman, D. K. Extracellular electron transfer. *Cell. Mol. Life Sci.* **58**, 1562–1571 (2001).

41. Cereda, A., Hitchcock, A., Symes, M.D., Cronin, L., Bibby, T.S. and Jones, A. K. A bioelectrochemical approach to characterize extracellular electron transfer by *Synechocystis*. *PLoS One* **9**, e91484 (2014).

42. Bhaya, D., Bianco, N. R., Bryant, D. and Grossman, A. Type IV pilus biogenesis and motility in the cyanobacterium *Synechocystis* sp. PCC6803. *Mol. Microbiol.* **37**, 941–951 (2000).

43. Pirbadian, S. and El-Naggar, M. Y. Multistep hopping and extracellular charge transfer in microbial redox chains. *Phys. Chem. Chem. Phys.* **14**, 13802–13808 (2012).

44. Malvankar, N.S., Vargas, M., Nevin, K.P., Franks, A.E., Leang, C., Kim, B.C., Inoue, K., Mester, T., Covalla, S.F., Johnson, J.P. and Rotello, V. M. Tunable metallic-like conductivity in microbial nanowire networks. *Nat. Nanotechnol.* **6**, 573–579 (2011).

45. Wang, F., Gu, Y., O'Brien, J.P., Sophia, M.Y., Yalcin, S.E., Srikanth, V., Shen, C., Vu, D., Ing, N.L., Hochbaum, A.I., Malvankar, N .S and Egelman, E. H. Structure of Microbial Nanowires Reveals Stacked Hemes that Transport Electrons over Micrometers. *Cell* **177**, 361–369 (2019).

46. Leang, C., Qian, X., Mester, T. and Lovley, D. R. Alignment of the c-type cytochrome OmcS along pili of *Geobacter sulfurreducens*. *Appl. Environ. Microbiol.* **76**, 4080–4084 (2010).

47. Altamura, L., Horvath, C., Rengaraj, S., Rongier, A., Elouarzaki, K., Gondran, C., Maçon, A.L., Vendrely, C., Bouchiat, V., Fontecave, M. and Mariolle, D. A synthetic redox biofilm made from metalloprotein-prion domain chimera nanowires. *Nat. Chem.* **9**, 157–163 (2017).

48. Richter, K., Schicklberger, M. and Gescher, J. Dissimilatory Reduction of Extracellular Electron Acceptors in Anaerobic Respiration. *Appl. Environ. Microbiol.* **78**, 913–921 (2012).

49. Rev, A. and Lovley, D. R. Dissimilatory metal 1 red1uction. *Annu. Rev. Microbiol. 47.1 263-290.* **47.1**, 263–290 (1993).

50. Liu H, Ramnarayanan R, L. B. Production of Electricity during Wastewater Treatment Using a Single Chamber Microbial Fuel Cell. **38**, 2281–2285 (2004).

51. Lovley, D.R., Phillips, E.J., Gorby, Y.A. and Landa, E.R., Microbial reduction of uranium. *Nature* **350**, 413 (1991).

52. Shi, L., Richardson, D.J., Wang, Z., Kerisit, S.N., Rosso, K.M., Zachara, J.M. and Fredrickson, J. K. The roles of outer membrane cytochromes of *Shewanella* and *Geobacter* in extracellular electron transfer. *Environ. Microbiol. Rep.* **1**, 220–227 (2009).

53. Hartshorne, R.S., Reardon, C.L., Ross, D., Nuester, J., Clarke, T.A., Gates, A.J., Mills, P.C., Fredrickson, J.K., Zachara, J.M., Shi, L. and Beliaev, A. S. Characterization of an electron conduit between bacteria and the extracellular environment. *Proc. Natl. Acad. Sci. U.S.A* **106**, 22169–22174 (2009).

54. Myers, C.R. and Myers, J.M., Localization of Cytochromes to the Outer Membrane of Anaerobically Grown *Shewanella putrefaciens* MR-1. *J. Bacteriol.* **174**, 3429–3438 (1992).

55. Pirbadian, S., Barchinger, S.E., Leung, K.M., Byun, H.S., Jangir, Y., Bouhenni, R.A., Reed, S.B., Romine, M.F., Saffarini, D.A., Shi, L. and Gorby, Y. A. *Shewanella oneidensis* MR-1 nanowires are outer membrane and periplasmic extensions of the

extracellular electron transport components. *Proc. Natl. Acad. Sci. U.S.A* **111**, 12883–12888 (2014).

56. Marsili, E., Baron, D.B., Shikhare, I.D., Coursolle, D., Gralnick, J.A. and Bond, D. R. *Shewanella* secretes flavins that mediate extracellular electron transfer. *Proc. Natl. Acad. Sci U.S.A.* **105**, 3968–3973 (2008).

57. Von Canstein, H., Ogawa, J., Shimizu, S. and Lloyd, J.R., Secretion of flavins by *Shewanella* species and their role in extracellular electron transfer. *Appl. Environ. Microbiol.* **74**, 615–623 (2008).

58. Yang, Y., Ding, Y., Hu, Y., Cao, B., Rice, S.A., Kjelleberg, S. and Song, H., Enhancing Bidirectional Electron Transfer of *Shewanella oneidensis* by a Synthetic Flavin Pathway. *ACS Synth. Biol.* **4**, 815–823 (2015).

59. Watanabe, K., Manefield, M., Lee, M. and Kouzuma, A. Electron shuttles in biotechnology. *Curr. Opin. Biotechnol.* **20**, 633–641 (2009).

60. Glasser, N.R., Saunders, S.H. and Newman, D.K.,The colorful world of extracellular electron shuttles. *Annu. Rev. Microbiol.* **71**, 731–751 (2017).

61. Kotloski, N. J. and Gralnick, J. A. Flavin Electron Shuttles Dominate Extracellular Electron Transfer by *Shewanella oneidensis*. *MBio* **4**, 10–13 (2013).

62. Saffarini, D., Brockman, K., Beliav, A., Bouhenni, R. and Shirodkar, S. *Shewanella oneidensis* and extracellular electron transfer to metal oxides. in *Bacteria-Metal Interactions,Springer, Cham* 21–40 (2015).

63. Okamoto, A., Saito, K., Inoue, K., Nealson, K.H., Hashimoto, K. and Nakamura, R. Uptake of self-secreted flavins as bound cofactors for extracellular electron transfer in *Geobacter* species. *Energy Environ. Sci.* **7**, 1357–1361 (2014).

64. Xu, S., Jangir, Y. and El-Naggar, M. Y. Disentangling the roles of free and cytochrome-bound flavins in extracellular electron transport from *Shewanella oneidensis* MR-1. *Electrochim. Acta* **198**, 49–55 (2016).

65. Tokunou, Y., Hashimoto, K. and Okamoto, A. Acceleration of Extracellular Electron Transfer by Alternative Redox-Active Molecules to Riboflavin for Outer-Membrane Cytochrome *c* of *Shewanella oneidensis* MR-1. *J. Phys. Chem. C* **120**, 16168–16173 (2016).

66. Richter, H., Nevin, K.P., Jia, H., Lowy, D.A., Lovley, D.R. and Tender, L. M. Cyclic voltammetry of biofilms of wild type and mutant *Geobacter sulfurreducens* on

fuel cell anodes indicates possible roles of OmcB, OmcZ, type IV pili, and protons in extracellular electron transfer. *Energy Environ. Sci.* **2**, 506 (2009).

67. Francis Jr, R.T. and Becker, R.R.,Specific indication of hemoproteins in polyacrylamide gels using a double-staining process. *Anal. Biochem.* **136**, 509–514 (1984).

68. Hayashita, T., Taniguchi, S., Tanamura, Y., Uchida, T., Nishizawa, S., Teramae, N., Jin, Y.S., Lee, J.C. and Bartsch, R. A. A dibenzo-16-crown-5 fluoroionophore for selective emission ratio sensing of Na+ in basic aqueous dioxane solution. *J. Chem. Soc. Perkin Trans. 2* 1003–1006 (2002).

69. Pechsrichuang, P., Songsiriritthigul, C., Haltrich, D., Roytrakul, S., Namvijtr, P., Bonaparte, N. and Yamabhai, M. OmpA signal peptide leads to heterogenous secretion of *B. subtilis* chitosanase enzyme from *E. coli* expression system. *Springerplus* **5**, 1200 (2016).

70. Thony-Meyer, L., Fischer, F., Kunzler, P., Ritz, D. and Hennecke, H. *Escherichia coli* genes required for cytochrome c maturation. *J. Bacteriol.* **177**, 4321–4326 (1995).

71. Okamoto, A., Hashimoto, K., Nealson, K. H. and Nakamura, R. Rate enhancement of bacterial extracellular electron transport involves bound flavin semiquinones. *Proc. Natl. Acad. Sci. U. S. A.* **110**, 7856–61 (2013).

72. Macheroux, P. UV-visible Spetroscopy as a Tool to Study Flavoproteins. *Humana Press* **131**, 1–7 (1999).

73. Weber, G. Fluorescence of riboflavin and flavin-adenine dinucleotide. *Biochem. J.* **47**, 114 (1950).

74. Smith, J.A., Tremblay, P.L., Shrestha, P.M., Snoeyenbos-West, O.L., Franks, A.E., Nevin, K.P. and Lovley, D. R. Going Wireless: Fe(III) Oxide Reduction without Pili by *Geobacter sulfurreducens* Strain JS-1. *Appl. Environ. Microbiol.* **80**, 4331–4340 (2014).

75. Edwards, M.J., White, G.F., Norman, M., Tome-Fernandez, A., Ainsworth, E., Shi, L., Fredrickson, J.K., Zachara, J.M., Butt, J.N., Richardson, D.J. and Clarke, T. A. Redox Linked Flavin Sites in Extracellular Decaheme Proteins Involved in Microbe-Mineral Electron Transfer. *Sci. Rep.* **5**, 11677 (2015).

76. Jensen, H.M., Albers, A.E., Malley, K.R., Londer, Y.Y., Cohen, B.E., Helms, B.A., Weigele, P., Groves, J.T. and Ajo-Franklin, C. M. Engineering of a synthetic electron conduit in living cells. *Proc. Natl. Acad. Sci. U. S. A.* **107**, 19213–8 (2010).

77. Jensen, H. M., TerAvest, M. A., Kokish, M. G. and Ajo-Franklin, C. M. CymA and Exogenous Flavins Improve Extracellular Electron Transfer and Couple It to Cell Growth in Mtr-Expressing *Escherichia coli*. *ACS Synth. Biol.* **5**, 679–688 (2016).

78. Celeste Yanisch-Perron, J. V. and J. M. Improved M13 phage cloning vectors and host strains:nucleotide sequence of the M13mp18 and pUC19 vectors. *Gene* **33**, 103–119 (1985).

79. Arslan, E., Schulz, H., Zufferey, R., Künzler, P. and Thöny-Meyer, L. Overproduction of the *Bradyrhizobium japonicum c*-Type Cytochrome Subunits of the cbb3Oxidase in *Escherichia coli*. *Biochem. Biophys. Res. Commun.* **251**, 744–747 (1998).

80. Studier, F. W. and Moffat, B. A. Selective expression of cloned genes directed by T7 RNA polymerase. *J. Mol. Biol.* **189**, 113–130 (1986).

81. Kotloski, N. J., Gralnick, J. A. and Newman, D. K. Flavin Electron Shuttles Dominate Extracellular Electron Transfer by *Shewanella oneidensis*. *MBio* **4**, 1–4 (2013).

82. Kracke, F., Vassilev, I. and Krömer, J. O. Microbial electron transport and energy conservation - The foundation for optimizing bioelectrochemical systems. *Front. Microbiol.* **6**, 1–18 (2015).

83. Rabaey, K. and Verstraete, W. Microbial fuel cells: Novel biotechnology for energy generation. *Trends Biotechnol.* **23**, 291–298 (2005).

84. Gorby, Y.A., Yanina, S., McLean, J.S., Rosso, K.M., Moyles, D., Dohnalkova, A., Beveridge, T.J., Chang, I.S., Kim, B.H., Kim, K.S. and Culley, D.E. ,Electrically conductive bacterial nanowires produced by *Shewanella oneidensis* strain MR-1 and other microorganisms. *Proc. Natl. Acad. Sci. U.S.A* **103**, 11358–11363 (2006).

85. Holmes, D. E., Dang, Y., Walker, D. J. F. and Lovley, D. R. The electrically conductive pili of *Geobacter* species are a recently evolved feature for extracellular electron transfer. *Microb. Genomics* **2**, 1–20 (2016).

86. Stroml, M. S. and Lory, S. Structure-function and biogenesis of the type IV. *Fish. Sci.* **47**, 565–96 (1993).

87. Tichý, M., Bečková, M., Kopečná, J., Noda, J., Sobotka, R. and Komenda, J. Strain of *Synechocystis* PCC 6803 with Aberrant Assembly of Photosystem II Contains Tandem Duplication of a Large Chromosomal Region. *Front. Plant Sci.* **7**, 1–10 (2016).

88. Ikeuchi, M. and Tabata, S. *Synechocystis* sp. PCC 6803 – a useful tool in the study of the genetics of cyanobacteria. 73–83 (2001).

89. Lovley, D. R. Electromicrobiology. *Annu. Rev. Microbiol.* **66**, 391–409 (2012).

90. Tajima, N., Sato, S., Maruyama, Kaneko, Sasaki, N.V., Kurokawa, Ohta, H., Kanesaki, Y.U., Yoshikawa, H., Tabata, S. and Ikeuchi, M. Genomic Structure of the Cyanobacterium *Synechocystis* sp. PCC 6803 Strain GT-S. *DNA Res.* **18**, 393–399 (2011).

91. Bouhenni, R.A., Vora, G.J., Biffinger, J.C., Shirodkar, S., Brockman, K., Ray, R., Wu, P., Johnson, B.J., Biddle, E.M., Marshall, M.J. and Fitzgerald, L. A. The role of *Shewanella oneidensis* MR-1 outer surface structures in extracellular electron transfer. *Electroanalysis* **22**, 856–864 (2010).

92. Danika, T., Bjorn, V., Annegret, W., Salim, A. and Wolfgang, R. H. Microevolution in Cyanobacteria: Re-sequencing a Motile Substrain of *Synechocystis* sp PCC 6803. *DNA Res.* **19**, 435–448 (2012).

93. Williams, J. G. K. Construction of Specific Mutations in Photosystem II Photosynthetic Reaction Center by Genetic Engineering Methods in *Synechocystis* 6803. *Methods Enzymol.* **167**, 766–778 (1988).

94. Kamei, A., Yuasa, T., Geng, X. and Ikeuchi, M. Biochemical examination of the potential eukaryotic-type protein kinase genes in the complete genome of the unicellular cyanobacterium *Synechocystis* sp. PCC 6803. *DNA Res.* **9**, 71–78 (2002).

95. Kaneko, T., Sato, S., Kotani, H., Tanaka, A., Asamizu, E., Nakamura, Y., Miyajima, N., Hirosawa, M., Sugiura, M., Sasamoto, S. and Kimura, T. Sequence Analysis of the Genome of the Unicellular Cyanobacterium *Synechocystis* sp. Strain PCC6803. II. Sequence Determination of the Entire Genome and Assignment of Potential Protein-coding Regions. *DNA Res.* **3**, 185–209 (1996).

96. Williams, R. J. P. Overview of Biological Electron Transfer. *Adv. Chem. Transf. Biol. Solid State* 3–23 (2009).

97. Amdursky, N., Marchak, D., Sepunaru, L., Pecht, I., Sheves, M. and Cahen, D., Electronic Transport via Proteins. *Adv. Mater.* **26**, 7142–7161 (2014).

98. Gralnick, J. A. and Newman, D. K. Extracellular respiration. *Mol. Microbiol.* **65**, 1–11 (2007).

99. Shi, L., Dong, H., Reguera, G., Beyenal, H., Lu, A., Liu, J., Yu, H.Q. and Fredrickson, J. K. Extracellular electron transfer mechanisms between microorganisms and minerals. *Nat. Rev. Microbiol.* **4**, 651–662 (2016).

100. Malvankar, N. S. and Lovley, D. R. Microbial nanowires: A new paradigm for biological electron transfer and bioelectronics. *ChemSusChem* **5**, 1039–1046 (2012).

101. Malvankar, N. S. and Lovley, D. R. Microbial nanowires for bioenergy applications. *Curr. Opin. Biotechnol.* **27**, 88–95 (2014).

102. Angenent, L.T., Karim, K., Al-Dahhan, M.H., Wrenn, B.A. and Domíguez-Espinosa, R. .,Production of bioenergy and biochemicals from industrial and agricultural wastewater. *Trends Biotechnol.* **22**, 477–485 (2004).

103. El-Naggar, M.Y., Gorby, Y.A., Xia, W. and Nealson, K. H. The molecular density of states in bacterial nanowires. *Biophys. J.* **95**, 10–12 (2008).

104. Feliciano, G.T., da Silva, A.J., Reguera, G. and Artacho, E. ,Molecular and electronic structure of the peptide subunit of *Geobacter sulfurreducens* conductive pili from first principles. *J. Phys. Chem. A* **116**, 8023–8030 (2012).

105. Vargas, M., Malvankar, N.S., Tremblay, P.L., Leang, C., Smith, J.A., Patel, P., Synoeyenbos West, O., Nevin, K.P. and Lovley, D. R. Aromatic Amino Acids Required for Pili Conductivity and Long-Range Extracellular Electron Transport in *Geobacter sulfurreducens*. *MBio* **4**, 1–6 (2013).

106. Malvankar, N. S., Tuominen, M. T. and Lovley, D. R. Lack of cytochrome involvement in long-range electron transport through conductive biofilms and nanowires of *Geobacter sulfurreducens*. *Energy Environ. Sci.* **5**, 8651 (2012).

107. Malvankar, N. S., Yalcin, S. E., Tuominen, M. T. and Lovley, D. R. Visualization of charge propagation along individual pili proteins using ambient electrostatic force microscopy. *Nat. Nanotechnol.* **9**, 1012–1017 (2014).

108. Malvankar, N.S., Vargas, M., Nevin, K., Tremblay, P.L., Evans-Lutterodt, K., Nykypanchuk, D., Martz, E., Tuominen, M.T. and Lovley, D. R. Structural basis for metallic-like conductivity in microbial nanowires. *MBio* **6**, e00084 (2015).

109. Filman, D.J., Marino, S.F., Ward, J.E., Yang, L., Mester, Z., Bullitt, E., Lovley, D.R. and Strauss, M. Structure of a cytochrome-based bacterial nanowire. *bioRxiv* 492645 (2018).

110. Qian, Y., Paquete, C.M., Louro, R.O., Ross, D.E., LaBelle, E., Bond, D.R. and Tien, M. Mapping the Iron Binding Site(s) on the Small Tetraheme Cytochrome of *Shewanella oneidensis* MR-1. *Biochemistry* **50**, 6217–6224 (2011).

111. Hudalla, G.A., Sun, T., Gasiorowski, J.Z., Han, H., Tian, Y.F., Chong, A.S. and

Collier, J. H. Gradated assembly of multiple proteins into supramolecular nanomaterials. *Nat. Mater.* **13**, 829–36 (2014).

112. Collier, J. H. and Messersmith, P. B. Enzymatic modification of self-assembled peptide structures with tissue transglutaminase. *Bioconjug. Chem.* **14**, 748–55 (2003).

113. Fourmond, V. QSoas: A Versatile Software for Data Analysis. *Anal. Chem.* **88**, 5050–5052 (2016).

114. Leys, D., Meyer, T.E., Tsapin, A.S., Nealson, K.H., Cusanovich, M.A. and Van Beeumen, J. J. Crystal structures at atomic resolution reveal the novel concept of 'electron-harvesting' as a role for the small tetraheme cytochrome *c*. *J. Biol. Chem.* **277**, 35703–11 (2002).

115. Paquete, C. M. and Louro, R. O. Unveiling the details of electron transfer in multicenter redox proteins. *Acc. Chem. Res.* **47**, 56–65 (2014).

116. Burgess, M., Moore, J. S. and Rodríguez-López, J. Redox Active Polymers as Soluble Nanomaterials for Energy Storage. *Acc. Chem. Res.* **49**, 2649–2657 (2016).

117. Wang, J., Li, D., Yang, M. and Zhang, Y. A novel ferrocene-tagged peptide nanowire for enhanced electrochemical glucose biosensing. *Anal. Methods* **6**, 7161–7165 (2014).

118. Yemini, M., Reches, M., Rishpon, J. and Gazit, E. Novel electrochemical biosensing platform using self-assembled peptide nanotubes. *Nano Lett.* **5**, 183–186 (2005).

119. Tan, Y., Adhikari, R.Y., Malvankar, N.S., Pi, S., Ward, J.E., Woodard, T.L., Nevin, K.P., Xia, Q., Tuominen, M.T. and Lovley, D. R. Synthetic Biological Protein Nanowires with High Conductivity. *Small* **12**, 4481–4485 (2016).

120. Amdursky, N. Enhanced solid-state electron transport via tryptophan containing peptide networks. *Phys. Chem. Chem. Phys.* **15**, 13479–13482 (2013).

121. Creasey, R.C., Mostert, A.B., Solemanifar, A., Nguyen, T.A., Virdis, B., Freguia, S. and Laycock, B. Biomimetic Peptide Nanowires Designed for Conductivity. *ACS Omega* **4**, 1748–1756 (2019).

122. Clarke, T.A., Edwards, M.J., Gates, A.J., Hall, A., White, G.F., Bradley, J., Reardon, C.L., Shi, L., Beliaev, A.S., Marshall, M.J. and Wang, Z. Structure of a bacterial cell surface decaheme electron conduit. *Proc. Natl. Acad. Sci. U.S.A* **108**, 9384–9389 (2011).

123. Blauch, D. N. and Savéant, J. M. Dynamics of Electron Hopping in Assemblies of Redox Centers. Percolation and Diffusion. *J. Am. Chem. Soc.* **114**, 3323–3332 (1992).

124. Xu, S., Barrozo, A., Tender, L.M., Krylov, A.I. and El-Naggar, M.Y. ,Multiheme Cytochrome Mediated Redox Conduction through *Shewanella oneidensis* MR-1 Cells. *J. Am. Chem. Soc.* **140**, 10085–10089 (2018).

125. Malvankar, N.S., Tuominen, M.T. and Lovley, D. R. Lack of cytochrome involvement in long-range electron transport through conductive biofilms and nanowires of *Geobacter sulfurreducens*. *Energy Environ. Sci.* **5**, 8651–8659 (2012).

126. Christopher Fry, H., Wood, A. R. and Solomon, L. A. Supramolecular control of heme binding and electronic states in multi-heme peptide assemblies. *Org. Biomol. Chem.* **15**, 6725–6730 (2017).

127. Ing, N.L., Spencer, R.K., Luong, S.H., Nguyen, H.D. and Hochbaum, A. I. Electronic Conductivity in Biomimetic α-Helical Peptide Nanofibers and Gels. *ACS Nano* **12**, 2652–2661 (2018).

128. Kajihara, R., Oohora, K. and Hayashi, T. Photoinduced electron transfer within supramolecular hemoprotein co-assemblies and heterodimers containing Fe and Zn porphyrins. *J. Inorg. Biochem.* **193**, 42–51 (2019).

129. Amdursky, N., Wang, X., Meredith, P., Riley, D.J., Payne, D.J., Bradley, D.D. and Stevens, M. M. Electron Hopping Across Hemin-Doped Serum Albumin Mats on Centimeter-Length Scales. *Adv. Mater.* **29**, 1700810 (2017)

130. Chong, G.W., Karbelkar, A.A. and El-Naggar, M. Y. Nature's conductors: what can microbial multi-heme cytochromes teach us about electron transport and biological energy conversion *Curr. Opin. Chem. Biol.* **47**, 7–17 (2018).

131. Babanova, S., Matanovic, I., Cornejo, J., Bretschger, O., Nealson, K. and Atanassov, P., Outer membrane cytochromes/flavin interactions in *Shewanella* spp.—A molecular perspective. *Biointerphases*, **12**(2),021004 (2017).

132. Schuergers, N., Werlang, C., Ajo-Franklin, C.M. and Boghossian, A.A. A synthetic biology approach to engineering living photovoltaics. *Energ Environ Sci*, **10**(5),1102-1115 (2017).

133. TerAvest, M.A. and Ajo-Franklin, C.M., Transforming exoelectrogens for biotechnology using synthetic biology. *Biotechnol. Bioeng*, **113**(4), 687-697 (2016).

134. Tang, H.Y., Holmes, D.E., Ueki, T., Palacios, P.A. and Lovley, D.R., Iron Corrosion via Direct Metal-Microbe Electron Transfer. *Mbio*, **10**(3), e00303-19 (2019).

135. Li, F., Wang, L., Liu, C., Wu, D. and Song, H., Engineering exoelectrogens by synthetic biology strategies. *Curr. Opin. Echem*, **10**, 37-45 (2018).

136. Glaven, Sarah M. Bioelectrochemical systems and synthetic biology: more power, more products. *Microbiol. Biotechnol,* **12**, 819-823 (2019).

APPENDIX

A. PLASMID MAPS

A. Plasmid maps

Plasmid Map of pJ411 Plasmid with OmcZs

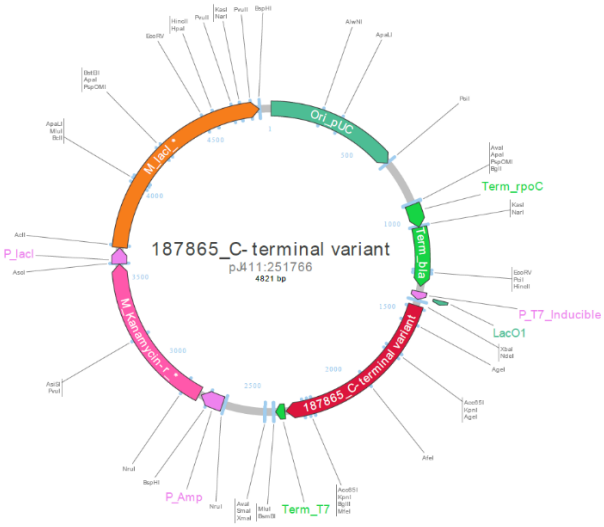

Plasmid Map of pJ411 Plasmid with β-STC